ABSTRACT

Title of Document: **ULTRASENSITIVE CITP-MS BASED TARGETED PROTEOMICS TECHNOLOGIES FOR PROTEIN IDENTIFICATION AND QUANTIFICATION**

Chenchen Wang, Doctor of Philosophy, 2014

Directed By: Professor Cheng S. Lee
Department of Chemistry and Biochemistry

Mass Spectrometry (MS) based technologies have enabled efficient and comprehensive proteomic profiling for biomarker discovery. However, due to sample complexity and large concentration variation, the obtained data is usually biased to endogeneous high abundance proteins while the important disease-related information went missing. Targeted proteomics enables the delivery of precise and sensitive qualitative/quantitative data of interest to researchers by focusing analysis on a preselected population of cells or proteins. This project aims to develop targeted proteomic technologies through capillary isotachophoresis (CITP)-based technique which is capable of selectively enriching trace compounds for a further improved sensitivity in both discovery and validation studies.

By employing tissue microdissection and a CITP-based multidimensional separation platform, homogeneous glioma cells were isolated from unwanted cells and analyzed in search of glioblastoma biomarker. Comparative proteomic profiling of pure tumor cells from different grades of infiltrative astrocytomas revealed disease specific protein expression variation among grades. Further validation using immunohistochemistry demonstrated consistent results. This targeted tissue analyzing platform provided a

sensitive and confident methodology for biomarker discovery within minute amount of samples.

With the demonstrated outstanding analyzing capacity on targeted biomarker discovery, we moved on to developing ultrasensitive targeted quantitation techniques. We demonstrated online coupling of transient-CITP/CZE (capillary zone electrophoresis) with selective reaction monitoring (SRM) MS for the first time via a sheathliquid interface for improved sensitivity and selectivity. Ultrasensitive targeted quantitation was achieved through the incorporation of the selective enrichment capability of CITP/CZE with SRM MS, giving a limit of quantitation (LOQ) of 50 pM with a total sample loading of 50 attomoles.

In order to further improve the sensitivity, we developed a novel sheathless interface which enables increased loading capacity and nanoflow operation by assembling a large size separation capillary and a small size porous emitter. LOQ was improved 5 times comparing to using the first sheathliquid interface, giving a LOQ of 10 pM with a total sample loading of 25 attomoles. This novel interface optimally preserved the high resolution and efficiency of CITP/CZE while improving the limited sample loading capacity, demonstrating a powerful analytic platform for targeted proteomic quantitation and validation.

ULTRASENSITIVE CITP-MS BASED TARGETED PROTEOMICS TECHNOLOGY FOR PROTEIN IDENTIFICATION AND QUANTIFICATION IN BIOMARKER DISCOVERY

By

Chenchen Wang

Dissertation submitted to the Faculty of the Graduate School of the
University of Maryland, College Park, in partial fulfillment
of the requirements for the degree of
Doctore of Philosophy
2014

Advisory Committee:
Professor Cheng S. Lee, Chair
Professor Shuwei Li
Professor Dorothy Beckett
Professor Neil Blough
Professor David Mosser

Table of Contents

List of Figures

List of Tables

List of Abbreviations

ApoA1	Apolipoprotein A-1
AUC	Area Under Curve
BGE	Background Electrolyte
BPC	Base Peak Ion Chromatograms
BSA	Bovine Serum Albumin
CE	Capillary Electrophoresis
CE-MS	Capillary Electrophoresis-Mass Spectrometry
CITP	Capillary Isotachophoresis
CZE	Capillary Zone Electrophoresis
CV	Coefficient of Variation
CIEF	Combined Capillary Isoelectric Focusing
DIGE	Difference Gel Electrophoresis
DTT	Dithiothreitol
ESI-MS	Electrospray Ionization
ELISA	Enzyme-Linked Immunosorbent Assay
EIC	Extracted Ion Chromatograms
FDRs	False Discovery Rates
GBM	Glioblastoma
HCV	Hepatitis C Virus
HCC	Hepatocellular Carcinoma
HER2	Human Epidermal Growth Factor Receptor 2
IHC	Immunohistochemistry

IAM	Iodoacetamide
iTRAQ	Isobaric Tag For Relative And Absolute Quantitation
LCM	Laser-Capture Microdissection
LE	Leading Electrolyte
LOD	Limit of Detection
LOQ	Limit of Quantitation
LTQ	Linear Ion-Trap Mass Spectrometer
LC-MS	Liquid Chromatography-Mass Spectrometry
MALDI-MS	Matrix Assisted Laser Desorption/Ionization Mass Spectrometry
MALDI-TOF/TOF	Matrix-Assisted Laser Desorption/Ionization-Time of Flight/Time of Flight
MS	Mass Spectrometry
MuDPIT	Multidimensional Protein Identification Technique
nano-RPLC	Nano-Reversed Phase Liquid Chromatography
OMSSA	Open Mass Spectrometry Search Algorithm
FFPE	Paraffin-Embedded
PSA	Prostate-Specific Antigen
RT	Retention Time
SRM	Selected Reaction Monitoring
S/N	Signal to Noise Ratio
SPE	Solid-Phase Extraction
SCX	Strong Cation-Exchange

SELDI-MS	Surface Enhanced Laser Desorption/Ionization-Mass Spectrometry
TMA	Tissue Microarray
HF	Hydrofluoric Acid

Chapter 1 : Introduction

Section 1.3 Capillary electrophoresis in biomarker discovery and recent advances is reproduced with permission from Wang, C.; Fang, X.; Lee, C.S.: Recent advances in capillary electrophoresis-based proteomic techniques for biomarker discovery. *Methods Mol Biol* **2013**; *984*,1-12.

1.1 Introduction

Despite the continued progress of drug development and surgery procedure, cancer has still remained to be a leading cause of mortality in both developed and developing countries. In order to combat cancer and other high mortality diseases, researchers have been actively looking for biomolecules in tissus and biofluids with diagnostic, predictive and prognostic functions. Such biomolecules termed as biomarkers are defined as "biological molecules found in blood, other body fluids, or tissues that are a sign of a normal or abnormal process or of a condition or disease" by the National Cancer Institute.

This definition only speaks of the diagnostic function of biomarker while successful biomarkers actually can do so much more in patient care. Biomarkers can be used to predict the probability of the occurrence or recurrence of cancers in certain individuals or populations; biomarkers can be utilized to estimate the likely outcome of the disease and develop the best therapeutic method (personalized medication); biomarkers can also be employed to monitor and assess the effectiveness and adverse effects of a treatment.

Some well-known and widely applied biomarkers are prostate-specific antigen (PSA), human epidermal growth factor receptor 2 (HER2).

PSA is a diagnostic biomarker used in large scope screening for early detection and treatment of prostate cancer which is normally associated with elevated PSA level in urine or blood . HER2 on the other hand, is a predictive and prognostic biomarker for breast cancer. HER2 testing is performed in breast cancer patients to assess the prognosis and the suitability of trastazumab therapy as trastazumab is restricted to HER-2 positive individuals due to the severe side effect and low efficacy in HER-2 negative patients. Currently, the number of biomarkers approved by the Food and Drug Administration is still very limited due to the lengthy, costly development procedure as well as the demanding technical requirements for biomarker discovery and verification.

Mass Spectrometry (MS) has played a critical role in biomarker discovery in the recent years. Though this technology itself is only 20-30 years old, it has been evolving at a magnificent speed and has become a very effective technique for biomarker discovery and verification. Reproducible and comprehensive assessment of the complex human proteome has been achieved; thousands of proteins as well as various types of post-translational modifications can be confidently identified in a single analysis. The development of MS based assays has brought revolution in human proteome research and has led to an exponential increase in the number of candidate biomarkers for specific diseases. Most recently, potential biomarkers for pancreatic cancer[1-5], lung cancer[6-12], prostate cancer[13-15], breast cancer[16-22], brain cancer[23-25] and other high influence cancers have been reported by various groups using different types of MS technologies like matrix assisted laser desorption ionization-mass spectrometry (MALDI-MS), surface

enhanced laser desorption ionization-mass spectrometry (SELDI-MS), liquid chromatography-mass spectrometry (LC-MS) and capillary electrophoresis-mass spectrometry (CE-MS) for protein detection in both intact and digested forms.

Initially, proteomic studies using MS are perofrmed with their primary goal to identify as many proteins as possible. As technology evolves, researchers realized that this so called global proteomics method is not always effective to solve specific biological problems such as specific disease related biomarker discovery and verification. Therefore, scientists have knowingly started to shift the focus from global discovery to targeted proteomics that is more closely related to their specific problems. Initially, the idea of MS based targeted proteomics was limited to the targeted quantification of a predefined set of analytes. It has since evolved into a hypothesis-driven methodology effectivly applied to much broad biological applications. Targeted proteome experiments are in general designed to identify and quantify a set of targeted proteins that show significant abundance change and/or post translational modification under different biological conditions or disease states.

1.2 Targeted proteomics

1.2.1 Targeted proteomics study of homogenous tumor cells

In biomarker discovery, plasma is the most studied sample type because it is easily accessible with minimally invasive, fast and cost-effective clinical collection procedure. Plasma biomarker is also highly desirable for clinical screening test in general population for early detection of potential disease. However, extensive studies on plasma samples have revealed several barriers that pose enormous analytical challenge in identifying

cancer-related biomarker in plasma. Firstly, plasma composition varies significantly among different persons and over the time; Secondly, plasma proteome is extremely complex and heavily influenced by individual organs in the circulation.

Still, the most challenging problem is the identification/quantification of analytes that exist in extremely low concentrations in the complex matrix of plasma which often exceeds the achievable sensitivity of current techniques. These analytes are typically small proteins or fragments that shed or secreted by the tissue at the primary site of cancer into the circulation with significant dilution. This situation is further complicated by endogenous high abundance proteins which constitute 99% of the total protein mass in plasma. The presence of these very high abundance proteins heavily interferes with the ability to detect disease-specific proteins whose concentrations are at least 10 million times less abundant. The dynamic range of protein concentration in human plasma samples can reach up to 12 orders of magnitude. Tissue sample[2,19,26] or proximal fluids[27-33] like cerebrospinal fluid, seminal plasma, and tumor interstitial fluids are better alternatives, in which tumor-derived proteins are present at significantly high local concentration to be detected by conventional mass spectrometers.

Among all the different types of samples studied, tumor tissue from the primary site provides the best chance to identify rare disease-specific biomarkers since less interference and dilution is involved. Moreover, in tumor tissue studies, related-genomic information can be obtained to increase confidence in the discovery and verification of a particular candidate biomarker through corroborating information between genomic and proteomic data[34].

One important factor to be considered for tissue biomarker studies is the heterogeneity of the cells in constituting tumor tissues which includes fibroblasts, nerve cells, endothelial cells, infiltrating lymphocytes and epithelial cells. While the complexity of tumor tissue is greatly reduced comparing with plasma samples, these different groups of cells can still be sources of interfering and misleading information. Laser-capture microdissection (LCM) (Figure 1.1) is a method that permits isolation and procuring of homogeneous cell types from a tissue under microscopic visualization. Cells are sorted based on their histomorphology after a specific staining that enables accurate isolation of malignant, premalignant, and normal cells from a tumor tissue[35].

LCM allows targeted analysis on specific cell populations to obtain disease-specific information. Studies have shown that targeted proteomics facilitated by LCM enables direct comparison of protein profiles between the normal and tumor cell types for a more accurate molecular profile and a valid approach for better understanding of molecular mechanisms[36-38]. For example, Karring and co-workers have applied LCM technology on corneal samples to isolate corneal amyloid deposits and the surrounding corneal stroma for in-depth proteomic proteomic analysis[39].

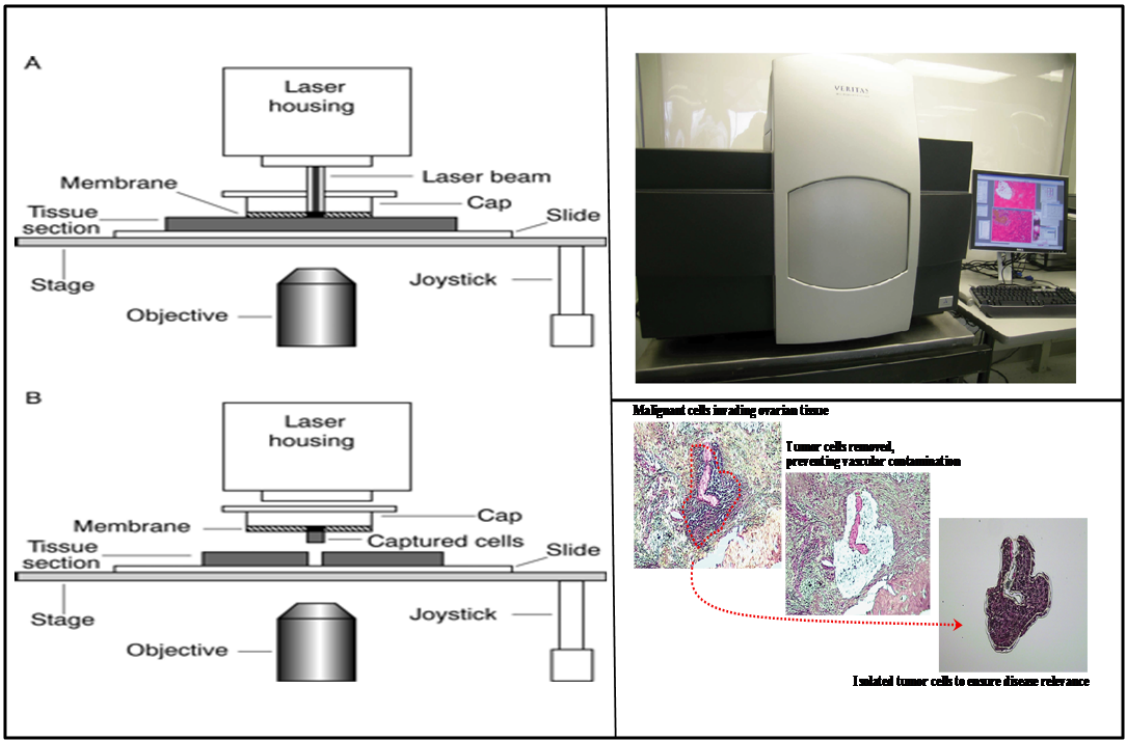

Figure 1.1 Laser capture microdissection (LCM) illustrating cell isolation (left); Real view of LCM instrument (upper right) and tissue sections before and after LCM (bottom right).

In LCM, a cap coated with thermo labil film is used and placed in contact with stained tissue section. The cell selection is performed through microscopic visualization. A focused laser beam is then utilized to generate localized melting of the the film so that the underlying cells become fused to the cap and get selectively removed when the cap is lifted. The stained tissue biopies before LCM and the isolated cells after LCM demonstrated precise and clear cell selection

Sugihara et al. have used LCM to isolate tumor cells from ulcer floor, central area, and invasive front and compare against normal colorectal epithelial cells to examine the intra-tumor heterogeneity in colorectal cancer. They discovered that though the overall proteome is not statistically different among tumors cells from different locations, the proteins that are differently expressed between normal and tumor cells are found to be associated with different functions such as stress response in ulcer floor, glucose metabolism in central area and mitochondria-mediated apoptosis in invasive front, indicating effects of tissue microenvironment on tumor cells. Their results suggest that tissue localization should be taken into consideration in sampling process and well defined targeting is critical in obtaining meaningful and enlightening information.

1.2.2 Targeted quantification through selected reaction monitoring (SRM) MS

Once biomarker candidates are recognized, the next key step is to validate the specificity, sensitivity and reproducibility of the biomarkers in a large cohort of samples. There is very distinct difference between analysis of proteins at the discovery and validation stages. In discovery stage, relative change in protein expression level between samples is measured with low stringency required. In contrast, accurate absolute quantification of potential biomarkers has to be achieved in validation phase in order to differentiate normal and disease samples with a high confidence in clinical application.

Immunoassay, such as enzyme-linked immunosorbent assay (ELISA), has been an effective tool for candidate biomarker quantification with an excellent sensitivity and specificity. However, developing individual ELISA assays for a large number of biomarker candidates is very time consuming and expensive, and thus impractical.

Selective reaction monitoring (SRM)-MS based assay can be used to relieve the bottleneck in the biomarker pipeline presented by immunoassay. The SRM-MS technology has recently been adapted for targeted quantification of candidate biomarkers using stable-isotope labeled peptide surrogates, and has become a gold standard in MS based quantification technologies.

SRM-MS is usually performed using a triple quadrupole mass spectrometers because their short duty cycles. As illustrated in Figure 1.2 below, in SRM-MS analysis, precursor ion with specific m/z is selected in the first quadrupole (Q1), then fragmented in Q2 and the optimum fragment ions/product ions are then monitored using Q3. The pair of selected precursor ion m/z and product ion m/z is termed a 'transition'. Through the combination of isolating precursor peptide ions within a narrow mass window in Q1 and monitoring product ions corresponding to the specific precursor ions in Q3, outstanding sensitivity and specificity is achieved. Typically, 3-5 transitions for each targeted peptide and 3-5 peptides per protein are used in SRM-MS analysis. The absolute abundance for each targeted peptide is calculated based on the comparison against the MS intensity of the isotope labeled counterparts spiked into the sample with known concentration[40].

Addona et al[41] conducted systematic assessment of the transferability and reproducibility of SRM-MS based targeted assay at eight different laboratories using a three-phase study. This three-phase study sequentially introduced additional source of variability from phase I to III in both sample preparation and instrument analyses while the SRM assay development was configured at a single site and kept consistent across all the laboratories. This study demonstrated the excellent inter- and intra-laboratory reproducibility of SRM-MS assay even in a highly complex matrix such as plasma. This

study also helps established some baseline parameters for SRM-MS based assay using isotope labeled internal standards for biomarker verification in complex biological matrix. Overall, this invaluable study provided insightful evaluation of SRM-MS technology, made suggestions on ways to minimize experimental variations and served guidance for future development and application. A recent study by Prakash et al[42] took a step further and analyzed the reproducibility of SRM-MS assay with various upfront enrichment strategies and different types of clinical samples across several laboratories. Again, reproducible results were demonstrated, proving the feasibility of SRM-MS based assay to verify biomarker at low abundance in clinical specimens.

Mustafa et al.[43] discovered and confirmed the down regulation of ApoA1 in hepatitis C virus (HCV) patients as compared to ApoA1 in hepatocellular carcinoma (HCC) patients by 2-dimensional difference gel electrophoresis (DIGE)-MALDI/MS/MS and SRM-MS assay, respectively. Heavy ^{18}O labeled internal standards were used for absolute quantification. Their study demonstrated the confidence of SRM assay for biomarker verification and reported ApoA1 as a candidate biomarker for HCC.

Everley et al.[44] in Dr. Gygi's lab recently presented a work on multiplexed targeted quantitation to improve the throughput of SRM assay in order to apply SRM-MS assay for high-throughput screening, clinical diagnositic and biomarker verification on large cohorts of samples. They utilized isobaric tag for relative and absolute quantitation (iTRAQ) along with two novel 6-plex isobaric tags in combination with three mass variants of the target peptide, achieving a total of up to 54-plex quantitation in a single run.

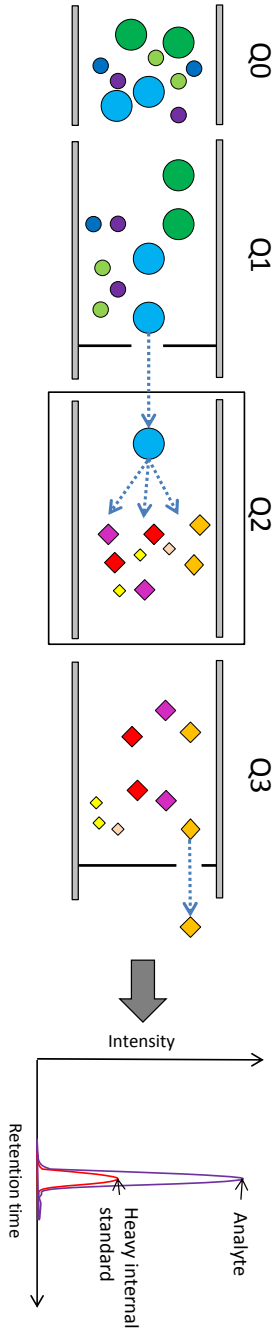

Figure 1.2 Schematic of absolute quantification using SRM-MS in combination with isotope-labeled internal standard

1.3 Capillary electrophoresis in biomarker discovery and recent advances

The inherent disadvantage of biomarker dilution in biofluids such as serum/plasma, urine, and saliva has directed increasing attention at using tissues from the primary site of pathology for the discovery of disease biomarkers. It has been well accepted that molecular profiling in tumor lesion is fundamental to understand the molecular etiology in tumor development. However, in the absence of PCR-like protein amplification, comprehensive analysis of protein expression within small populations of tumor cells microdissected from limited tissue samples represents a significantly technological challenging. Especially the size of human tissue biopsies are getting increasingly smaller as a result of advent of minimally-invasive methods and early detection and treatment of lesions. In addition to sample amount constraints, the greatest bioanlytical challenge facing comprehensive proteomic analysis of microdissected tumor specimens is related to the large variation of protein relative abundances, particularly in the identification of low abundance proteins. For example, the protein concentration dynamics range from 10^6-fold in cells to 10^{12}-fold in blood[45, 46]. A more effective proteomic technology is critically needed to efficiently handle the small sample amount as well as to enable comprehensive and comparative studies of protein profiles that will have diagnostic and therapeutic relevance.

Capillary electrophoresis (CE) has been known for its high separation efficiency, high resolving power and its broad utility in various analyses from small molecules like metabolites to large intact proteins. In addition, CE is intrinsically compatible with small sample amount which makes it an attracting technique in analyzing clinical samples.

Over the years, CE has evolved into an important technology for biological sample analysis in biomarker studies through coupling with MS detection.

1.3.1 Single Dimension Capillary Electrophoretic Separation Coupled With Mass Spectrometry

Capillary zone electrophoresis (CZE) resolves proteins and peptides based on their differences in electrophoretic mobility which is a function of the charge-to-size ratio. Due to its high throughput and excellent resolving power, the coupling of CZE with electrospray ionization-mass spectrometry (ESI-MS) has been employed for the analysis of low molecular weight proteins (below 20 kDa) and peptides for the discovery of biomarkers in human urine. Samples were investigated from patients suffering from a variety of diseases including ureteropelvic junction obstruction[47], cancer[48, 49, 50], vasculitis[51], coronary artery diseases[52, 53, 54], kidney diseases[55, 56, 57], lithium-induced nephropathy[58], graft-versus-host disease[59], and diabetes[54].

The CZE-ESI-MS data were presented by plotting the measured molecular masses against their migration times and compared among healthy and diseased patients. Known and potential new urine biomarkers have been identified using subsequent MS/MS experiments[60, 61.] Although a variety of different proteins/peptides were discovered, most of these putative markers are derived from the most abundant proteins in the body such as collagen - mainly type I, II, and III, albumin, β-2-macroglobulin, and uromodulin[62].

In addition to human urine, single dimension CZE separation was also employed for the proteomic analysis of other body fluids such as human plasma[63] and ventricular cerebrospinal fluid[64]. Potential biomarkers of vascular disease in plasma from patients with chronic kidney disease were discovered by CZE-ESI-MS[63]. In contrast to the use of

ESI-MS or ESI-MS/MS for the detection and identification of protein and peptide markers, off-line matrix-assisted laser desorption/ionization-time of flight/time of flight (MALDI-TOF/TOF) MS coupled with iTRAQ labeling[65] was employed for multiplexed quantification of proteins in human ventricular cerebrospinal fluid samples collected from a patient with traumatic brain injury during patient recovery[64].

1.3.2 Capillary Electrophoretic-Based Multidimensional Separations Coupled With Mass Spectrometry

1.3.2.1 Capillary Isoelectric Focusing (CIEF)

Combined CIEF/nano-reversed phase liquid chromatography (nano-RPLC) separations have been developed and demonstrated to achieve comprehensive and ultrasensitive analysis of minute protein digests extracted from microdissected tissue specimens[66, 67]. In addition to protein identification, the capabilities of the CIEF-based proteomic platform coupled with the spectral counting approach[68, 69] to confidently and reproducibly quantify proteins and changes in protein expression levels among samples were evaluated by the measurements of coefficient of variation (CV) and the Pearson correlation coefficient[70]. Analytical reproducibility of relative protein abundance was determined to exhibit a Pearson R^2 value greater than 0.99 and a CV of 14.1%. The platform was capable of measuring changes in protein expression as low as 1.5 fold with confidence as determined by t-test followed by Benjamini-Hochberg multiple testing adjustments.

The protein expression profiles from two distinct ovarian endometrioid tumor-derived cell lines have been compared using CIEF-based multidimensional separations coupled with ESI-MS/MS [71]. Differentially expressed proteins were further investigated by

ingenuity pathway analysis to reveal their association with important biological functions and signaling pathways such as the P13K/AKT pathway. The results illustrated the utility of high throughput proteomic profiling combined with bioinformatic tools to provide insights into the mechanisms of deregulation in neoplastic cells.

In addition to CIEF, microscale in solution IEF was employed as the first separation dimension for the fractionation of intact proteins, followed by tryptic digestion and subsequent CZE peptide separation coupled off-line to MALDI-TOF/TOF MS[72]. The platform was used for the analysis of human follicular fluid with clinical implication. A total of 73 unique proteins were identified, including mostly acute phase proteins and proteins that are known to be extensively involved in follicular development.

1.3.2.2 Transient capillary Isotachophoresis/Capillary Zone Electrophoresis

In contrast to universally enriching all analytes by a similar degree, the result of the capillary isotachophoresis (CITP) stacking process is that major components may be diluted, but trace compounds are concentrated[73]. CITP employs a discontinuous electrolyte consisting of leading electrolyte such as ammonium acetate which has a mobility greater than any of the sample components and a terminating electrolyte such as acetic acid. The stacking and separation of analytes occurred in the boundary region between the sample and leading or terminating electrolytes under the application of an electric field (Figure 1.3). Under the influence of constant current across the separation capillary generated by applied voltage, the sections containing the high-mobility leading electrolyte would therefore experience lower and higher electric fields, respectively. The analyte ions in the sample zone initially migrating at fast speed induced by high electric field are slowed down and stacked at the interface of the sample and leading electrolyte

sections. Stable boundaries formed between analytes and analytes are aligned according on their relative mobility. The concentration of the analytes after focusing is mainly determined by the concentration of the leading electrolyte. As a result, the CITP stacking process can selectively enrich low abundance analytes according to their original concentration relative to LE concentrationg. Furthermore, CITP offers the benefits of speed and straightforward manipulation/switching between the stacking and separation modes in transient CITP/CZE. Transient CITP/CZE further provides seamless combination with nano-RPLC (Figure 1.3) as two highly resolving and completely orthogonal separation techniques critically needed for analyzing complex proteomes[74, 75]. While CITP has been widely used for analyte pre-concentration prior to electrophoretic separation, the application of CITP to selectively enrich trace amounts of proteins/peptides in complex proteome mixtures represents a completely untapped avenue in proteomic technology development. As illustrated by Fang and co-workers for the analysis of human saliva and mouse brain mitochondrial proteomes[74, 75], the application of CITP to selectively enrich trace amounts of proteins in targeted cells significantly augments the ability to perform ultrasensitive and global proteomic analysis, particularly toward the identification of low abundance proteins.

The ultrahigh resolving power of transient CITP/CZE as the first separation dimension has been demonstrated by significantly low peptide fraction overlapping for the analysis of protein expression within glioblastoma multiforme derived cancer stem cells[76]. Approximately 89% of distinct peptides were identified in only a single CITP fraction. In contrast, a high degree of peptide overlapping in strong cation-exchange (SCX) chromatography, as the first separation dimension of the multidimensional protein

identification technique (MuDPIT)[77], was observed with at least 40% of carry over peptides that were identified in previous salt gradients. A high degree of peptide overlap in SCX unnecessarily burdens the subsequent nano-RPLC separation and greatly reduce the overall peak capacity in a multidimensional separation system. The presence of high abundance peptides in multiple SCX fractions further negatively impacts the selection of low abundance peptides for tandem MS identification.

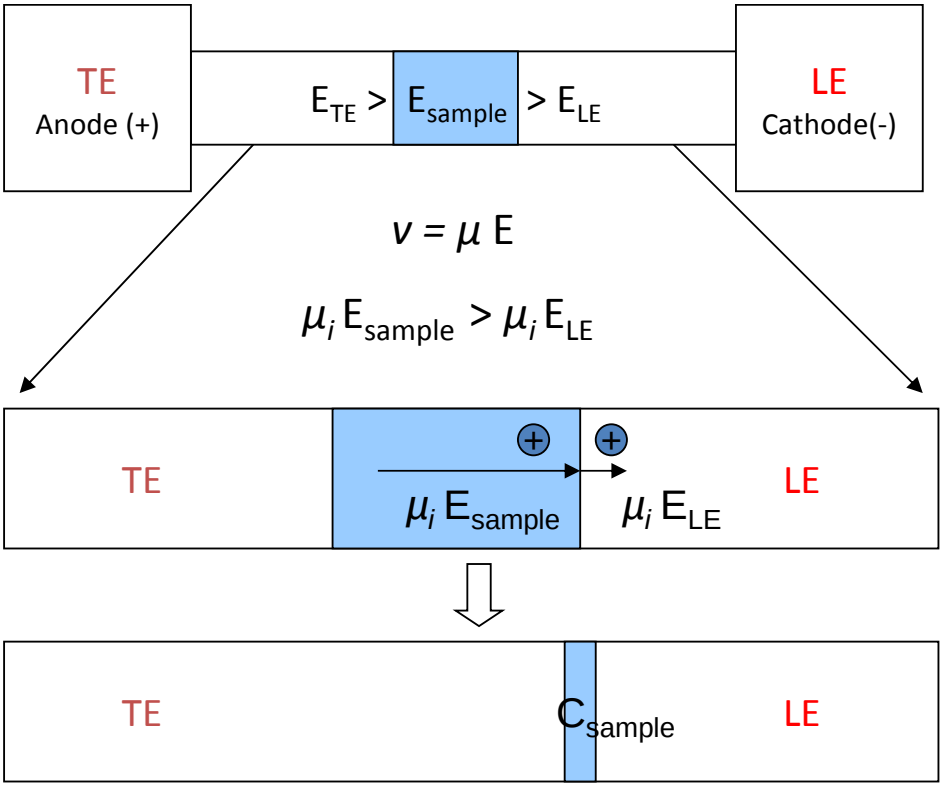

Figure 1.3 Schematic view of the CITP-based electrokinetic stacking mechanism.

C: concentration; E: applied electric field strength; LE: leading electrolyte; TE: terminating electrolyte; μ: mobility; v: velocity.

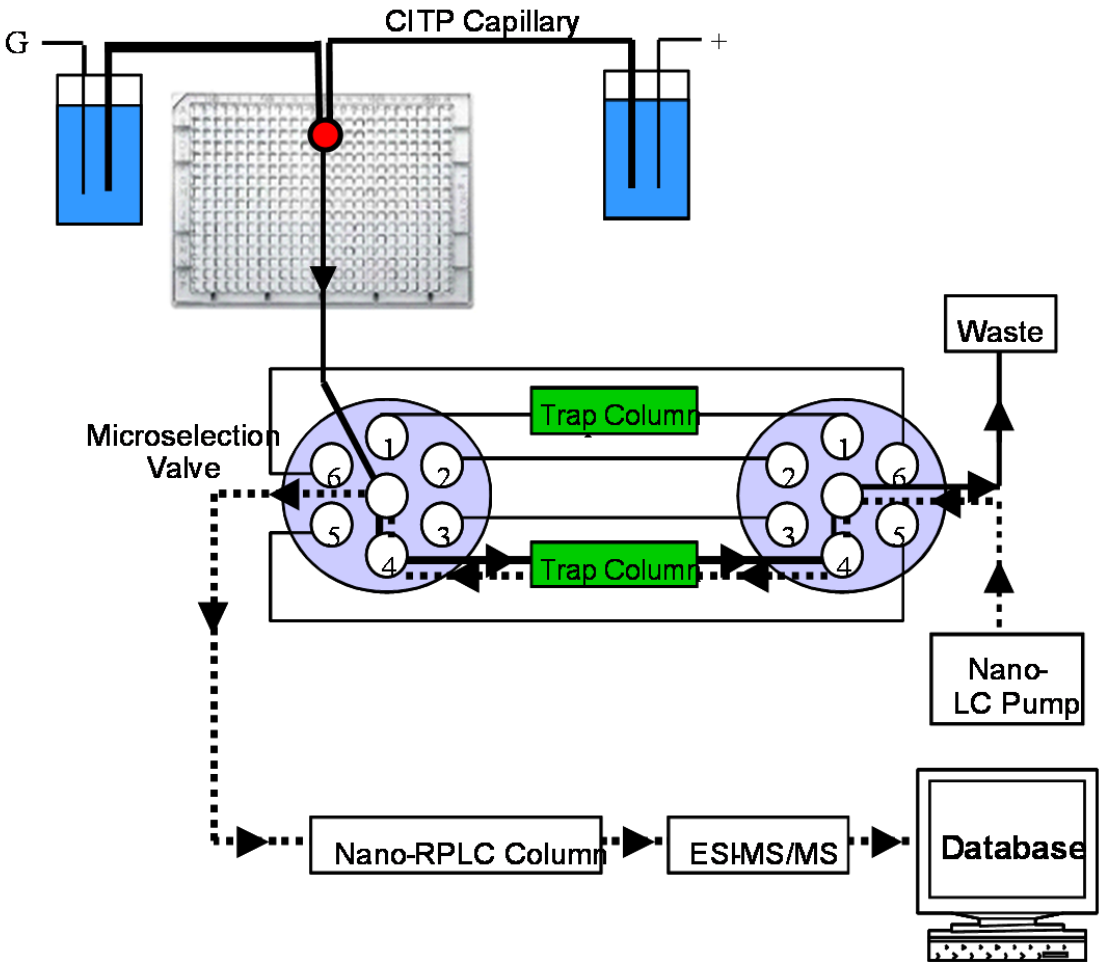

Figure 1.4 Schematic of on-line ntegration of CITP with nano-RPLC for achieving selective analyte enrichment and multidimensional proteome separation.

Solid and dashed lines represent the flow paths for the loading of CITP fractions and the injection of fractions into a nano-RPLC column, respectively.

For the evaluation of overall cancer stem cells proteome performance[76], the CITP proteomic platform demonstrated significant enhancements in total peptide, distinct peptide, and distinct protein identifications over a corresponding MuDPIT run by 119%, 192%, and 79%, respectively. The CITP proteomic technology, equipped with selective analyte enrichment and ultrahigh resolving power, further accomplished superior coverage in key pathways than that of the MuDPIT. For example, many biologically relevant proteins, including MKP, the Raf family, and Src in the ERK/MAPK pathway, were only identified by the CITP technology (Figure 1.4).

Jinawath and co-workers[78] applied the CITP proteomic technology to perform comparative proteomic analysis of paired primary and recurrent post-chemotherapy ovarian high grade serous carcinomas from nine ovarian cancer patients. A total of 30,884 distinct peptides were identified using a 0.1% false discovery rate for total peptide identifications, leading to the identification of 5,063 non-redundant proteins from the SwissProt human database. Of the proteins identified from primary ovarian tumor cells, a number of them, including merlin, ezrin, moesin[79], selenium binding protein 1[80], glutathione-S-transferase, epidermal growth factor receptor, E-cadherin, α- and β-catenins[81], β-tubulin, ubiquitin carboxyl-terminal hydrolase, glyoxalase 1, F-actin α subunit, and cofilin[82], have been reported to be present in ovarian epithelial cells.

Furthermore, the increase in ovarian cancer proteome coverage, attributed to CITP-based selective analyte enrichment, allowed the application of protein network and pathway analysis toward the discovery of ovarian carcinoma biomarkers. For example, low abundance proteins such as cytokine IL-6 and signal transducer and activator of transcription 3 (STAT3), as well as many other proteins known to participate in the IL-6 signaling pathway, have been identified and compared for their expression levels within primary and recurrent ovarian tumors (Fig. 1.6). Both STAT3 and IL-6 were found to be

over-expressed in the recurrent tumor cells. As supported by recent in vitro studies of ovarian[83] and non-small cell lung[84] cancer cell lines, the STAT3 pathway plays a significant role in the development of high-grade ovarian cancer and the drug-resistant ovarian cancer. STAT3 can be activated by various protein tyrosine kinases including epidermal growth factor receptor, interleukin, and IFN ligands. Inhibition of the STAT3 pathway has been shown to enhance paclitaxel-induced apoptosis. In addition, IL-6 expression was found to be associated with the generation of drug resistance. The comparative proteomic results have further identified RELA which is the p65 subunit of the NF-κB complex (Figure 1.6). p65 was over-expressed more than 3 folds in recurrent tumors as compared to the primary tumors. The NF-κB/RELA family of transcription factors is one of the most important and well-characterized signaling pathways in both normal and pathological conditions. It controls a variety of cellular functions including inflammatory and immune responses, cell growth and survival, and drug resistance to several chemotherapeutic agents[85].

1.4 CE-MS interface development

CE has been proven to be a highly efficient separation technique and is considered a powerful technique for the analysis of biological samples. In addition, it's relatively inexpensive and it is ideal in handling small amount of sample and reagent. As a result, online coupling of CE with MS provides an intriguing and attractive solution to combine high-resolution separation with high-sensitivity/selectivity detection.

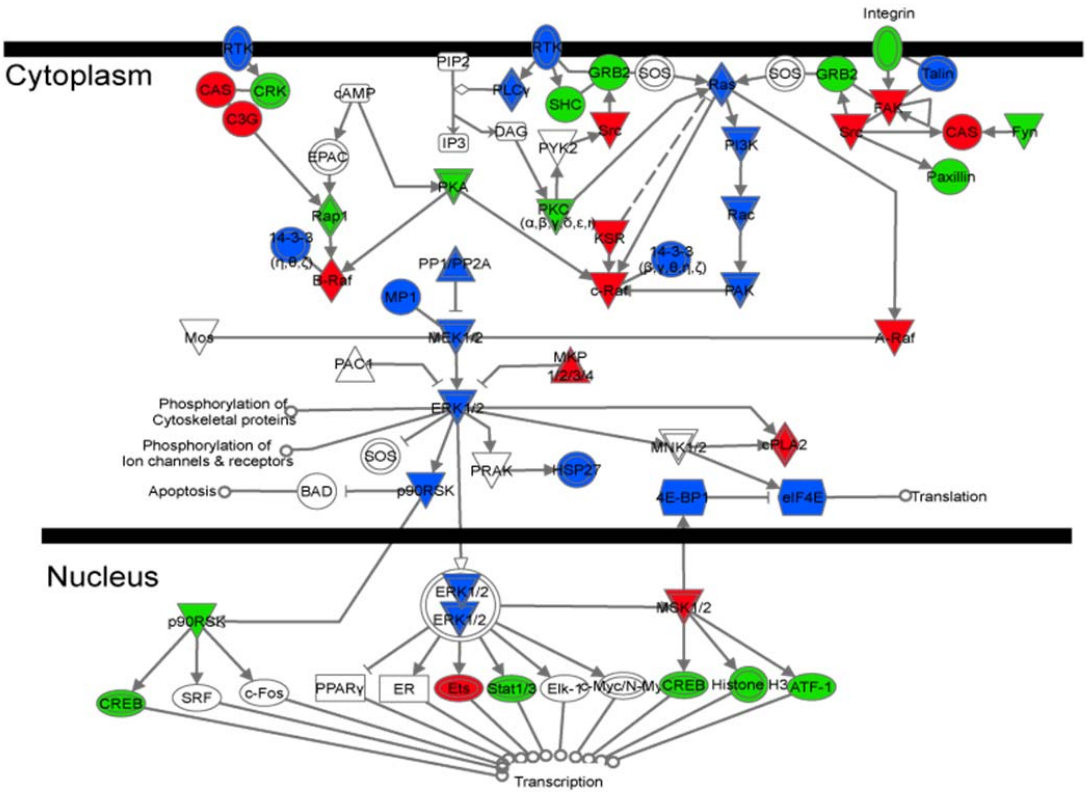

Figure 1.5 Comparison of the coverage in the ERK/MAPK pathway achieved by the MuDPIT and CITP proteomic platform. [1]

Red: proteins only identified by CITP; blue: proteins identified by CITP with higher confidence (larger numbers of spectral counts and distinct peptide identifications per protein) than that achieved by MuDPIT; green: proteins identified by both CITP and MuDPIT with approximately equal confidence

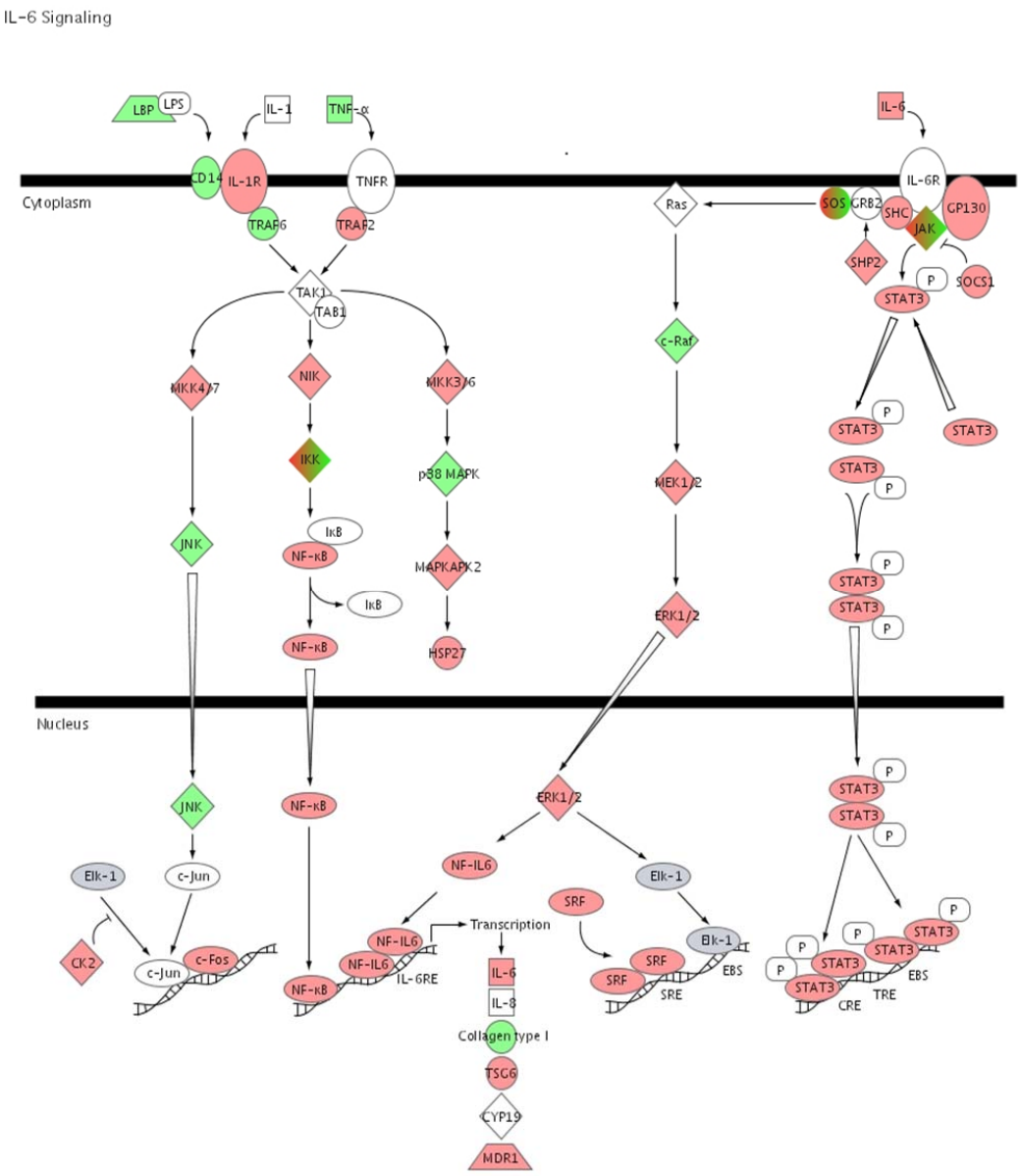

Figure 1.6 differentially expressed proteins among primary and recurrent ovarian tumors in the IL-6 signaling canonical pathway using the Ingenuity System™. [79]

The coupling of CE to MS is not straightforward because of the requirement of a closed electric circuit that provides different electric fields for capillary electrophoresis separation and electrospray ionization (ESI). After the first online CE-ESI-MS introduced in 1987 using sheathless design via metalized ESI emitter tip[86], a variety of designs of both sheathless and sheath liquid interfaces have been proposed to maximize the coupling efficiency of CE-MS. By far, sheath liquid interfaces employing a sheath-flow or make-up liquid is more commonly used than sheathless interfaces, especially in commercial applications, due to a variety of reasons including issues of stability, longevity and ease of use. There lies a great compromise between interfaces with optimal performances and those practical for commercial platforms. Those interfaces offering the lowest detection limit have been among the most fragile thus impractical for commercial use. As this hyphenated technique continuously gains popularity as a promising alternative to LC-MS for proteomic, metabolomics and pharmaceutical studies, active efforts have been devoted to reliably and optimally couple CE separation with MS.

1.4.1 Sheathliquid Interfaces

Sheathliquid interfaces can be achieved through the use of additional flow or liquid that mixes with the CE effluent to establish electrical contact between an electrode and the background electrolyte to accomplish CE separation as well as stable electrospray operation. Coaxial sheath-liquid is the most common interface of this type which was first introduced by Smith et al in 1988[87] (Figure 1.7) which is configured by a continuous flow being delivered through a tube of larger diameter in a coaxial setting and merging with the CE effluent at the capillary outlet. Another function of the sheath flow is to modify the composition of the CE electrolyte to optimize the ESI process, so the sheath-

liquid is usually composed of a mixture of water and organic modifier containing volatile acid. A gas flow is applied through a third coaxial capillary to neumatically assist electrospray process as well as facilitate the charged droplet desolvation. A rather firm electric contact is achieved using this co-axial sheath flow design making it a reliable CE-MS interface. This type of interface is commonly adapted by most commercial CE instruments. However, this interface usually requires rather high operating flow rate of the sheath-liquid ranging from 1 to 10 μL/min while CE separation is operated at 100 nL/min. Thus, the sheath-liquid are usually several times or even one order of magnitude higher than the intrinsic CE flow which causes significant analyte dilution as well as greatly compromised ionization efficiency, limiting the achievable detection sensitivity of the CE-MS platform. Additionally, the sheath flow is reported to influence the peak efficiency by introducing a parabolic flow and reduces the achievable peak efficiency[88,89]. Overall, the sheath-flow interface is considered a robust system and the availability of commercial sprayers enables it to become the most commonly used interface.

Alternative to using a straight tube to deliver sheath liquid, sheath-flow interfaces can also be achieved using a tapered tube with the CE capillary sitting slightly back from the tip. The advantage of this design is that the mixing of the CE effluent and sheath liquid is more sufficient which leads to improved electric contact and ESI stability. Also sheath liquid is able to operate at lower flow rate because of the smaller tip aperture from the tapered emitter.

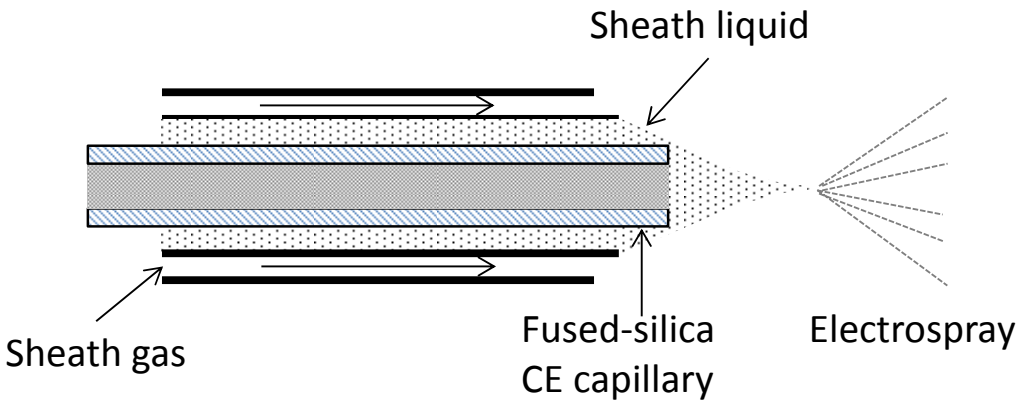

Figure 1.7 Schematic of a sheath-flow interface for CE-MS through coaxial sheath-flow with sheath gas

Electric contact is achieved through the mixing of sheath liquid with CE eluent to drive both CE separation and electrospray ionization processes. Additional sheath gas is used to help the formation of talor cone to promote the ionization process.

Recently, Dovichi's[90] group published a nanospray sheath-flow interface design using tapered sheath flow tube for electric contact and electrokinetic flow to drive both the separation and the electrospray[91]. In this design, the separation capillary is placed inside a tapered glass emitter and ESI voltage is applied in the sheath liquid reservoir. They performed large scale E. coli proteome analysis using this sheath flow CZE-ESI-MS platform after simple fractionation using solid-phase extraction (SPE) column. With less than 1 μg sample loading, they were able to identify 4902 peptides and 871 protein groups, which was even better than other three published work with more than 4 times the sample loading analyzed using RPLC based separation platforms[92-94]. This work also reported the largest proteome dataset using CE-MS/MS to date, demonstrating CZE-ESI-MS/MS as a useful tool for proteomic analysis.

The design from Dovichi's group can also be categorized as liquid-junction interface which is another approach to couple CE and MS. The liquid-junction interface was first reported by Henion and co-workers[95] where a small gap was used to separate CE capillary and ESI emitter to allow mixing between the CE eluent and sheath-liquid before entering the ESI emitter to complete the electric circuit. One advantage and distinguishable feature of liquid-junction designs from sheath-flow interfaces is the flow rates of the sheath-liquid are typically in the range of 60-200 nl/min, which significantly reduces the dilution factor while retaining the solution-modifying benefits.

Up till now, the liquid junction interfacing has not been widely applied in proteomic studies. However, the results obtained so far are promising and intriguing for further development and applications.

1.4.2 Sheathless interfaces

Sheathless interfacing is no doubt the most straightforward and ideal way for coupling CE with MS as no dilution is involved and the intrinsically low-flow rate operation of CE can be optimally reserved. Since nanoESI improves ionization efficiency[96,97] and is friendlier towards hydrophilic compounds[98] and aqueous solution[96], the employment of sheathless CE-MS usually provides better flexibility in separation buffers as well as more sensitive and comprehensive detection. Various sheathless designs have been proposed in attempts to achieve robust and stable nanoESI operation.[99] To name a few, ideas like tapered emitter coated with metal,[73,100] electrically conductive polymer[101] or carbon,[102] or insertion of metal wire in the CE capillary[103] as well as connecting the separation capillary with stainless tubing[104] have all been proposed. While most of these interfaces have been proven to provide very high performances, there has been major bottlenecks in concern of dead volume dilution, electrolysis interference, manufacturing complexity, low mechanical duration, poor reproducibility, flow disturbance and costly.

Sheathless interface via a porous tip reported by Moini seems to provide a better alternative[105]. The porous emitter approach is very straightforward and does not require any fluidic connection or material deposition. The fabrication of porous emitter is achieved through chemically etching a 3 cm portion from one end of the capillary using hydrofluoric acid to reduce the wall thickness to 5-10 μm. The thin wall at the emitter permits exchange of small ions through the size selective porous interface while minimizing the analytes leakage. Part of the porous portion is inserted in a stainless tube containing conductive buffer on which electric contact are being made. The relative simplicity in this approach provides significant advantage as compared to previous

sheathless interfaces. As a result, commercial instrument using this interface is being developed by Beckman Coulter and various applications with outstanding performance have been reported[106-112]. Significant improvement of urinary metabolome coverage over classical sheath-liquid interface was presented using this sheathless interface[110] by Ramautar et al.

The suitability of this sheathless interfacing was also evaluated by the group of Lindner where it was compared with nano-RPLC-ESI-MS by analyzing rat testis linker histones digests[113]. They observe a 60% increase in the number of identified peptides with sheathless CE-ESI-MS at comparable amounts of sample loading. They also observed more identifications in low-molecular weight peptides (usually lower than 1400 Da) by CE-ESI-MS as this group of peptides usually interacts poorly with the reverse-phase material in LC system.

With the proven performance on peptides and intact proteins using this porous sprayer[107,109], Bonvin et al. further evaluated the performance stability of this porous sprayer in terms of sensitivity and in analyzing low molecular weight pharmaceutical compounds. They carefully studied the operating parameters such as interface positioning and fragmentor voltage and source parameters. Methamphetamine, methadone and acebutolol were used as model compounds in this study and high sensitivity with LOD at 5 ng/ml using a single quadrupole MS was demonstrated.

1.5 Project description

In order to obtain biomarkers to predict disease behavior and therapeutic response in combat with cancer, analyzing techniques and platforms that can overcome the great complexity of human proteome and the heterogeneity among different cell types with

high efficiency and sensitivity are necessary. Targeted proteomic studies enabled through microdissection for homogeneous cell population and targeted quantification through SRM MS greatly reduces the sample complexity and improves specificity and sensitivity. CITP/CZE's unique feature of selective enrichment of low abundant analytes works ideally to solve the large dynamic range problem for protein abundance in biological samples which is one of the greatest challenges in proteomic analysis. Synergetic effort of CITP/CZE and targeted proteomic will be able to provide a better methodology for biomarker studies in terms of sensitivity, specificity and reproducibility.

In order to demonstrate the capability of CITP/CZE based targeted proteomics, chapter 2 described a multidimensional CITP/CZE-nano-RPLC separation platform coupled with MS in analyzing homogeneous tumor cell population obtained via LCM from a set of human astrocytoma tissues in search of glioblastoma biomarkers. Proteins extracted from homogeneous tumor cells from different grades of astrocytoma were fractionated and concentrated in CITP/CZE separation in the first dimension and then sequentially loaded onto nano-RPLC for additional separation and detected using tandem MS. Comparative proteomics among different grades relative to glioblastoma (GBM) was performed and the proteins up-regulated in GBM were further analyzed using statistic and biology tools in order to derive biological significant and confident information for potential glioblastoma specific biomarkers. The ultrahigh resolving power of CTIP/CZE was evidenced by the large number of distinct peptide identifications measured from each CITP fraction together with the low peptide fraction overlapping among identified peptides. Over 3000 proteins were identified while only 177, 120 and 594 proteins were uniquely found in grade II, grade III and IV astrocytomas samples respectively,

demonstrating high confidence and outstanding reproducibility of proteomic measurement performed using CITP. Meanwhile, 650 membrane proteins which count for 19% of the total identification represents the most extensive tissue proteomics identified so far in human Astrocytoma, also proved the advantage of CITP based technology in targeted tissue proteomics. Through the employment of this platform, over 30 candidate biomarkers of glioblastoma that are highly associated with cancer function were discovered. A rigid validation process through immunohistochemistry (IHC) on tissue microarray (TMA) was also performed in this study and displayed consistent results.

Starting from chapter 3, a series of effort was devoted into exploring ultrasensitive and high throughput targeted quantification platform for biomarker validation. Validation phase has been a main bottleneck in the pipeline of biomarker discovery as much more rigid criteria and larger sample cohorts are required before a valid biomarker can be established and applied into clinical use. Conventional immunology methodology is efficient, sensitive and low cost under the premise that the antibody against target biomarker candidate already exists. However, in most cases this premise does not stand and the development of immunoassay for the relatively large scale of biomarker candidates is very time-consuming and costly. LC-MS systems are widely used in proteomic studies, but its low throughput is proved to be problematic in biomarker validation. In chapter 3, we explored the targeted quantitation platform through online CITP/CZE-ESI-SRM MS via liquid junction interface. This work represnts the first effort to couple CITP/CZE online with SRM MS to the best of our knowledge. Through the combination of large sample loading capacity, analyte enrichment capability of

CITP/CZE and the improved sensitivity and selectivity provided by SRM-MS, the platform presents outstanding sensitivity and accuracy with a demonstrated LOQ at 50 pM along with excellent signal to noise ratio (S/N). Systematic optimization and evaluation of this platform in terms of sample loading, focusing effect and reproducibility. were performed. The results demonstrated that this online CITP/CZE-ESI-SRM MS is a potential powerful tool for targeted quantification in serve of biomarker validation.

Chapter 4 describes an improved online CITP/CZE-ESI-SRM MS platform by using a novel sheathless interface which preserves large sample loading capacity while allows low nano-ESI operation. We developed a CE setup consisting of large bore separation capillary and a porous small size emitter in order to optimally exert the capability of CITP/CZE while eliminating the dilution caused by sheathliquid. We evaluated the advantage of this novel interface in terms of increased sample loading. Up to 2.5 μL of sample loading capacity was demonstrated with the new CITP/CZE setup while sample amount in low nano liter range could only be used in CZE separation. Commercial sheathless interface, in order to perform stable ESI, is restricted to small size capillary which results in an over 10 times signal intensity loss comparing to our interface. Systematic evaluation of resolving power, flow rate and sensitivity was performed which demonstrated a stable ESI operation at flow rate as low as 30 μl/min and a LOQ at 10 pM while good coefficient of variation (CV<20%) was obtained.

Chapter 2 : Targeted Tissue Proteomic Analysis of Human Astrocytomas

This work was initially started by Dr. Xueping Fang and was completed as a collaborative work by Dr. Fang, me and all the contributing authors between multiple research organizations. My work in this project includes tryptic digest sample preparation, 2D CITP/CZE-nanoRPLC-ESI-MS/MS analyzing platform configuration/optimzation/operation, sample analysis, data collection and interpretation as well as data presentation for publication.

2.1 Introduction

Gliomas are the most common primary tumors of the brain, with an incidence of about 30,000 new cases per year in the United States[114,115]. Most gliomas (> 80%) appear to arise from astrocytes, the most abundant type of glial cells, and are known as astrocytomas. Astrocytomas are divided into four grades by the World Health Organization (WHO). Grade I tumors are histologically benign and may be cured by surgical resection; most are found in children.

The tumors seen in adults are infiltrative and are generally grade II-IV gliomas. Grade II tumors exhibit mild cellular proliferation, have moderate cellular pleomorphism, and infiltrate the surrounding brain which makes curative resection difficult. Grade III tumors are hypercellular, have a higher degree of proliferation, and are malignant and lead to

death in two to five years. Grade IV tumors, the glioblastoma (GBM), are exceptionally-aggressive malignancies with increased mitotic activity, pronounced angiogenesis (microvascular proliferation), necrosis, and proliferative rates 3-5 times higher than grade III tumors[114-116]. Patients with GBM have a median survival of 12-15 months with aggressive therapy; fewer than 5% will survive more than five years[114,117].

The majority of human gliomas have a set of genetic alterations that cause the loss of protein regulation[118]. Studies based on DNA microarray analyses have indicated that GBMs overexpress various gene families related to cell adhesion, motility, invasion, and angiogenesis[119]. Approximately 50% of all GBMs are primary in origin while the other half arises secondarily from lower grade tumors. Current models of gliomagenesis coincide with the two clinically-recognized forms of GBM, *de novo* or primary and secondary or progression. In primary GBMs, *EGFR* gene amplifications, often combined with gene rearrangements that lead to a constitutively active, truncated receptor, occur in GBMs that generally express wild type *p53*[114,117,120,121]. In secondary GBMs, progression from a low grade to a high grade glioma involves the serial accumulation of genetic alterations that inactivate tumor suppressor genes such as *p53, p16, Rb, PTEN*, or activate oncogenes such as *MDM2, CDKs 4* and *6*[114,117].

While proteomic measurements provide a wealth of information complementary to the transcriptomic data, the inherent disadvantage of biomarker dilution in complex biological fluids such as cerebrospinal fluids[122,123] and serum/plasma[124] of GBM patients necessitates highly sensitive analytical approaches, often exceeding the dynamic range of currently available proteomic platforms. Thus, investigative studies directed at tissues obtained from the primary site of pathology currently afford the best opportunity for the

discovery of disease biomarkers[125-127]. For example, Melchior and co-workers[128] employed the shotgun-based multidimensional protein identification technique (MuDPIT)[77] and a semi-top-down approach involving combined intact protein/peptide separations in proteomic studies of whole GBM tissues.

Still, biologically relevant proteomic data can only be generated if the tissue samples investigated consist of homogeneous cell populations, in which no unwanted cells of different types and/or development stages obscure the results. For example, SM22, a dominant protein in smooth muscle cells, has been widely reported to be abnormally expressed in many solid tumors. However, Li and co-workers found that the highly expressed SM22 was mainly found in smooth muscle layers, blood vessels, and myofibroblasts instead of gastric cancer cells[129]. While limited two-dimensional polyacrylamide gel electrophoresis analyses of microdissected GBM tissues have been attempted[130-133], these studies required significant manual effort and time to extract sufficient levels of protein for analysis, while providing little information on protein expression beyond a relatively small number of high abundance proteins.

Besides sample amount constraints from microdissection-procured tissues[134], the large variation of protein relative abundances having potential biological significance in mammalian systems presents a major analytical challenge for achieving comprehensive proteomic studies of clinical specimens. In contrast to universally enriching all analytes by a similar degree, the result of the capillary isotachophoresis (CITP) stacking process is that major components may be diluted, but trace compounds are concentrated[135-137]. Such selective enhancement toward low abundance proteins drastically reduces the range of relative protein abundances and greatly enhances the proteome coverage for the analysis

of human saliva and mouse brain mitochondrial proteomes[74,75]. In this work, we used CITP proteomic technology coupled with the label-free spectral counting approach[68,69,138] to compare protein expression profiles within microdissected astrocytoma tissues, including WHO grade II, III, and IV astrocytomas.

2.2 Experimental Section

2.2.1 Materials and Reagents

Fused-silica capillaries (50 μm i.d./365 μm o.d. and 100 μm i.d./365 μm o.d.) were acquired from Polymicro Technologies (Phoenix, AZ). Acetic acid, dithiothreitol (DTT), and iodoacetamide (IAM) were obtained from Sigma (St. Louis, MO). Acetonitrile, ammonium acetate, hydroxypropyl cellulose (average MW 100,000), tris(hydroxymethyl)aminomethane (Tris), and urea were purchased from Fisher Scientific (Pittsburgh, PA). Pharmalyte 3-10 was acquired from Amersham Pharmacia Biotech (Uppsala, Sweden). Sequencing grade trypsin was obtained from Promega (Madison, WI). All solutions were prepared using water purified by a Neu-Ion system (Baltimore, MD) equipped with a UV sterilizing lamp and a 0.05 μm membrane final filter.

2.2.2 Tissue Microdissection and Proteomic Sample Preparation

A set of fresh frozen brain biopsies, including grade II astrocytoma (n = 4), grade III anaplastic astrocytoma (n = 3), and grade IV GBM (n = 5), were obtained under an Institutional Review Board-approved protocol at the Cleveland Clinic Foundation. By following the procedures described in our previous studies[139,140], these tissue sections (1 cm x 1 cm x 10 μm) were microdissected using the Arcturus Laser Capture

Microdissection (LCM) System of Applied Biosystems (Foster City, CA) to gather approximately 100,000 tumor cells from each clinical specimen (Figure 2.1).

The microdissected cells obtained from each specimen were individually processed and placed directly into a microcentrifuge tube containing 8 M urea and 20 mM Tris-HCl at pH 8.0. The soluble proteins were collected in the supernatant by centrifugation at 20,000 g for 30 min. Proteins in the supernatant were reduced and alkylated by sequentially adding DTT and IAM with final concentrations of 10 mg/mL and 20 mg/mL, respectively. The solution was incubated at 37 ^{0}C for 1 hr in the dark and then diluted 8-fold with 100 mM ammonium acetate at pH 8.0. Trypsin was added at a 1:40 (w/w) enzyme to substrate ratio and the solution was incubated at 37 ^{0}C overnight. Tryptic digests were desalted using a Peptide MacroTrap column (Michrom Bioresources, Auburn, CA), lyophilized to dryness using a SpeedVac (Thermo, San Jose, CA), and then stored at -80 ^{0}C.

2.2.3 CITP-Based Tissue Proteomic Analysis

A total of 12 proteomic samples, containing proteolytic digests processed from 4 grade II, 3 grade III, and 5 grade IV astrocytoma tissue specimens, were prepared using a 2% pharmalyte solution with a final total protein concentration of approximately 1 μg/μL. Each proteomic sample was analyzed in duplicate. Similar to the procedures described in our previous studies[74-76], a 80-cm long CITP capillary (100 μm i.d./365 μm o.d.) coated with hydroxypropyl cellulose was initially filled with a background electrophoresis buffer of 0.1 M acetic acid at pH 2.8. A 50-cm long sample plug, corresponding to a 4.0 μL

sample volume or 4 μg total protein loading, was hydrodynamically injected into the capillary.

A positive electric voltage of 24 kV was applied to the inlet reservoir, which was filled with a 0.1 M acetic acid solution. The cathodic end of the capillary was housed inside a stainless steel tube (460 μm i.d./785 μm o.d.) using a coaxial liquid sheath flow configuration[141]. A sheath liquid composed of 0.1 M acetic acid was delivered at a flow rate of 1 μL/min using a Harvard Apparatus 22 syringe pump (South Natick, MA). The stacked and resolved peptides in the CITP capillary were sequentially fractionated and loaded into individual wells on a moving microtiter plate. The entire capillary content was separated and sampled into 18 individual fractions in less than 2 hr. The CITP separation and fractionation apparatus was operated on an in-house built robotic platform controlled by LabView (National Instruments, Austin, TX).

To perform combined CITP/nano-reversed phase liquid chromatography (nano-RPLC) separations, peptides collected in individual wells were sequentially injected into dual trap columns (3 cm x 100 μm i.d. x 365 μm o.d.) packed with 5 μm porous C_{18} particles. Each peptide fraction was subsequently analyzed by nano-RPLC equipped with an Ultimate dual-quaternary pump (Dionex, Sunnyvale, CA) and a dual nano-flow splitter connected to two pulled-tip fused-silica capillaries (50 μm i.d. x 365 μm o.d.). These two 15-cm long capillaries were packed with 3.5-μm Zorbax Stable Bond (Agilent, Palo Alto, CA) C_{18} particles.

Nano-RPLC separations were performed in parallel in which a dual-quaternary pump delivered two identical 2-hr organic solvent gradients with an offset of 1 hr. Peptides were eluted at a flow rate of 200 nL/min using a 5-45% linear acetonitrile gradient over

100 min with the remaining 20 min for column regeneration and equilibration. The peptide eluants were monitored using a linear ion-trap mass spectrometer (LTQ, Thermo, San Jose, CA) equipped with an electrospray ionization interface and operated in a data dependent mode. Full scans were collected from 400 - 1400 *m/z* and 5 data dependent MS/MS scans were collected with dynamic exclusion set to 30 sec.

Figure 2.1 Demonstration of selective tissue microdissection of a relatively pure population of tumor cells.

Left, a hypercellular focus of GBM cells, abutting the acellular space to the left of the slide, surrounded on the right by white matter (brain) infiltrated by tumor cells, but at a substantially lower cellular density; middle, the tumor cells selectively removed by LCM; and, right, the tumor cells isolated on the LCM cap.

2.2.4 MS Data Analysis

Raw LTQ data were converted to peak list files by msn_extract.exe (Thermo). Open Mass Spectrometry Search Algorithm (OMSSA)[142] developed at the National Center for Biotechnology Information was used to search the peak list files against the SwissProt sequence library with decoyed sequences appended. This decoyed database was constructed by reversing all sequences and appending them to the end of the sequence library. Searches were performed using the following parameters: fully tryptic, 1.5 Da precursor ion mass tolerance, 0.4 Da fragment ion mass tolerance, 1 missed cleavage, alkylated Cys as a fixed modification and variable modification of Met oxidation. Searches were run in parallel on a 14 node, 28 CPU Linux cluster (Linux Networx, Bluffdale, UT).

False discovery rates (FDRs) were determined using a target-decoy search strategy introduced by Elias and co-workers[143] and employed in our previous study for a comparative evaluation among commonly used tandem MS identification search algorithms[144]. An E-value threshold corresponding to a 1% FDR in total protein identifications was used as a cutoff in this analysis as this correlates with the maximum sensitivity versus specificity in our previous work[144]. Furthermore, proteins were reported as being identified by at least two distinct peptides among which contain at least one unique peptide. For a protein family with shared redundancy peptides sequences, only one member of a protein family was reported which has the best scoring in the search results. After generation of search data, the OMSSA XML result files were parsed using a Java parser and loaded into an Oracle 10g database for analysis and reporting using in-house software

2.2.5 Protein Validation Using Immunohistochemistry (IHC)

One of highly confident and differentially expressed proteins among astrocytomas, IQGAP1, was chosen from MS-based proteomic measurements for validation using IHC. IHC was performed on tissue microarray (TMA) sections by removing three 1.5 mm diameter cores (> 90% tumor cells) of tissue from each block at the laboratory of US Biomax (Rockville, MD). Negative and positive controls were conducted using the normal cerebral tissue and the skin tissue of malignant melanoma, respectively.

The mouse primary antibody against IQGAP1 was purchased from Santa Cruz Biotechnology (Santa Cruz, CA) and incubated with a dilution ratio of 1:150 at 4 ^{0}C overnight. The biotinylated anti-mouse immunoglobulin was employed as the link antibody and was incubated for 30 min. The avidin-biotin-peroxidase complex (Vector Laboratories, Burlingame, CA) was utilized as the labeling reagent and incubated for 30 min. A 10-min wash step with Tris buffered saline was carried out between each step. TMAs were counterstained by hematoxylin and mounted for examination by microscope.

2.3 Results and Discussion

Besides selective analyte enrichment, CITP further provides high resolving power to analyze complex proteomic mixtures. As demonstrated in our previous studies of human saliva and mouse brain mitochondrial proteomes[74,75], approximately 85-90% of distinct peptides are identified in only a single CITP fraction. For the investigation of microdissected astrocytoma tissues, about 80-85% of distinct peptides were identified in each of 18 CITP fractions. In contrast, a high degree of peptide overlapping in strong cation-exchange chromatography, as the first separation dimension of MuDPIT[77], is

generally observed with at least 40% of carryover of peptides that are identified in previous salt gradient fractions. The combination of selective analyte enrichment with excellent resolving power contributed to superior astrocytoma proteomic results with regard to the analytical reproducibility, the confidence in protein identification, and the overall tissue proteome coverage.

2.3.1 Overall Performance of Human Astrocytoma Proteomes

The overall tissue proteomic results are summarized in Table 2-1 with the complete protein lists provided in the Supporting Information. The number of proteins which are predicted to contain at least one or more transmembrane domains using TMHMM[145] is also included in Table 2-1 and accounts for approximately 19% of total protein identifications. To the best of our knowledge, these data sets represent the most extensive tissue proteomics confidently identified so far in human astrocytomas. The coupling of tissue microdissection for tumor cell enrichment with CITP-based selective analyte concentration serves as a synergistic strategy to greatly increase tissue proteome coverage, including the characterization of low abundance proteins.

Identification reproducibility was evaluated and was determined to be around 83-88% in identified proteins among technical duplicates of the same tissue specimen. Furthermore, the average number of distinct peptides leading to each protein identification was around 6.8 and illustrated the broad sequence coverage of protein identification. The enhanced analytical reproducibility, together with the confidence of protein identification, ensures high impact inferences to be drawn from the proteomic investigations of archival astrocytoma tissues.

Table 2-1 Number of Distinct Proteins Identified from Duplicated Runs for Each Microdissected Astrocytoma Tissue Specimen

Specimen Number	Grade II	Grade III	Grade IV
1	2,014 (403)*	2,196 (396)	2,663 (511)
2	2,007 (454)	2,314 (415)	2,566 (440)
3	2,483 (467)	2,346 (455)	2,327 (417)
4	2,395 (478)		2,540 (495)
5			2,207 (413)

* Number of identified membrane proteins is included in parentheses.

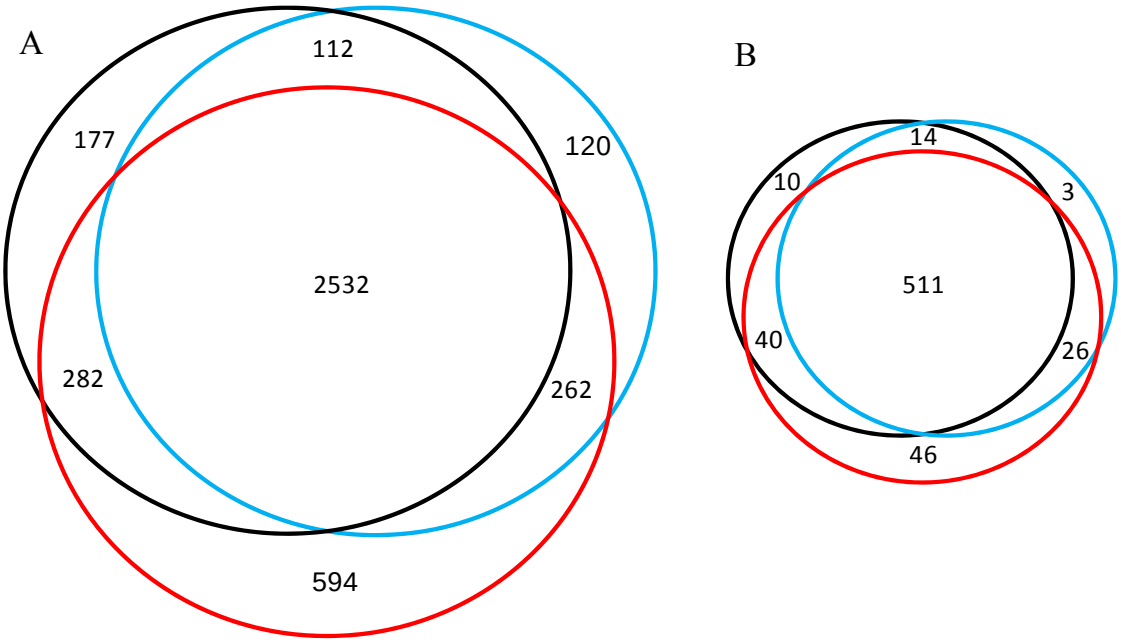

Figure 2.2 The Venn diagrams comparing (A) total proteins and (B) membrane proteins identified from grade II astrocytoma (black), grade III anaplastic astrocytoma (blue), and grade IV GBM (red).

2.3.2 Comparisons among Different Grades of Astrocytomas

GBMs (grade IV) are aggressive malignancies with an increased mitotic activity, pronounced angiogenesis (microvascular proliferation), necrosis, and more rapid proliferative rates than grade III tumors[114-116]. GBMs, in general, exhibited the largest number of identified proteins than those of grades II and III (Table 2-1). Besides the identification of many common proteins among different grades of astrocytomas (Figure 2.12 A), only 177, 120, and 594 proteins were detected uniquely in grades II, III, and IV, respectively. Of the 650 membrane proteins identified, only 10, 3, and 46 membrane proteins were detected uniquely in grades II, III, and IV, respectively (Figure 2.2 B). Such high degree of overlapping in protein identification further supports the high confidence and the enhanced reproducibility of proteomic measurements performed with CITP.

In addition to protein identification, monitoring quantitative changes in identified peptides, and by inference, proteins, is essential for the discovery of cancer-associated biomarkers. Due to constraints requiring the study of proteins in a tissue environment with limited sample availability, the protein expression profiles within targeted tumor cells selectively procured from astrocytoma tissues were quantitatively compared by coupling the CITP technology with the label-free MS-based spectral counting measurements[68,69,138]. Even though major components may be diluted and trace compounds are concentrated as a result of selective analyte enrichment in the CITP process[135-137], the bandwidth of individual peptides/proteins, however, is proportional to the amount injected into the CITP capillary and therefore the abundance in the original proteome sample[73]. Thus, the analyte bandwidth established during the CITP separation,

correlated with the quantity of analyte, affects the distribution of each peptide within single or multiple CITP fractions, the peak width of peptide in subsequent nano-RPLC separation, and the number of total peptide hits (or tandem MS events) leading to individual protein identification and quantification through the spectral counting approach[68,69,138].

The Pearson correlation coefficient was employed to measure how well a linear equation describes the quantitative correlation between two proteomic runs to assess analytical reproducibility and allow for easy visual identification of outlier features (proteins). The calculation of the Pearson correlation coefficient was performed using the MATLAB Statistics Toolbox (MathWorks, Natick, MA). As shown in Figure 2.3, technical replicates of two adjacent GBM sections of the same specimen give a Pearson coefficient of greater than 0.99 over a dynamic range of around 10^4.

A Student's *t*-test was performed to compare the protein expression profiles within microdissected tumor cells among different grades of gliomas. Despite sharing over 2,532 common proteins (Figure 2.2 A), highlighted areas shown in Figure 2.4 A and 2.4 B specifically denote a large number of highly confident (*p*-value of less than 0.01) and differentially expressed (greater than 2-fold change) proteins discovered in comparative proteomic studies of astrocytomas.

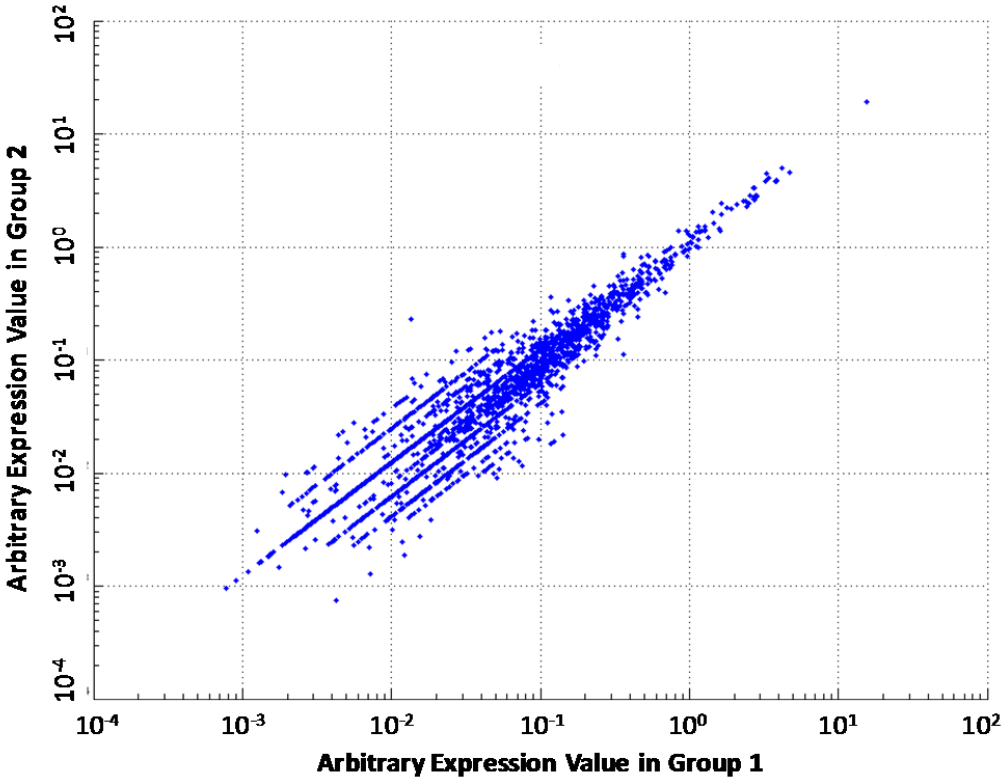

Figure 2.3 Pearson correlation coefficient plot of two proteomic runs analyzing adjacent GBM sections of the same tissue specimen.

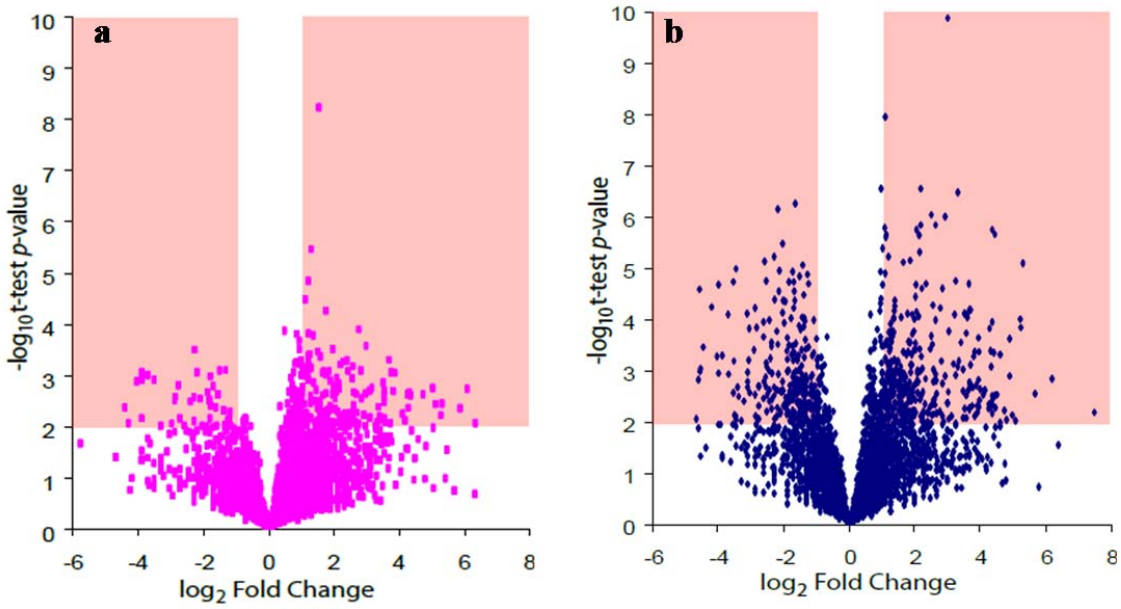

Figure 2.4 Volcano plots of (a) grade IV vs. grade III and (b) grade IV vs. grade II.

Comparison of expression difference of proteins between grade IV verses lower astrocytomas grades. Highly confident proteins (p value smaller than 0.01) with expression difference more than 2 fold are concluded in the highlighted area in the plot.

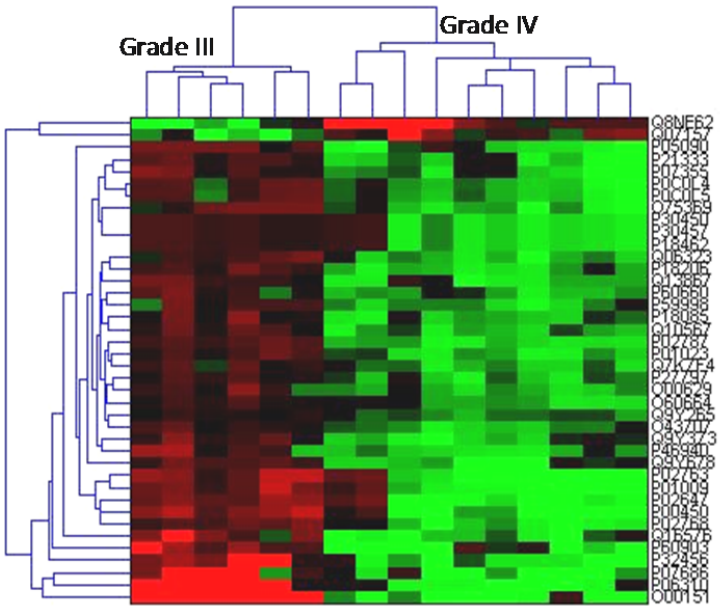

Figure 2.5 Unsupervised hierarchical clustering of forty proteins with the most significant t-test values resulting from the comparison of grade III and grade IV astrocytomas.

Unsupervised hierarchical clustering was conducted using Cluster 3.0[146]. Arrays and genes were both clustered using the Euclidian distance similarity metric. The complete linkage method was applied for clustering grade III anaplastic astrocytoma with grade IV GBM. Forty proteins with the most significant *p*-values by *t*-test are shown in Figure 2.5. This clustering analysis reveals significant and consistent expression differences between the two disease grades and provides a tractable set of proteins as potential candidates for follow-on validation studies and functional investigation.

2.3.3 Function and Network Analysis of Proteins Up-regulated in GBM

Besides monitoring and comparing the protein expression profiles among different grades of astrocytomas, the approach of grouping individual expression changes into pathways of actions is not only useful in trying to interpret genome and proteome datasets, but also allows common biological themes to emerge from the comparative proteomic analyses[147]. Comparative proteomics involving measurements in changes of pathways or functional processes are expected to provide relevant tumor-associated markers and networks, molecular relationships among different stages of disease, and molecular mechanisms that drive the progression of cancer. From a practical perspective, the evaluation of comparative proteomic dataset within a biological context is essential for high-throughput data authentication, prioritization of follow-on biomarker selection, and validation.

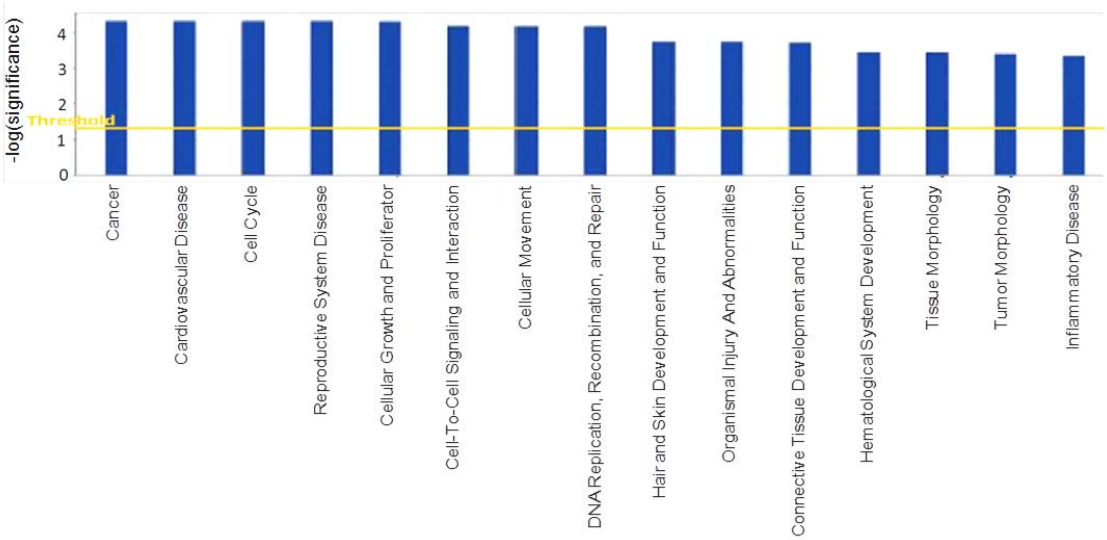

Figure 2.6 Top functional pathways constructed from the up-regulated GBM proteome dataset using the Ingenuity Pathway AnalysisTM.

Table 2-2 Proteins Related to Cancer Function and Up-Regulated in GBM

Name	Description	Accession	Location	Family	Spectral Counts (Grades II/III/IV)
B4GALNT1	β-1,4-N-acetyl-galactosaminyl Transferase 1	Q00973	cytoplasm	enzyme	(0/2/4)
BAG1	BCL2-associated athanogene	Q99933	cytoplasm	other	(0/0/2)
CASP1	caspase 1, apoptosis-related cysteine peptidase (interleukin 1, β, convertase)	P29466	cytoplasm	peptidase	(0/2/4)
CD97	CD97 molecule	P48960	plasma membrane	G-protein coupled receptor	(0/0/4)
COL6A3	collagen, type VI, α 3	P12111	extracellular Space	other	(6/14/87)
CTSS	cathepsin S	P25774	cytoplasm	peptidase	(0/0/5)
DCN	decorin	P07585	extracellular Space	other	(2/2/9)
EGFR	epidermal growth factor receptor (erythroblastic (leukemia viral (v-erb-b) oncogene homolog, avian)	P00533	plasma membrane	kinase	(5/9/47)
ERBB2	v-erb-b2 erythroblastic eukemia viral oncogene homolog2, neuro/ glioblastoma derived oncogene homolog (avian)	P04626	plasma membrane	kinase	(0/0/4)
GBP1	guanylate binding protein 1, interferon- inducible, 67kDa	P32455	cytoplasm	enzyme	(2/4/16)
IGFBP7	insulin-like growth factor Binding protein 7	Q16270	extracellular space	transporter	(0/0/5)
IL18	interleukin 18 (interferon-γ-inducing factor)	Q14116	extracellular space	cytokine	(0/0/3)
IQGAP1	Ras GTPase-activating-like protein IQGAP1	P46940	plasma membrane	other	(7/25/57)
ITGA2	integrin, α 2 (CD49B, α 2 subunit of VLA-2 receptor)	P17301	plasma membrane	other	(0/0/4)
ITGB2	integrin, β 2 (complement component 3 receptor 3 and 4 subunit)	P05107	plasma membrane	other	(0/2/5)

LGALS3	lectin, galactoside-binding, soluble, 2 (galectin 3)	P17931	extracellular space	other	(0/0/6)
LRPAP1	low density lipoprotein receptor-related protein associated protein 1	P30533	plasma membrane	transmembrane receptor	(0/2/5)
MCM7	MCM7 minichromosome Maintenance deficient 7 (S. cerevisiae)	P33993	nucleus	enzyme	(0/0/6)
MMP2	matrix metallopeptidase 2 (gelatinase A, 72kDa gelatinase, 72kDa type IV collagenase)	P08253	extracellular space	peptidase	(0/0/3)
MRE11A	MRE11 meiotic recombination 11 homolog A (S. cerevisiae)	P49959	nucleus	enzyme	(0/0/3)
NEK9	NIMA (never in mitosis gene a)-related kinase 9	Q8TD19	nucleus	kinase	(0/2/5)
N QO1	NAD(P)H dehydrogenase, quinone 1	P15559	cytoplasm	enzyme	(0/0/5)
OAS3	2'-5'-oligoadenylate synthetase 3, 100kDa	Q9Y6K5	cytoplasm	enzyme	(0/2/8)
PML	promyelocytic leukemia	P29590	nucleus	transcription regulator	(2/3/6)
S100A10	S100 calcium binding protein A10 (annexin II ligand, calpactin I, light polypeptide (p11))	P60903	cytoplasm	other	(2/2/10)
SMARCA4	SWI/SNF related, matrix associated, actin dependent regulator of chromatin, subfamily a, member 4	P51532	nucleus	transcription regulator	(0/0/3)
TBXAS	thromboxane A synthase 1 (platelet, cytochrome P450, family 5, subfamily A)	P24557	plasma membrane	enzyme	(0/0/4)
TFRC	transferrin receptor (p90, CD71)	P02786	plasma membrane	transporter	(2/4/9)
TIMP1	TIMP metallopeptidase inhibitor 1	P01033	extracellular space	other	(0/0/3)
TIMP2	TIMP metallopeptidase inhibitor 2	P16035	extracellular space	other	(0/0/3)
TYMS	thymidylate synthetase	P04818	nucleus	enzyme	(0/0/3)

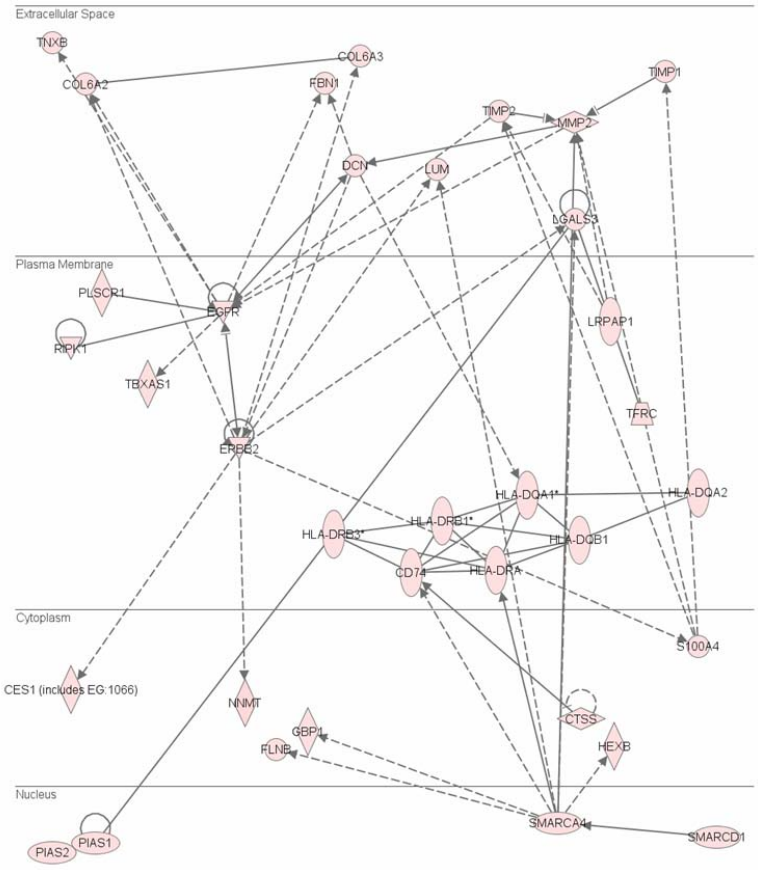

Figure 2.7 An up-regulated GBM protein network containing EGFR and Erbb2.

Proteins in this network were up-regulated in GBM more than 2 fold. This protein network were completely revealed as benefited from improved proteome coverage and well know cancer related plasma membrane proteins like EGFR and ERBB2 were noticed.

By employing the proteome dataset that is up-regulated in GBMs, the top functional pathways were mapped using the Ingenuity Pathway Analysis™ program (Ingenuity Systems, Redwood City, CA), as shown in Figure 2.6. The significance value associated with the functional analysis for a dataset is a measure of how likely the proteins from the dataset under investigation participate in that function. The significance is expressed as a *p*-value, which is calculated using the right-tailed Fisher's Exact Test. The *p*-value is calculated by comparing the number of user-specified proteins of interest that participate in a given function or pathway, relative to the total number of occurrences of these proteins in all functional/pathway annotations stored in the Ingenuity Pathway Knowledge Base. Table 2 lists the proteins that have been associated with the "cancer function" and that are uniquely up-regulated in GBM. Their spectral counting results among different grades of astrocytomas are also included in Table 2-2.

Since CITP's selective analyte enrichment greatly increases proteomic coverage, several protein networks were partially or completely revealed in these gliomas. For example, one of the protein networks, containing tyrosine kinase receptors of EGFR and its ErbB family member of Her2 (Erbb2), shown in Figure 2.7, is associated with the cell cycle dys-regulation and oncogenesis. Proteins shown in this network were up-regulated over 2 fold in GBM relative to lower grade astrocytomas. Previous studies have shown that EGFR amplification, over-expression and/or mutation are commonly observed in primary GBM. EGFR is involved in several major cellular signal transduction pathways such as the Ras, NF-κB, and PTEN pathways. It is believed that constantly activating these pathways contributes to cancer cell proliferation and survival. In addition to these well known cancer related plasma membrane proteins, two proteins expressed in the nucleus,

PIAS1 and PIAS2, were over-expressed in GBM. These two proteins regulate STAT expression in the Jak-Stat signaling pathway, which can promote astrocyte differentiation through cross-talk between Notch and the BMP-Smad signaling pathways[148].

2.3.4 Selection and Validation of IQGAP1 Using IHC

The cell membrane protein IQGAP1, which was differentially expressed between different grades of gliomas (Figure 2.8) as measured by the spectral counting approach[68,69,138], was selected for validation using IHC. IQGAP1 was chosen because of its role in key protein networks and pathways associated with the progression of brain tumors[149-151]. IHC was performed on TMA by removing three cores from each tissue block. For example, A1-A3 shown in Figure 2.9 were the cores removed from the same tissue block of patient diagnosed with grade 1 astrocytoma.

A total of 60 tissue blocks, including 9 grade 1, 19 grade 2, 18 grade 3, and 14 grade 4, were employed for the validation studies of IQGAP1. Additionally, normal cerebral tissue (L5-M15) and the skin cancer, melanoma (M16), served as negative and positive controls, respectively. As shown in Figure 2.9, both the staining intensity and the percentage score are reproducible among the cores removed from the same tissue block. Furthermore, the staining index, given for each case as the product by multiplying the percentage score with the staining intensity, increases with increasing tumor grade from grade 1 to grade 4 astrocytomas.

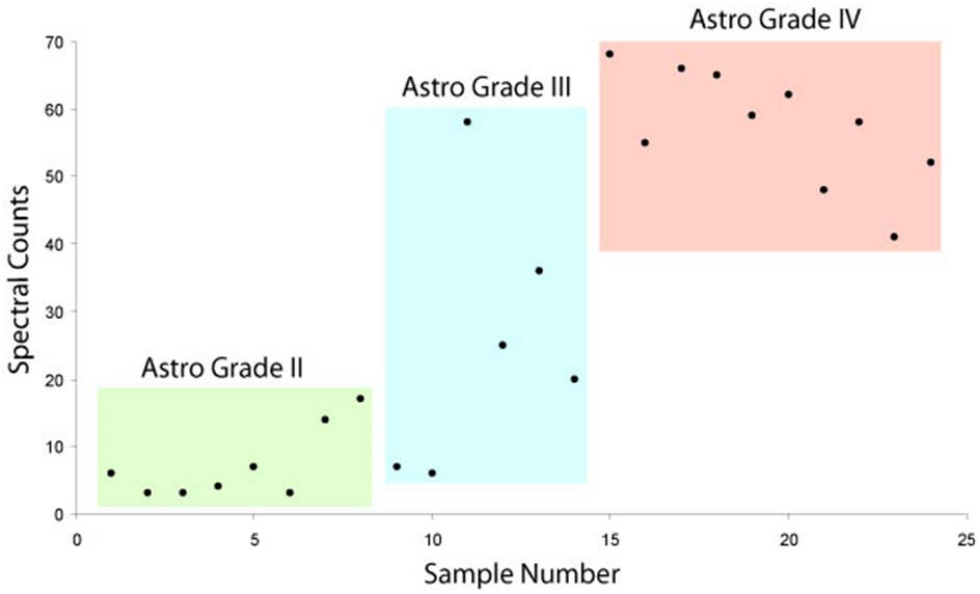

Figure 2.8 IQGAP1 expression relative to correlation with astrocytoma grade.

Quantification of protein IQGAP1 through label free spectral counting plotted along with astrocytomas grades demonstrated elevated expression level with increasing astrocytomas grades.

	1	2	3	4	5	6	7	8	9	10	11	12	13	14	15	16
A	1C	1C	1B	1D	1D	1D	1D	1D	1C	1A	1B	1B	1C	1B	1B	1D
B	1C	1D	1C	1B	1D	1C	1B	1D	1D	1C	1D	1B	1B	1B	1C	1C
C	1A	1D	1D	2D	1D	1D	1D	2D	2D	2D	1B	1B	1D	1C	1C	1B
D	1D	1C	1D	1B	1B	1C	2D	2D	2D	1D	1C	1D	2D	2D	2D	1C
E	1B	1B	2D	2D	1B	1B	1B	1C	1B	1B	1A	1B	1B	1B	1B	1B
F	1B	2D	2D	2D	2D	2D	2D	2D	1D	2D	1C	1C	1C	2D	2D	2C
G	2D	2D	2D	3D	3D	3D	2B	2C	2C	3D	3D	3D	3D	3D	3D	2D
H	3D	3D	2D	2C	2C	3C	3D	3C	2C	2C	2B	1D	1B	1A	2D	2B
I	2C	3D	3D	3D	3D	3D	3D	2D	2D	2D	3D	3D	3D	3D	3D	3D
J	3D	3D	3D	2D	2D	2D	2D	2D	3D	3D	3D	3D	2D	2D	2D	2B
K	2B	2B	3D	3D	3D	3D	3D	3D	3D	3D	3D	3D	3D	3D	2C	2B
L	2C	3D	3D	3D	0A	0A	0A	0A	0A	0A	0A	0A	0A	0A	0A	0A
M	0A	0A	0A	0A	0A	0A	0A	0A	0A	0A	0A	0A	0A	0A	0A	3D

Intensity	
0	Negative
1	Weak positive
2	Moderate positive
3	Strong positive

Percentage	
A	0-25%
B	26-50%
C	51-75%
D	76-100%

Grade	
1	
2	
3	
4	
cerebral tissue	
melanoma tissue	

Figure 2.9 Scoring of TMA with IHC staining of IQGAP1.

"Intensity" refers to staining intensity using IHC; "percentage" refers to the percentage of tumor cells within each TMA that were positive by IHC; and "grade" refers to WHO grade I-IV gliomas.

2.4 Conclusion

Comprehensive and comparative proteomic profiling of relatively pure populations of glioma cells obtained from selectively microdissected tumors demonstrates the ability of this combined approach to accurately and reliably discover and validate proteins that may correlate directly with and predict prognosis, survival, and response to therapy in patients. This work represents the largest catalog of proteins indentified and quantified among different grades of astrocytomas reported to date. Our proteomic results, including an enhanced analytical reproducibility, a high confidence in protein identification, and the broad tissue proteome coverage, illustrate the utility of proteomic discovery using targeted tissue microdissection in combination with CITP's selective analyte enrichment and its elevated resolving power prior to tandem MS measurements.

Despite sharing many common proteins, there are significant differences in protein expression among different grades of the infiltrative astrocytomas. The greatest number of differentially-expressed proteins was found in GBM, many of which are proteins frequently identified in other cancer types, including the plasma membrane proteins EGFR and Erbb2. Furthermore, two nuclear proteins up-regulated in GBM, PIAS1 and PIAS2, regulate STAT expression in the Jak-Stat signaling pathway, which can promote astrocyte differentiation through cross-talk between Notch and the BMP-Smad signaling pathways[148].

IQGAP1, a cell membrane protein, was selected from comparative proteomic studies for validation using IHC. IQGAP1 is a prominent member of several key protein networks and pathways that have been associated with the progression of brain tumors[149-151]. To facilitate high-throughput IHC measurements, analysis of IQGAP1 expression was

performed in a large TMA, including 60 astrocytoma specimens and validated MS-based proteomic profiling of microdissected astrocytoma tissues.

2.5 Acknowledgement

This work was supported by NIH grants CA 143177 to CSL and RR 21239 to XF and BMB. We wish to thank the Melvin Burkhardt chair in neurosurgical oncology and the Karen Colina Wilson research endowment within the Burkhardt Brain Tumor and Neuro-oncology Center at the Cleveland Clinic Foundation for additional support and funding.

Chapter 3 : Ultrasensitive Sample Quantitation via Selected Reaction Monitoring Using CITP/CZE-ESI-Triple Quadrupole MS

This is an independent work accomplished by me under guidance of Dr. Cheng Lee, Dr. Richard Smith and Dr. Keqi Tang.

3.1 Introduction

Capillary electrophoresis (CE) coupled with mass spectrometry (MS) has been well recognized as a complementary analytical technology to more conventional liquid chromatography-mass spectrometry (LC-MS). By combining the high resolving power of CE with the highly sensitive and information-rich detection of MS, this hyphenated technique has enjoyed successful applications in many fields of scientific research, such as biomarker discovery and verification[62,152-154], metabolomics[155,156], identification and quantification of environmental pollutants[157] and food quality control[158]. While much less widely applied than LC-MS, the number of publications related to development and application of CE-MS continues to increase due to its potential capability in performing sensitive and high throughput sample analysis[159-161]. Online coupling of CE with electrospray ionization (ESI)-MS has been demonstrated via a co-axial sheath-flow interface[162] or a sheathless interface using either a metal sheath capillary[86], a metal coated capillary[163] or a T-junction design that connects separation capillary with electrospray

tip[164]. With the goal to refine this technology and broaden its utility, every aspect of the CE-MS technique has attracted attention, including CE capillary modification[165-167], ESI emitter fabrication[168] and high efficiency CE-MS interface design[169]. Recently, Maxwell and co-workers have designed a stainless hollow needle with a beveled spray tip as a more robust sheath liquid interface[170]. A conductive tip made by HF etching a fused silica capillary to porous was introduced by Moini[105]. The performance of sheath-less setup utilizing the etched porous tip was demonstrated by Busnel *et al.*[109], showing its capability in performing CE-ESI-MS analysis in a broad range of flow rates (from low nL/min to sub μL/min) with exquisite sensitivity. Two CE operation modes, capillary zone electrophoresis (CZE) and transient capillary isotachophoresis/capillary zone electrophoresis (CITP/CZE), have shown to be most compatible with online MS analysis and have thus been most widely used. Heemskerk *et al.* reported an improved ionization efficiency for phosphopeptides using CZE-ESI-MS under ultra low ESI flow rate (below 20 nL/min) recently[111]. Ramautar and co-workers reported enhanced coverage of urinary metabolome using CITP/CZE-ESI-MS[110]. Busnel and co-workers applied both CZE and CITP/CZE in a sheathless CE-ESI-MS setup and reported nanomolar and subnanomolar detection limits respectively[109]. Thus far, CE-MS has been primarily used for the qualitative analysis of biomolecules or small molecules. With the growing interest in identifying biomarkers for diagnostic, prognostic and predictive applications, new analytical tools capable of effectively quantifying low abundant targets in complex biological matrix are needed.

Triple quadrupole MS operating in a selected reaction monitoring (SRM) mode has demonstrated extremely high sensitivity, dynamic range and specificity in quantifying

targeted analytes in a complex chemical or biological sample matrix[171]. The SRM MS-based quantitation method has been extensively investigated and primarily used in combination with LC for quantitation of metabolites[172,173], and increasingly for peptide measurements, e.g. verification of protein biomarkers[171,174,175]. Online coupling CE with SRM MS, though still in its infancy, has already demonstrated its unique capability in sample quantitation with significantly less sample consumption as compared to LC-SRM MS based technique. Jeong *et al.* recently demonstrated the detection and quantitation of underivatized amino acids using CZE-SRM MS via a sheathless interface[176]. Li and co-workers have reported a highly sensitive method using CZE-SRM MS[177], and 10- to 20-fold sensitivity improvements over HPLC-SRM MS were demonstrated as well as linear response for Leu-enkephalin from 1.5 nM to 10 μM in a BSA tryptic digest background.

Here we report the use of CITP/CZE for online SRM MS quantitation. CITP is a static-state electrophoresis, which utilizes the conductivity difference between sample ions and background ions to achieve a sample stacking mechanism. CITP has been mainly used as a preconcentration method prior to sample separation by which a concentration factor of ~1000 can be achieved when applied to dilute samples. CITP/CZE is a hybrid mode capable of achieving both sample concentration (selectively) and separation simultaneously[73]. As a result of the selective focusing and high resolving power, trace compounds are less masked by the major compounds after CITP/CZE and thus become more detectable by MS. Fang *et al.* have demonstrated the use of CITP/CZE MS for candidate biomarker discovery using tissue samples[74,75]. Our goal is to utilize the intrinsic focusing feature of CITP/CZE to achieve ultrasensitive sample quantitation and

evaluate the lower limit of quantitation using CITP/CZE-SRM MS for quantifying targeted peptides in complex biological matrix.

3.2 Experimental Section

3.2.1 Chemicals

Bovine serum albumin (BSA) tryptic digest standard was purchased from Protea (Morgantown, WV). Leu-enkephalin, angiotensin II, kemptide, ammonium acetate, methanol and acetic acid were purchased from Sigma (St. Louis, MO). Fused silica capillaries were purchased from Polymicro Technologies (Phoenix, AZ).

3.2.2 Sample Preparation

BSA tryptic digest solution was used to evaluate the performance of the online CE-ESI-MS platform. Stock solution of BSA digest was prepared by dissolving 500 pmol of BSA digest standard in 100 μL leading electrolyte (LE) solution consisting of 25 mM ammonium acetate in deionized water with the solution pH adjusted by adding acetic acid to pH=4. Working solutions with concentrations ranging from 10 nM to 3.75 μM were obtained by diluting stock solution with LE. Preparation of samples for CZE experiments was similar except LE was substituted with 0.1 M acetic acid in deionized water. 0.1 M acetic acid solution was subsequently mixed with methanol at volume ratio 9:1 as background electrolyte (BGE) solution for better electrospray operation.

A mixture of three peptides (Leu-Enkephalin, Angiotensin II and Kemptide) spiked into BSA tryptic digest at different concentrations were used in the CITP/CZE-SRM MS sample quantitation experiments. Stock solution with 10 μM concentration for each peptide was prepared in water and stocked in aliquots. The stock solution was then

diluted using BSA background matrix (50 nM BSA digest in 25 mM LE) to obtain a peptide concentration series for CITP/CZE-SRM MS quantitation.

3.2.2 CITP/CZE-ESI-MS Interface

Figure 3.1 shows the schematic of the interface developed to couple CITP/CZE online with an ESI-triple quadrupole (QQQ) mass spectrometer. The CITP/CZE separation capillary (75 μm i.d., 150 μm o.d., and 88 cm long) was inserted into a large bore capillary (200 μm i.d., 360 μm o.d., and 5 cm long) concentrically using a PEEK cross. The free end of the large bore capillary was first pulled into a fine tip using a Sutter P-2000 laser puller and then chemically etched to remove a part of the tip using HF solution[168] to form an ESI emitter with a ~50 μm opening, as shown by the inserted picture at the bottom right of the Figure 3.1. The tapered i.d. of the large bore ESI emitter capillary also allowed the separation capillary to be inserted as far as possible until it hit the inner wall of the emitter capillary to both minimize the dead volume and provide a consistent coupling between the CITP/CZE separation capillary and the ESI emitter, as shown by the inserted picture at the bottom middle of the Figure 3.1. Before each CITP/CZE-ESI-QQQ MS analysis, a sheath flow of BGE serving as electrically conductive solution was introduced to completely fill the annular space between the separation capillary and the ESI emitter capillary. The liquid junction formed at the ESI emitter allows a second voltage to be applied for stable electrospray operation and maintains the electric contact. To minimize the sample dilution, the sheath-flow was turned off during the CITP/CZE-ESI-QQQ MS analysis. To avoid electric contact interruption by the air bubbles generated from the redox reaction at the metal contact of the ESI voltage, which could rapidly damage the separation capillary due to the high

separation voltage (~30 kV), the second voltage for ESI was applied to the sheath flow waste line through a flow split design, as shown in Figure 3.1, which was flushed with the sheath liquid to avoid bubble accumulation after each experiment.

The separation capillary was coated with hydroxypropyl cellulose to minimize electroosmotic flow. The separation capillary was filled with BGE solution before each experiment. Samples were loaded into the separation capillary by the hydrodynamic method[178] at constant gas pressure (1 psi). Sample loading was adjusted by varying the length of loading time. The CITP/CZE separation voltage of 27 kV was applied to the sample inlet of the capillary using a Glassman high voltage power supply. A ~ 1 kV electric potential at the ESI emitter liquid junction was created under the separation voltage when the sheath flow liquid waste line was grounded. Analytes were eluted from the separation capillary hydrodynamically by applying 1 psi nitrogen back pressure to the trailing electrolyte (TE) reservoir (Figure 3.1) after a fixed separation time, determined experimentally for achieving optimum ion focusing and separation.

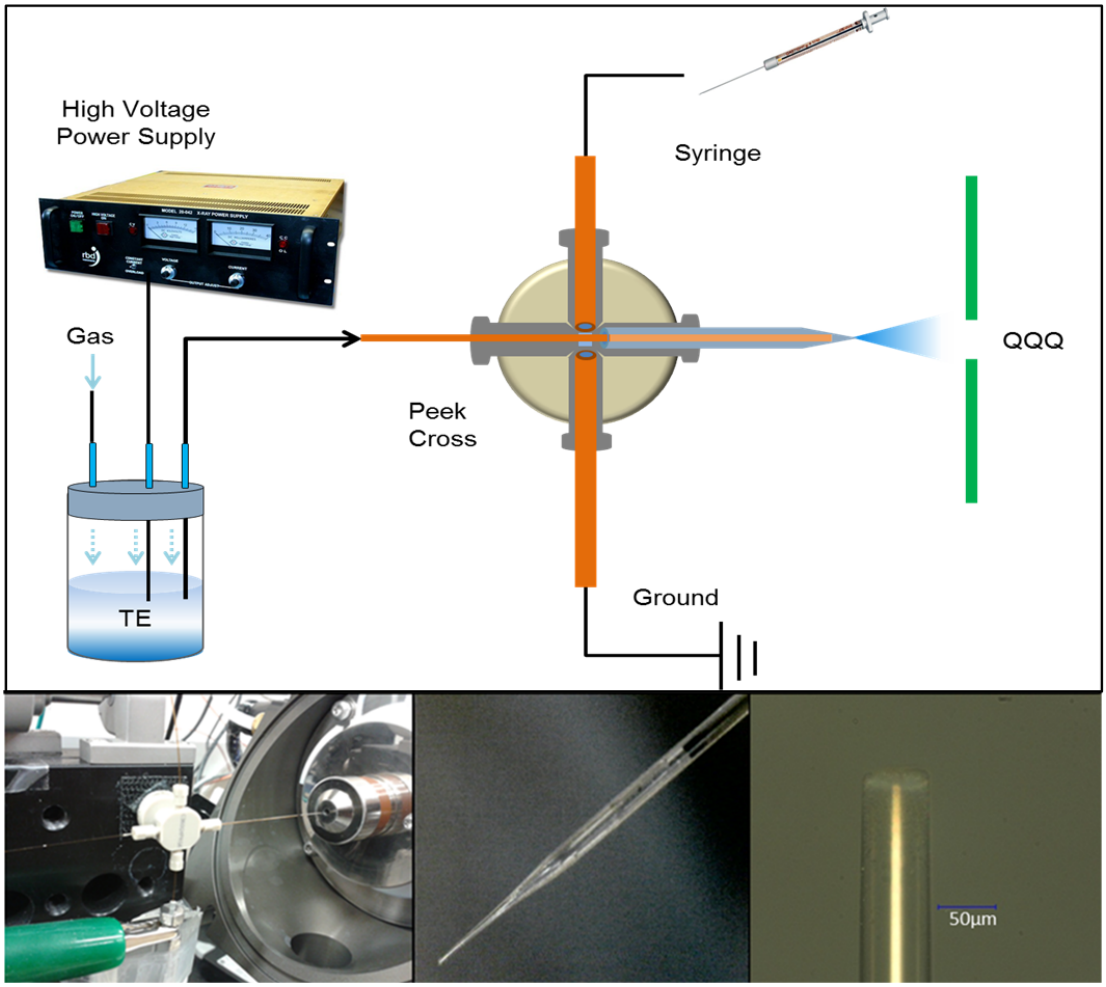

Figure 3.1 Graph of CITP/CZE-ESI-QQQ MS setup used in this study.

Upper part is the schematic of the whole setup (not to scale). Lower left shows the actual interface and the position of the emitter relative to MS inlet, as well as the off-flow path grounding design adapted to avoid redox reaction generated bubbles. Lower middle and lower right show close view of the in-house fabricated emitter and the size of the opening.

3.2.3 MS Optimization and Data Processing

An Agilent QQQ mass spectrometer (model 6430) was used for all sample analyses. The standard ESI interface of the instrument was modified with a multi-capillary/dual ion funnel interface[179] making the performance of the instrument similar to Agilent's latest triple quadrupole MS product (model 6490), as shown by the inserted picture at the bottom left of the Figure 3.1. The ESI voltage of the MS was varied in the range of -200 to -500 V for the optimum ESI sensitivity and signal stability considering the ~ 1 kV potential at ESI emitter liquid junction as described above under CITP/CZE operating condition. A dry nitrogen flow of 10 L/min and a gas temperature of 320 °C were used for optimum MS sensitivity. Both full scan MS and SRM were used in this study. In SRM mode, specific mass to charge ratio (*m/z*) precursor ions were selected in the first quadrupole (Q1) and fragmented in the second quadrupole (Q2 collision cell) via collision induced dissociation under sufficient collision energy. The specific *m/z* product ions were then selected in the third quadrupole (Q3) and monitored by the MS detector. Each selected precursor/product ion pair in SRM MS is referred to as a SRM transition. Through monitoring the unique transitions of the selected analytes, both high sensitivity and specificity can be achieved in sample quantification. SRM MS operating parameters for each peptide in this study were optimized using direct infusion of the peptide standard with 1 μM concentration at 500 nL/min. Three most intense fragments were selected for each peptide as SRM transitions regardless of the fragment ion types. The collision energy for each SRM transition was optimized and recorded for the highest product ion intensity. The dwell time for each SRM transition was set at 65 milliseconds to ensure at least 12 data points for each analyte peak in extracted CITP/CZE SRM MS

chromatogram. All the SRM transitions and their related optimum collision energies for three peptides selected for SRM MS quantitation in this study are listed in Table 3.1.

Data analysis was performed by using Agilent MassHunter Qualitative Analysis Software (version B.02.00). Symmetric 0.5 *m/z* tolerance was used to extract the selected ion chromatograms. Unit resolutions were used for both Q1 and Q3 in SRM data acquisition. Peak retention time, peak area and peak width were obtained through manual integration. In S/N calculation, peak height was used as signal and the software default setting, peak-to-peak definition, in the range of 3-minutes before and after the target peak was used for noise measurement. In this default setting, the noise value for the selected range is calculated as the difference between the highest and the lowest peak abundance values.

Table 3-1 SRM transitions and parameters used in this study

Compound Name	Sequence	Precursor Ion (*m/z*)	Product Ion (*m/z*)	Dwell Time (msec)	Collision Energy (eV)
Leu-enkephalin	$[YGGFL+H]^+$	**556.3**	**397.3 (a_4^+)**	**65**	**14**
		556.3	425.3 (b_4^+)	65	12
		556.3	278.3 (b_3^+)	65	22
Angiotensin II	$[DRVYIHPF+2H]^{2+}$	**523.8**	**784.5 (b_6^+)**	**65**	**14**
		523.8	756.5 (a_6^+)	65	20
		523.8	647.4 (b_5^+)	65	20
Kemptide	$[LRRASLG+2H]^{2+}$	**386.7**	**567.4 (b_5^+-NH_3)**	**65**	**17**
		386.7	549.4 (b_5^+-NH_3-H_2O)	65	18
		386.7	539.4 (a_5^+-NH_3)	65	22
BSA peptide	*$[VGTR+H]^+$*	*432.3*	*230.1 (a_3^+)*	*65*	*20*

The bolded transitions indicate the transition used for quantitation of each peptide. The non bolded/italicized transitions were used to confirm the peptide's identity. The italicized transition of BSA peptide was used to monitor the platform's reproducibility.

3.3 Results and Discussion

3.3.1 CITP/CZE Sample Loading Capability and Optimization

As one of the unique features, CITP is capable of selectively enriching/focusing the low abundance compounds in a complex mixture. During the CITP stacking process, analytes migrate into different bands under a constant electric field according to their different electric mobility. At the completion of the CITP stacking process, low abundance analytes are concentrated to a much greater extent than the major components in a mixture[73]. The CITP stacking mechanism enables relatively large (~μL) sample loading as compared to the much smaller (~nL) sample loading of traditional CZE, providing a basis for more sensitive detection for trace analytes. The CITP/CZE separation is a hybrid technique capable of simultaneously achieving high sensitivity and resolution by a combination of ion stacking and separation processes. To evaluate capability of CITP/CZE relative to CZE, both CITP/CZE and CZE were coupled online with ESI-MS. Figure 2 compares the analyte intensity between CITP/CZE-ESI-MS and CZE-ESI-MS at two different sample loading time using BSA tryptic digest. With 1.5 min sample loading time, which yielded a small sample plug, equivalent ion intensity was measured between CITP/CZE-ESI-MS and CZE-ESI-MS, as shown by the base peak ion chromatograms (BPC) in Figure 3.2A (the top two panels) and the extracted ion chromatograms (EIC) for selected peptide (m/z = 432.3) in Figure 3.2B (the top two panels). Similar peak widths (0.456 min and 0.499 min) were also observed between CITP/CZE-ESI-MS and CZE-ESI-MS at this short sample loading time. It is also expected that different peptide peaks will be more resolved in CZE-ESI-MS as compared to CITP/CZE-ESI-MS, as shown in Figure 3.2A, due to the additional time required to

complete the CITP ion stacking process before the analyte peaks are separated from each other in the CITP/CZE-ESI-MS. When the sample loading time was increased to 3 min, corresponding to an injection of a longer sample plug, the benefit of CITP/CZE-ESI-MS becomes more obvious, as shown by the bottom two panels of Figure 3.2A and B. While CZE-ESI-MS yielded essentially no gain in peak intensity and showed peak broadening (0.711 min), the analyte peak intensity in CITP/CZE-ESI-MS was increased by approximately 4-fold while the peak width remained essentially the same (0.477 min). The increased sample loading volume in CITP/CZE-ESI-MS also resulted in the detection of more analyte peaks due to the effective ion focusing. The apparent nonlinear dependence between sample loading time and the detected analyte peak intensity under these two loading time in CITP/CZE-ESI-MS is due to the hydrodynamic sample loading method used in the experiment. Under the small gas pressure (~1 psi), which was kept at constant by using a high precision digital gas pressure regulator, there is an approximately one minute time delay between the application of the gas pressure and fully developed liquid flow in the separation capillary. With this considered the detected peak intensity in CITP/CZE-ESI-MS is proportional to the sample loading time (i.e. the size of the sample plug).

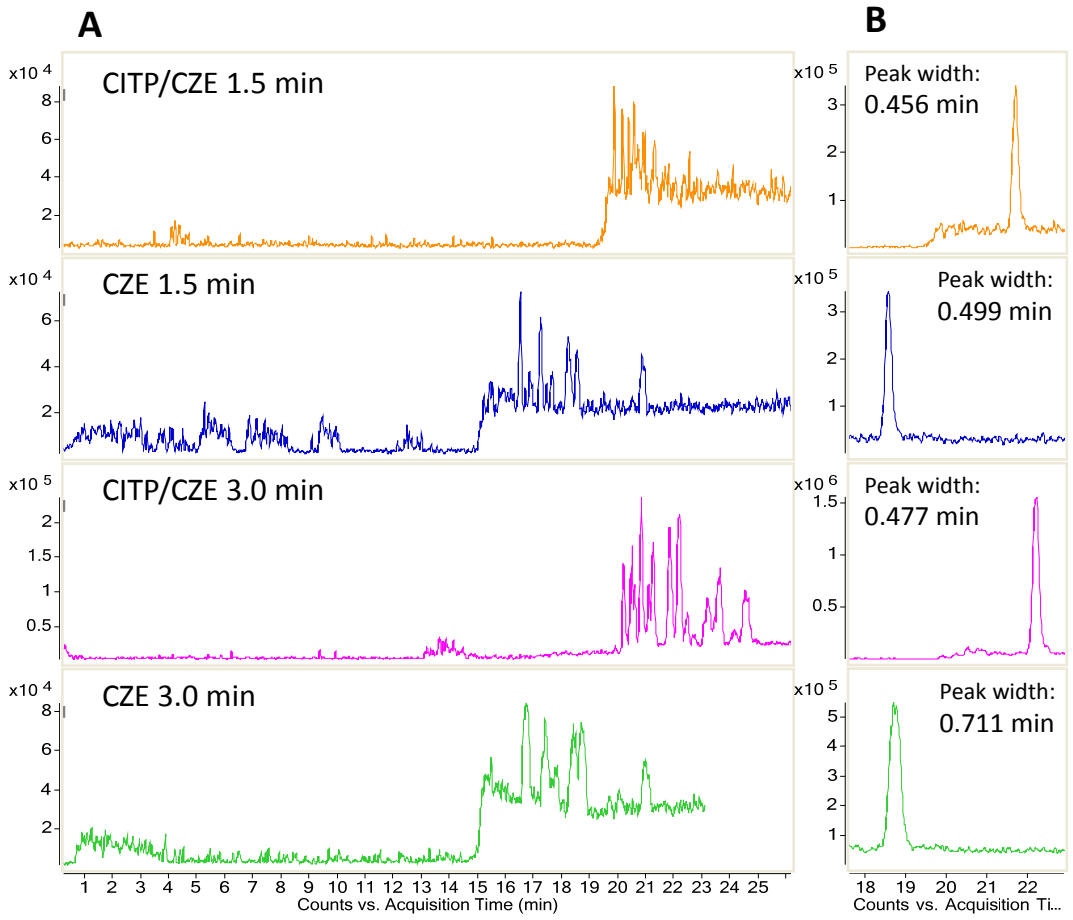

Figure 3.2 Comparison of CITP/CZE and CZE with different sample loading time using BSA digest for selected ion m/z 432.3 $[VGTR+H]^+$.

Comparison of CITP/CZE and CZE with different sample loading time using BSA digest for selected ion *m/z* 432.3 $[VGTR+H]^+$.

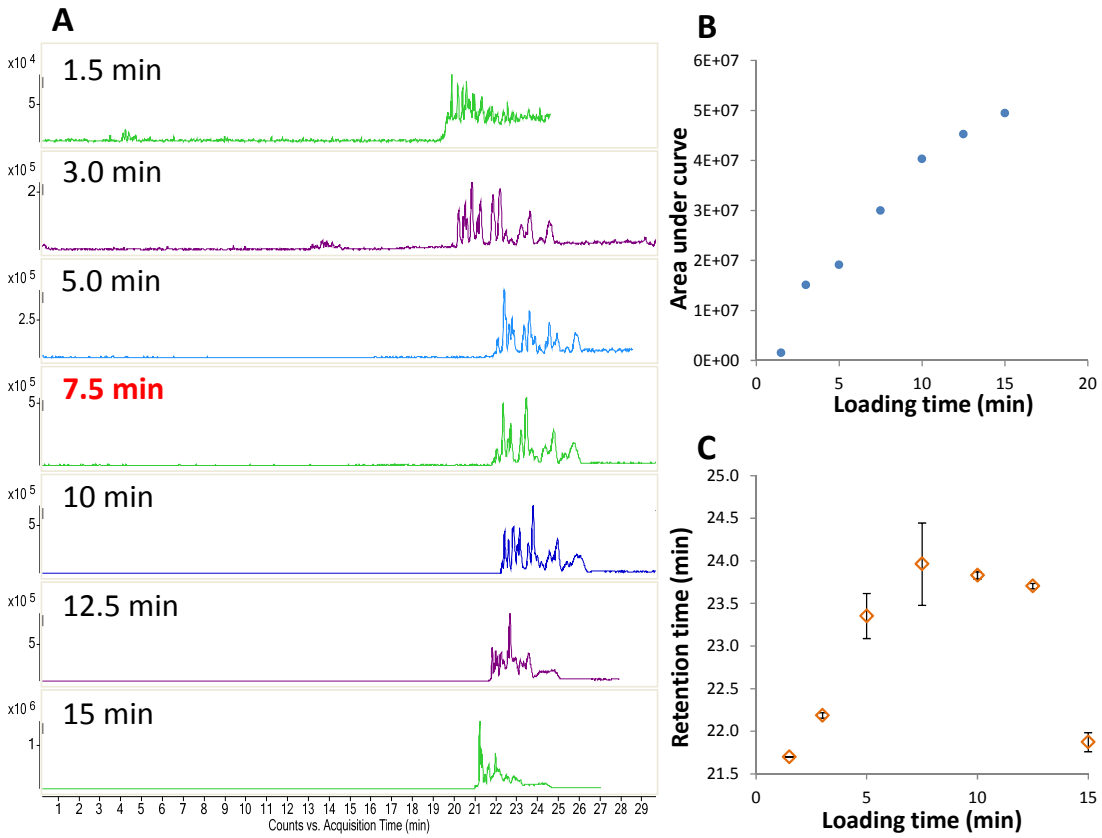

Figure 3.3 Sample loading capacity optimization.

(A) BPC from CITP/CZE-ESI MS with different sample loading time. (B) AUC (area under the curve) of BPC presented in panel A with different sample loading time. (C) Retention time of peptide *m/z* 432.3 $[VGTR+H]^+$. Sample condition: 3.75 µM BSA digest in 25 mM ammonium acetate (pH=4), loading condition: constant pressure at 1 psi.

In order to optimize the sample loading capacity of CITP/CZE for the length of the separation capillary and the separation voltage used in the experiment, a series of different sample loading times ranging from 1.5 minutes to 15 minutes were evaluated and the ion intensity was measured at each sample loading time using BSA tryptic digest. Figure 3.3A shows the BPCs from the CITP/CZE-ESI-MS measurements at different sample loading time. The optimum loading time under the current CITP/CZE setup is defined as the maximum sample loading volume to allow the sample stacking and separation to be fully developed in the remaining length of the capillary. As indicated by the experimental measurements in Figure 3.3A, peptide intensity continues to increase as the sample loading time increases from 1.5 minutes to 7.5 minutes while the electrophoresis peak width remains essentially the same. Beyond 10 minutes sample loading time, significant peak broadening and loss of separation quality was observed. This observation was further implied by the area under curve (AUC) of BPC vs. loading time in Figure 3.3B. As sample loading was increased beyond 10 minutes, the rate of area increase (e.g. the slope of the curve) was decreased. This is largely due to the peak overlapping as a result of insufficient separation time at large sample loading time. Consequently, 7.5 minutes sample loading time was selected as the optimum sample loading time, corresponding to about 1 μL of sample loading volume or 25% of the total separation capillary volume, since it provided the best balance among sample loading volume, completion of sample stacking and sufficient analyte separation. The variation of the retention time (RT) under different sample loading time, as shown in Figure 3.3C for BSA peptide *m/z* 432.3 $[VGTR+H]^+$, is due to a combination of ion focusing time and separation time change in CITP/CZE operation mode. In the pure CITP mode, the ion

focusing time is expected to increase as the sample loading time increases. In the pure CZE mode, the sample retention time decreases as the sample loading time increases. The final RT in CITP/CZE mode is determined by both ion focusing time and separation time. The data in Figure 3.3C indicate that RT increases initially as sample loading time increases due to the dominant change of ion focusing time. Beyond 7.5 min sample loading time, RT decreases as the sample loading time increases indicating the change of ion separation time becomes the dominant factor in determining the change of sample RT. Good reproducibility of RT was also measured with the variance smaller than 4%.

3.3.2 CITP/CZE-ESI-MS Sample Quantitation

The initial evaluation of CITP/CZE-ESI-MS for sample quantitation was performed by using BSA digest solution of different concentrations ranging from 20 nM to 3.75 μM. The peak areas for randomly selected BSA peptides were measured from triplicate CITP/CZE-ESI-MS analyses of each sample concentrations. Full scan MS from *m/z* 300 to 2250 was used in the experiments. Figure 3.4 shows the peak areas for two selected peptide ions *m/z* 582.5 $[LVNELTEFAK+2H]^{2+}$ and *m/z* 432.3 $[VGTR+H]^{+}$ at different BSA tryptic digest solution concentrations. Good reproducibility (CV<24%) and linearity were observed for both peptides in the tested BSA concentration range.

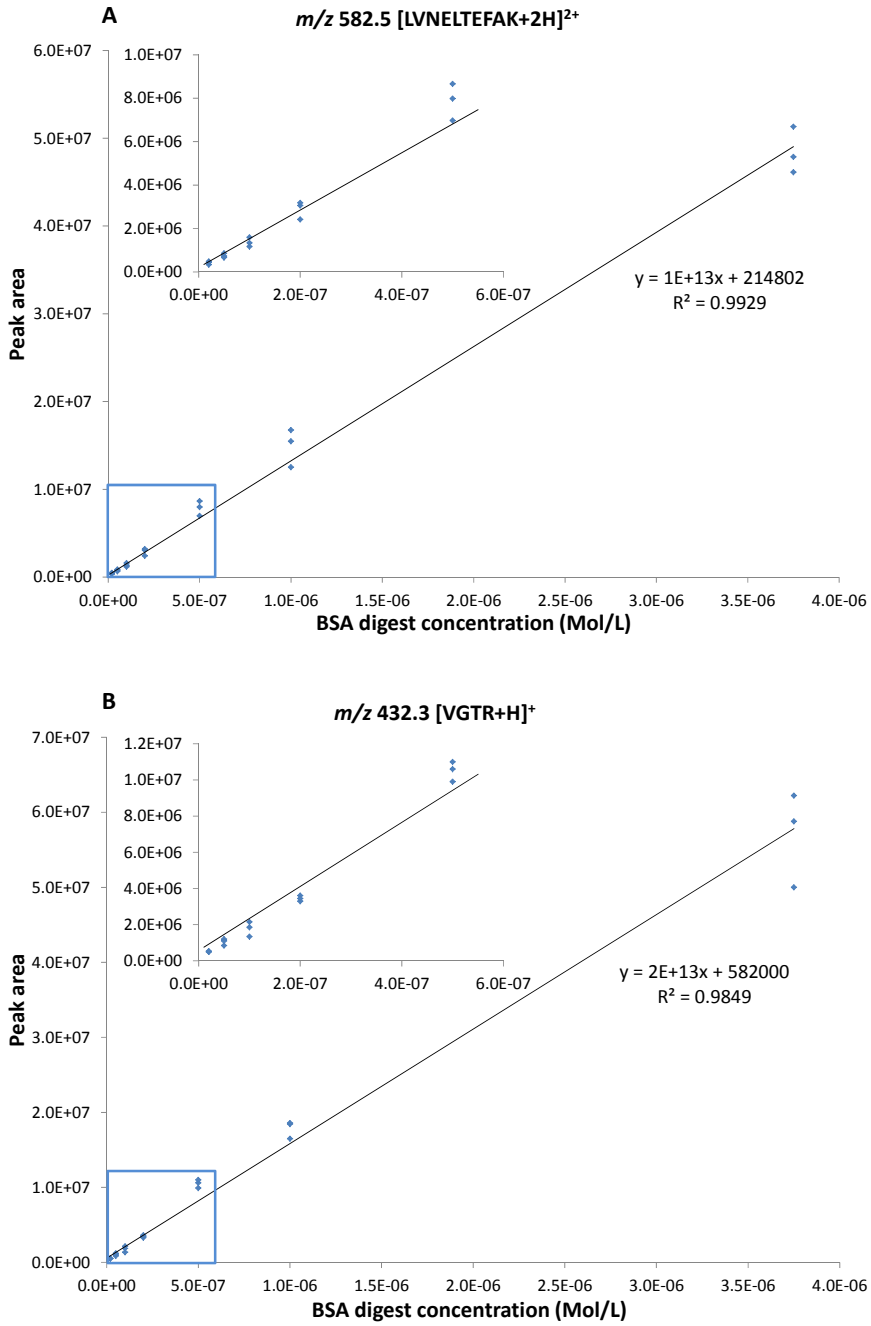

Figure 3.4 Peak area calibration curve, for selected BSA peptide ions of m/z 582.5 [LVNELTEFAK+2H]$^{2+}$

(A) and *m/z* 432.3 [VGTR+H]$^{+}$ (B) at different sample concentrations extracted from CITP/CZE-ESI MS measurements.

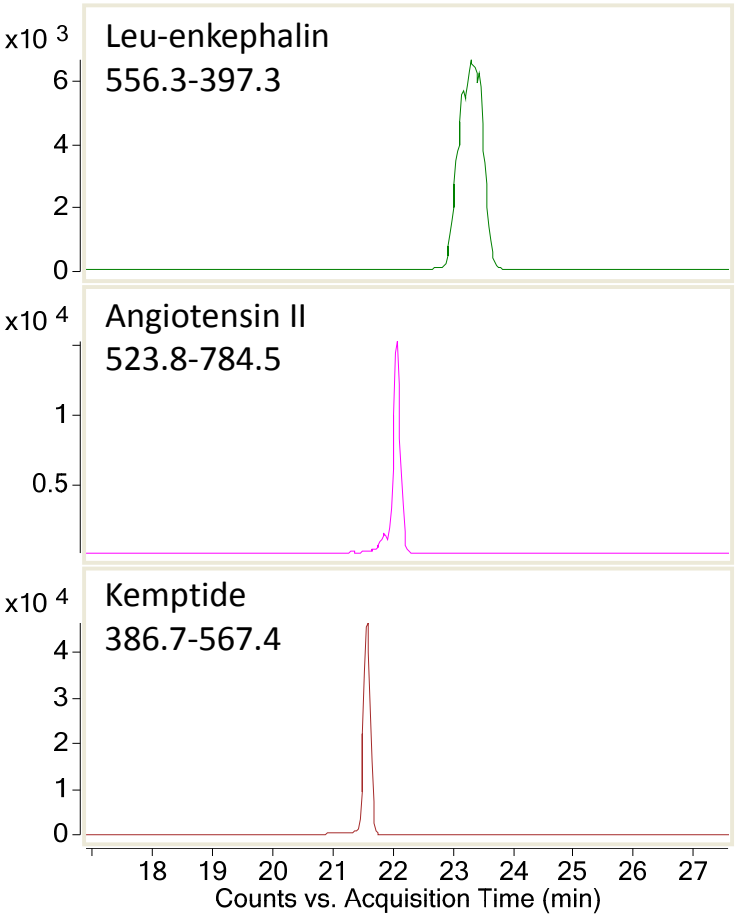

Figure 3.5 Different ion focusing effect observed for different ions.

EIC for Leu-Enkephalin (top), Angiotensin II (middle) and Kemptide (bottom) at 100 nM concentration spiked in 50 nM BSA digest sample matrix showing different CITP ion focusing characteristics.

To further determine the limit of quantitation (LOQ) for the CITP/CZE-ESI-MS instrument platform and investigate the matrix effect on the instrument LOQ, SRM MS analysis, as the most sensitive and specific MS operating mode, was used to quantify a set of samples containing three peptides (Leu-enkephalin, Angiotensin II and Kemptide) spiked into 50 nM BSA tryptic digest solution at different concentrations ranging from 50 pM to 5 μM. With an estimated 1 μL sample loading volume, the corresponding peptide loading amount was from 50 attomoles to 5 picomoles. Each sample solution also contains 25 mM LE as required by CITP/CZE separation. Three SRM transitions were monitored for each spiked in peptide and triplicate CITP/CZE-ESI-MS analyses were performed at each sample concentration. One additional SRM transition from a BSA peptide (m/z 432.3 $[VGTR+H]^+$) was also monitored during each CITP/CZE-ESI-MS analysis to ensure the stability of the instrument. This additional transition can also be used to normalize the peak intensity of the targeted peptides improving the precision of the quantification. (Table 2-1)

Different ion focusing was initially observed for three different spiked in peptides during the CITP/CZE-ESI-MS analyses under the current CITP/CZE-ESI-MS setup and operating conditions. Figure 3.5 shows the selected ion chromatograms for these peptides corresponding to SRM transitions 556.3 to 397.3 for Leu-enkephalin, 523.8 to 784.5 for Angiotensin II, and 386.7 to 567.4 for Kemptide respectively. Leu-enkephalin peak in Figure 3.5 is shown to be much broader than Kemptide and Angiotensin II peaks along with lower intensity indicating a poor CITP focusing for Leu-enkephalin ions. This different ion focusing characteristic can be explained by the Kohlrausch equation[137],

$$C_A = C_L/\{[\mu_L/(\mu_L + \mu_R)]\,[(\mu_A + \mu_R)/\mu_A]\}$$

Where C_A is the final analyte concentration, C_L is the concentration of LE, μ is electrophoretic mobility with A and R stands for analyte and counter ion respectively. Given constant leading electrolyte concentration, the final concentration of the analyte is determined by its electrophoretic mobility μ_A. The order of electrophoretic mobility for these three peptides is Kemptide > Angiotensin II > Leu-enkephalin based on their relative elution time. This electrophoretic mobility order is consistent with their peak width and peak intensity shown in Figure 3.5 as analyte with higher electrophoretic mobility gets better focused and thus forms a narrower peak with higher intensity.

Figure 3.6 shows the CITP/CZE-ESI-SRM MS quantitation curves for Angiotensin II (Figure 3.6A) and Kemptide (Figure 3.6B) using the same SRM transitions as Figure 3.5. Good linearity was observed from 50 pM to 500 nM for Angiotensin II and 50 pM to 100 nM for Kemptide. The EICs for the lowest concentration of each corresponding peptide from three replicates are also shown in the figure with signal-to-noise ratio (S/N) being 63.2, 32.6, 52.9 for Kemptide and 13.5, 21.1, 9.3 for Angiotensin II, respectively. Judging from the S/N, the LOQ for Angiotensin II is about 50 pM while the LOQ for Kemptide is significantly less than 50 pM. The shift of the linear dynamic range to a lower concentration range for Kemptide may be primarily attributed to the better electrospray ionization efficiency of Kemptide than that of Angiotensin II aside from their focusing ability difference, which is consistent with the larger slope of the trendline for Kemptide (e.g. $4x10^{12}$ and $2x10^{12}$ for Kemptide and Angiotensin II respectively), indicating a better CITP/CZE-ESI-SRM MS sensitivity for Kemptide. Due to the relative poor CITP focusing for Leu-enkephalin ions as compared to Kemptide and Angiotensin II ions, as discussed above, the LOQ for Leu-enkephalin was estimated to be about 500

nM (data not shown). Table 3-2 CV from triplicate SRM MS analyses of Kemptide and Angiotensin II at each concentration for selected SRM transitions. further lists the CV values for CITP/CZE-ESI-SRM MS measurements at each concentration for both peptides. Median CV values of 12% and 18% for Kemptide and Angiotensin II indicate a good reproducibility for CITP/CZE-ESI-SRM MS sample quantitation. Significantly better LOQ (~ 30 times better) is demonstrated through this study for the CITP/CZE-ESI-SRM MS sample quantitation as compared to a recent study using CZE-ESI-SRM MS[177]. The extracted ion chromatograms from the triplicate sample analyses shown in Figure 6 also indicate a good reproducibility in peak retention time (RSD 0.8% and 0.9% respectively). The retention time RSD among triplicate sample analyses across the concentration series is smaller than 5% with an average of 2.4% for Angiotensin II and 3.6% for Kemptide. Considering the RT variation introduced by the manual control of the data acquisition in, the RT reproducibility can be further improved by a fully automated data acquisition.

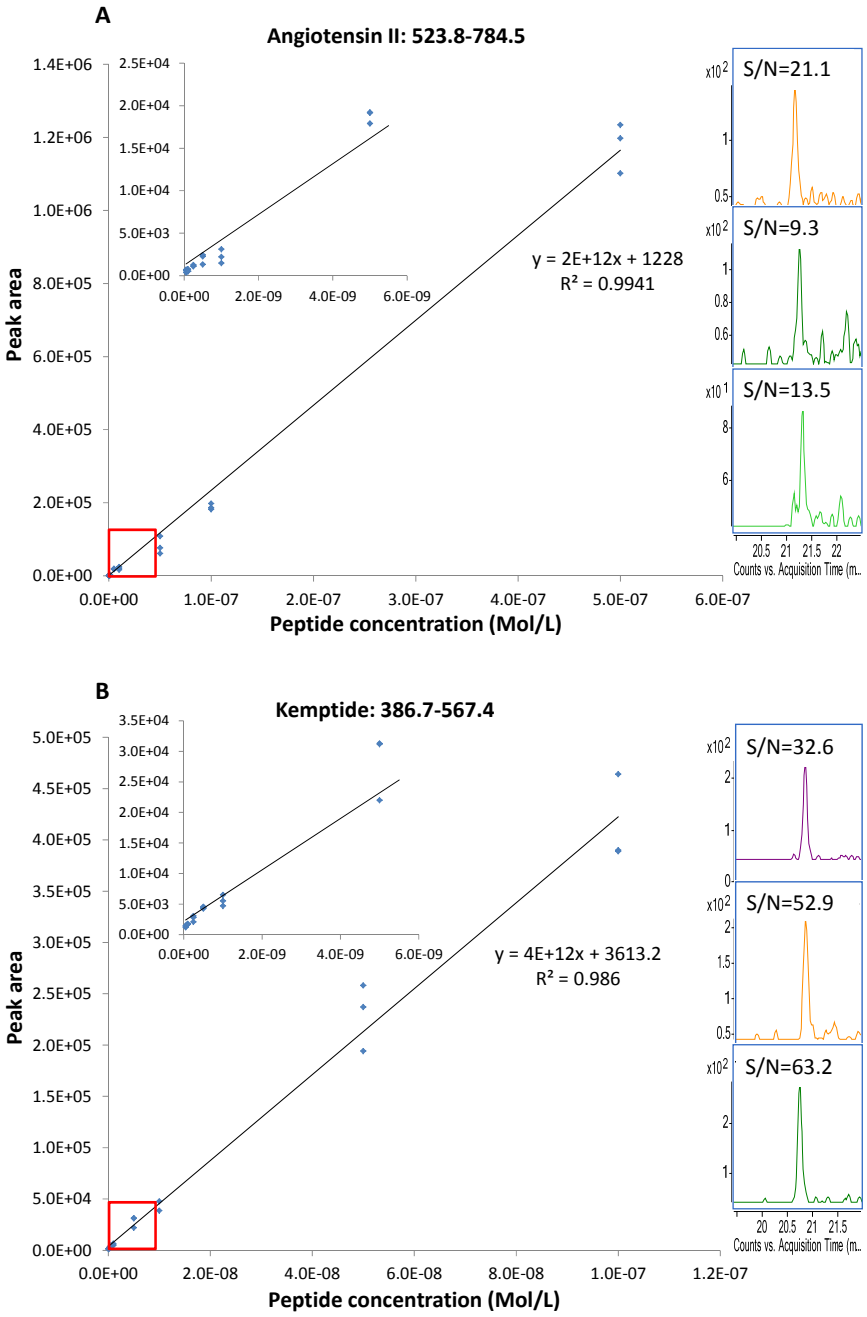

Figure 3.6 Calibration curve of CITP/CZE-ESI-SRM MS quantitation of Angiotensin II (A) and Kemptide (B) and EIC from three replicate SRM measurements at 50 pM sample concentration (right).

Table 3-2 CV from triplicate SRM MS analyses of Kemptide and Angiotensin II at each concentration for selected SRM transitions.

Sample Concentration (Mol/L)	Kemptide (386.7-567.4)	Angiotensin II (523.8-784.5)
	Peak area (%CV)	Peak area (%CV)
5.00E-11	9.3	25
1.00E-10	3.0	21
2.50E-10	16	6.1
5.00E-10	2.8	24
1.00E-09	13	29
5.00E-09	16	3.3
1.00E-08	11	15
5.00E-08	12	24
1.00E-07	8.5	16
5.00E-07		4.8

3.4 Conclusion

This study demonstrates the online coupling of CITP/CZE separations with triple quadrupole-based SRM MS by using a high efficiency interface. A LOQ of less than 50 pM was demonstrated using a mixture of 3 peptides spiked in a BSA digest sample matrix at different concentrations. A linear dynamic range of 4 orders of magnitude was achieved with excellent reproducibility. The relatively short (30 min) analysis time using CITP/CZE-ESI-SRM MS also makes it suitable for high throughput sample analysis. We also noted the importance of the peptide selection in the optimum CITP/CZE-ESI-SRM MS quantitation due to the different peptide focusing abilities and ionization efficiencies. The selection of peptide SRM transition and optimization of CITP/CZE-ESI-SRM MS operating condition largely dictated the achievable instrument LOQ.

3.5 Acknowledgements

We thank Dr. Yuqian Gao and Dr. Ioan Marginean and Dr. Erin Baker for help with Agilent triple quadrupole MS operation, ESI emitter etching and sample preparation. This work was partially supported by grants from the National Institutes of Health: National Cancer Institute (1R33CA155252), National Institute of General Medical Sciences (8 P41 GM103493-10) and partially supported by the grants from National Cancer Institute (R21 CA143177) and National Institute of General Medical Science (R21 GM103536). All the experiments were performed in the Environmental Molecular Sciences Laboratory, a U.S. DOE national scientific user facility located at the Pacific Northwest National Laboratory (PNNL) in Richland, Washington. PNNL is a multi-program national laboratory operated by Battelle for the DOE under Contract DE-AC05-76RL01830.

Chapter 4 : CITP/CZE-nanoESI-SRM MS via a Novel Sheathless Interface for High Sensitivity Sample Quantification

This is an independent work accomplished by me under guidance of Dr. Cheng Lee, Dr. Richard Smith and Dr. Keqi Tang.

4.1 Introduction

Capillary electrophoresis mass spectrometry (CE-MS) has been an attractive analytical technique since its inception[86,162,163] due to its high separation efficiency, broad sample compatibility and high sensitivity detection. The utility of the CE-MS has been well demonstrated in e.g., proteomics[169,180], metabolomics[155,181] and peptidomics[182] for performing glycoform profiling of intact proteins[183,184], metabolomic profiling of clinical samples[185-187] protein phosphorylation studies[188,189]. Key reasons that CE-MS is still not considered as the method of choice in the routine chemical or biological sample analysis compared to more conventional liquid chromatography (LC)-MS are its small sample loading capacity and less robust interface. Seeking effective solutions to these two challenge problems continues to be a primary focus of research and development in CE-MS instrumentation.

Capillary electrophoresis is intrinsically a small scale separation technique with a total volume of typically less than several microliters. The sample loading capacity in a typical capillary zone electrophoresis (CZE) separation is about 1% of the total capillary volume as required to maintain a good separation quality, which limits the sample loading volume to the nanoliter range. While small sample consumption is advantageous when sample amount is strictly limited, it is more often a drawback limiting the measurement dynamic range. To overcome this limitation, transient capillary isotachophoresis (CITP/CZE) was developed to increase the sample loading capacity through *in situ* sample enrichment[137]. A sample loading capacity over 30% of the total separation capillary volume has been demonstrated for CITP/CZE separations[73,137,190-192], increasing the sample loading volume to several microliters. In addition, the capability of CITP/CZE in selectively enriching low abundance analytes in a complex mixture also makes the technique effective in many biological applications as important disease related biomarkers often exist in a complex biomatrixes at extremely low abundances[73,75]. However, in order to achieve microliter sample loading volumes, larger i.d. (> 75 μm) separation capillary are needed, which poses a new challenge to the CITP/CZE-MS interface design. The most efficient CITP/CZE-MS interface benefits from the use of a smaller i.d. (< 30 μm) capillary emitter to operate electrospray ionization (ESI) in the nanoliters per minute flow rate range (nanoESI) as it is well documented that nanoESI both improves analyte ionization efficiency[97] and reduces ionization bias[98].

Online coupling of CE with MS is typically achieved by using a sheath liquid[87] or a sheathless interface. In the sheath liquid interface, either a sheath liquid flowing coaxially with the separation liquid or a liquid-junction[91,170,177] at the ESI emitter tip is used to

provide the electric contact for ESI voltage. Sample dilution due to the use of sheath liquid limits the achievable sensitivity. To overcome this problem, several sheathless interface designs were developed in which the electric contact for ESI voltage was realized by using a special metal[73,100], conductive polymer[101] and carbon[102] coated ESI emitter or inserting a metal wire into the CE separation capillary[103]. Other alternative sheathless interface designs involving the use of a micro-tee[193] or a stainless tubing[104] to connect the separation capillary with the ESI emitter to close electrical circuit for CE separation voltage and ESI voltage have also been reported. However, these interface designs, sheath liquid or sheathless, all suffer from one or multiple problems including sample dilution, low mechanical robustness, and poor reproducibility. The latest sheathless interface design developed by Moini using a chemically etched porous ESI emitter[105] showed a much improved CE-MS performance. This interface design has been recently commercialized by Beckman Coulter (Brea, CA), and has led to several successful applications[106-108,110,112,183,185,194,195]. While this latest sheathless interface design effectively addresses several of the common problems of earlier interface designs, the sample loading capacity is still limited by the need to use small i.d. separation capillary in order to accommodate stable nanoESI operation.

Here we report the development of a new sheathless CITP/CZE-MS interface design that combines the capability for large sample loading volume with stable nanoESI operation. The new interface effectively resolves the mismatch of existing interface designs between the need to use large i.d. separation capillary for large sample loading capacity and small i.d. emitter capillary for stable nanoESI operation. The overall novelty of the interface design includes a large bore separation capillary for large sample loading capacity, a

dilution free sheathless interface using porous emitter and a smaller emitter capillary for robust nanoESI operation. Detailed characterization of the new interface was performed to show its achievable sample loading capacity, separation peak capacity, reproducibility, and detection sensitivity. The use of the new sheathless CITP/CZE-MS interface to quantify targeted peptides in bovine serum albumin (BSA) digest matrix and its achievable system limit is also systematically evaluated in the study. Since the main focus of this study is on characterizing the new sheathless CITP/CZE-MS interface technology, samples with intermediate complexity were used in all the experiments. A follow up study will focus on the biological applications of this new interface technology using more complex human serum and plasma samples.

4.2 Experimental Section

4.2.1 Chemicals

BSA tryptic digest standard was purchased from Protea (Morgantown, WV). Bradykinin, angiotensin I, neurotensin, fibrinopeptide, substance P, kemptide, leu-enkephalin, angiotensin II, melittin, renin, ammonium acetate, methanol, acetic acid and hydrofluoric acid (49%) (HF) were purchased from Sigma (St. Louis, MO). Fused silica capillaries were purchased from Polymicro Technologies (Phoenix, AZ). Epoxy (EP42HT-2) was purchased from Masterbond (Hackensack, NJ).

4.2.2 Sample Separation

BSA tryptic digest standard was purchased from Protea (Morgantown, WV). Bradykinin, angiotensin I, neurotensin, fibrinopeptide, substance P, kemptide, leu-enkephalin,

angiotensin II, melittin, renin, ammonium acetate, methanol, acetic acid and hydrofluoric acid (49%) (HF) were purchased from Sigma (St. Louis, MO). Fused silica capillaries were purchased from Polymicro Technologies (Phoenix, AZ). Epoxy (EP42HT-2) was purchased from Masterbond (Hackensack, NJ).

A stock solution of ten peptide mixture (bradykinin, angiotensin I, neurotensin, fibrinopeptide, substance P, kemptide, leu-enkephalin, angiotensin II, melittin, and renin) at 10 μM concentration for each peptide was first prepared in deionized water and stocked in aliquots. The stock solution was subsequently diluted to 3.75 μM using LE solution to serve as a working solution for the performance evaluation and optimization of the online sheathless CITP/CZE-nanoESI-MS platform. The stock solution of ten peptide mixture was further mixed with 50 nM BSA tryptic digest in 25 mM LE at different concentrations ranging from 10 pM to 500 nM for each peptide in the CITP/CZE SRM MS sample quantification experiments. Among the 10 peptides in the sample mixture, leu-enkephalin, angiotensin II and kemptide were selected as representative targets in CITP/CZE-selected reaction monitoring (SRM) MS experiments due to their good signal intensity displayed in our previous study[190].

4.2.3 Sheathless CITP/CZE-MS Interface

The upper part of Figure 4.1 shows the experimental setup used in this study which is a modified setup used in our previous work.[1] Briefly, one end of the separation capillary was inserted in a sealed reservoir for hydrodynamic sample loading or system flushing as well as the application of separation voltage while the joint between the other end of the separation capillary and porous emitter capillary was enclosed in a metal tube containing electrically conductive liquid using a peek cross. A syringe filled with conductive liquid

was also connected to the peek cross to fill and refresh the metal tube prior and between each sample analysis. A second ESI voltage was applied directly on the metal tube and the CITP/CZE-nanESI was interfaced with a triple quadrupole mass spectrometry. The new sheathless CITP/CZE-MS interface design, as shown in the lower part of Figure 4.1, involves the use of two different capillaries. A larger i.d. fused silica capillary (360 μm o.d., 100 μm i.d., and 95 cm long) was used as the separation capillary with its inner surface coated with hydroxypropyl cellulose to minimize electroosmotic flow. The coating was prepared by first flushing capillary with 1 mL 1M HCL, by applying 15 psi N_2 back pressure to the solvent reservoir, and then flushing 200 μl 5% hydroxypropyl cellulose using 20 psi N_2 back pressure. Finally, the capillary was flushed with deionized water to remove excessive hydroxypropyl cellulose. A smaller i.d. capillary (90 μm o.d., 20 μm i.d., and ~4 cm long) was used as ESI emitter.

A section of the emitter capillary, ~ 3 cm long from one end, was chemically etched to make it porous using the method described by Moini [105] to provide electric contact and serve as ESI emitter without further sharpening the emitter tip (etching experiments using HF must be conducted in hood. Goggle, rubber gloves and aprons are required for personnel protection), and the other end of the emitter capillary was subsequently inserted into the separation capillary. The assembly was then sealed by carefully wrapping the acid resistant epoxy around the joint and the epoxy was cured at room temperature overnight. Extended epoxy cure time at elevated temperature may be needed if dealing with stronger acid and is optional with the current setup in this study. The joint was then enclosed in a short metal tube (0.04" i.d., 1/16" o.d., and 5 cm long) filled with the contact solution of 2% (by volume) acetic acid in deionized water to form a

sheathless CITP/CZE MS interface. The interface contact solution was refreshed after each CITP/CZE MS sample analysis to ensure a good electric contact for the measurement reproducibility.

Due to the existence of size change at the capillary joint, it is important to keep all the connecting union and cross clean to prevent capillary blockage. Moreover, buffers and samples should be prepared with filtered deionized water. Prior to each run, the separation capillary was filled with BGE solution and flushed for 15 min by applying 15 psi back pressure in the BEG reservoir (Figure 4.1). Samples were loaded into the separation capillary at the same back pressure with the loading amount adjusted by varying the length of loading time. After sample loading, the sample reservoir at the capillary inlet was replaced by the BGE reservoir and a 30 kV separation voltage was applied to the sample inlet using a Glassman high voltage power supply. A second voltage varying from 1.5 to 1.7 kV was applied to the metal tube at the emitter end of the capillary for stable electrospray operation using a Bertan high voltage power supply. The ESI voltage was adjusted for each emitter capillary to achieve optimum sensitivity and signal stability at each CITP/CZE flow rate. Position of the emitter relative to the MS inlet was also optimized for best signal intensity and stability. During CITP/CZE analysis, a smaller gas pressure varying from 1 psi to 3 psi, referred as eluting pressure, was applied at the BGE reservoir to maintain a stable flow rate in the low nL/min range.

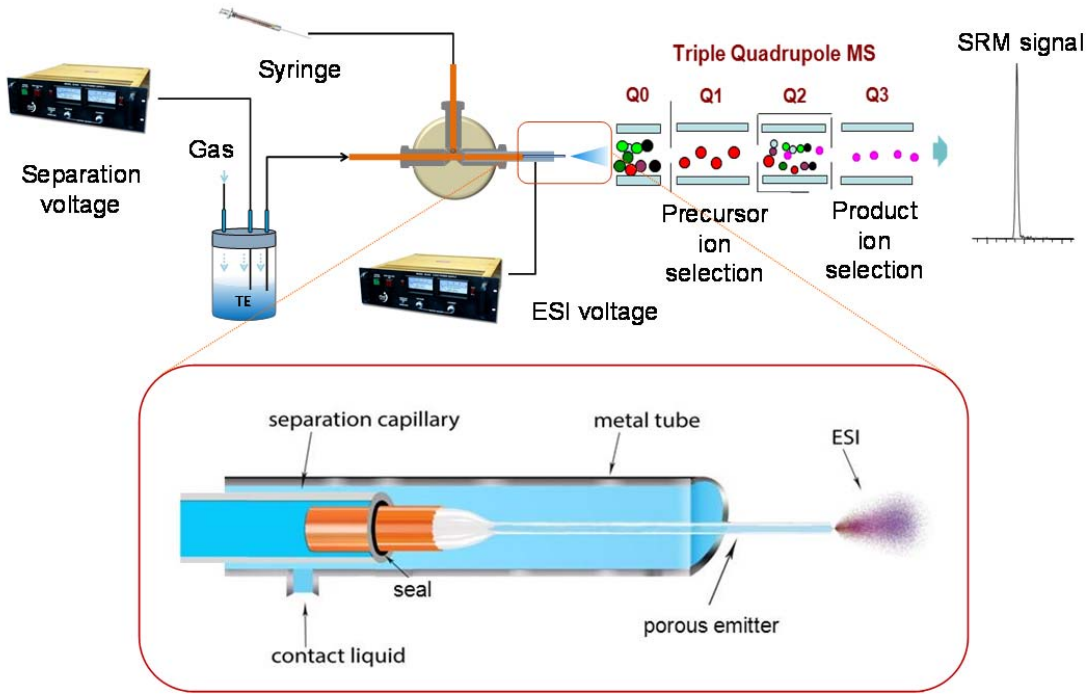

Figure 4.1 Schematic of CITP/CZE-nanoESI-QQQ MS setup used in this study. Lower part shows a detailed view of the sheathless interface design (not to scale).

The new sheathless CITP/CZE-MS interface developed in this study has the benefit of achieving both large sample loading capacity and dilution free nanoESI operation simultaneously for significantly better sensitivity. The detachable design between the large i.d. separation capillary and small i.d. ESI emitter capillary also provides more flexibility in accommodating different experiment requirements. As the separation capillary and emitter capillary are prepared separately, the sizes of the separation capillary and emitter capillary can be altered independently and special treatment of the separation capillary can be performed easily. In addition, the porous emitter can be readily replaced without the need to change the separation capillary with little effort in case of blockage or broken emitter.

For the performance comparison, a sheathless CITP/CZE-MS interface using a single capillary (140 μm o.d., 30 μm i.d., and 95 cm long) was also prepared. The capillary was first neutrally coated with hydroxypropyl cellulose and a 3 cm section from one end of the capillary was then chemically etched to porous. The sample loading volume and eluting pressure was adjusted to obtain the optimum operating conditions for the interface.

4.2.4 Flow Rate Calibration

To correctly determine the liquid flow rate based on the gas pressure applied at the separation capillary inlet reservoir, the complete CITP/CZE setup was first calibrated experimentally. The liquid flow rates at different gas pressures were determined by using a calibrated pipet (1 to 5 mL, Drummond Scientific, Broomall, PA) to collect the liquid exiting the ESI emitter and measure the time for collecting 1 μL liquid under a given gas pressure. The experimental measurements showed a linear dependence of liquid flow rate

on the gas pressure (Figure 4.2). Prior to each CITP/CZE-ESI-MS experiment, the flow rate at 15 psi gas pressure was measured so that the sample loading time and the eluting pressure could be adjusted accordingly to ensure the reproducibility of the sample loading volume and ESI flow rate.

4.2.5 MS Optimization and Data Processing

All the CITP/CZE-nanoESI-MS analyses were performed using a triple quadruple mass spectrometer (TSQ Quantum ultra, Thermo Fisher Scientific, MA). The inlet capillary of the mass spectrometer was maintained at 200 °C. Unit resolution (0.7 Da peak width) was used for Q3 in full scan MS and for both Q1 and Q3 in SRM operating mode. All the MS spectra were recorded in profile mode. In full scan MS mode, m/z range from 300 to 1400 was used with a scan time of 0.3 sec. Three most intense transitions and their corresponding collision energies for each targeted peptide in CITP/CZE-nanoESI-SRM MS sample quantification experiment were determined by using a fully automated compound optimization procedure in Thermo TSQ Tune view. Table 1 listed all the transitions and their corresponding collision energies for six targeted peptides used for sample quantification in which three peptides from BSA digest were used as quality control analytes to ensure measurement reproducibility.

All the data analyses of the raw MS files were carried out using Thermo Xcalibur Qual Browser 2.2. In the chromatogram ranges setting, peak algorithm was selected as ICIS. No smoothing or baseline subtraction was used and the default setting was used for mass tolerant. Auto peak detection with default parameters was used for all the peak extraction and peak area measurement while manual integration was also used to verify all the peak area measurements.

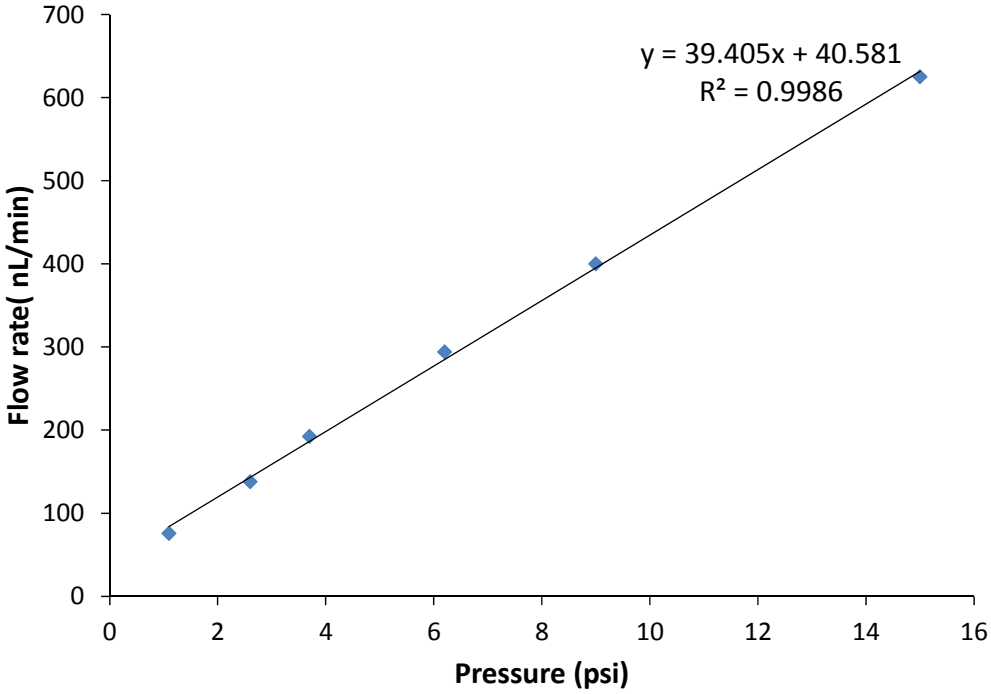

Figure 4.2 Measured liquid flow rate as a function of gas pressure applied at the inlet of the CITP/CZE separation capillary.

4.3 Results and Discussion

4.3.1 Sample Loading Optimization

The performance of the new CITP/CZE-MS interface was first evaluated for its sample loading capacity and separation quality. CITP/CZE separations were carried out under different sample volumes ranging from 0.27 μL to 3.07 μL using a 10 peptide mixture (3.75 μM concentration for each peptide) in 25 mM ammonium acetate. Sample loading volume was varied by adjusting the loading time at a given gas pressure (15 psi) as calculated according to the flow rate calibration described in the experimental section. Figure 4.3 shows the extracted ion chromatogram (EIC) at different sample loading volumes with the ESI flow rate measured at 60 nL/min. Well focused narrow peaks were achieved except two late eluting peaks (peak 9 and 10 in Figure 4.3) as focusing factor decreases as the electric mobility of analyte ion decreases. The focusing factor of the later eluting peptides can be further increased by increasing the LE concentration[190]. Baseline separation of the ten peptides was achieved at sample loading volumes of 1.39 μL (Figure 4.3A) and 1.95 μL (Figure 4.3B), which equal to 18% and 26% of the total separation capillary volume respectively. Good separation was still achieved even at 2.5 μL sample loading volume which accounted for 33% of the total capillary volume (Figure 4.3C). Significant peak overlapping and loss of separation quality was observed at the sample loadings beyond 2.5 μL due to incomplete CITP sample focusing and insufficient separation time. The loading capacity result shown in Figure 4.3 is consistent with our previous study using a sheath liquid interface[190] in which up to 1/3 of the total separation volume was allowed in CITP/CZE before a significant loss of separation quality was observed. The consistency between these two studies using completely different

interfaces implies that the size change from 20 μm to 100 μm at the junction between the emitter capillary and the separation capillary in the current sheathless interface has minor effect on the separation quality. A possible explanation could be that the analyte band speed under the experimental operating condition was significantly faster than the speed of the liquid flow, providing effective analyte peak compression in the ESI process. Despite some overlapping and peak broadening of the late eluting peaks 9 and 10 at 2.5 μL sample loading volume (Figure 4.3C), a separation window of more than 20 minutes was observed for all the sample loading volumes shown in Figure 4.3. In addition, the signal intensity keeps increasing as the sample loading volume increases. Since all of our selected peptide targets in the following sample quantification study elute much earlier than peaks 9 and 10, unless specified otherwise, 2.5 μL (33%) sample loading volume was chosen in all the subsequent experiments to maximize the measurement sensitivity. It was also observed experimentally that the CITP/CZE separation quality at a given sample loading volume improves as the analyte concentration decreases due to improved CTIP focusing[1].

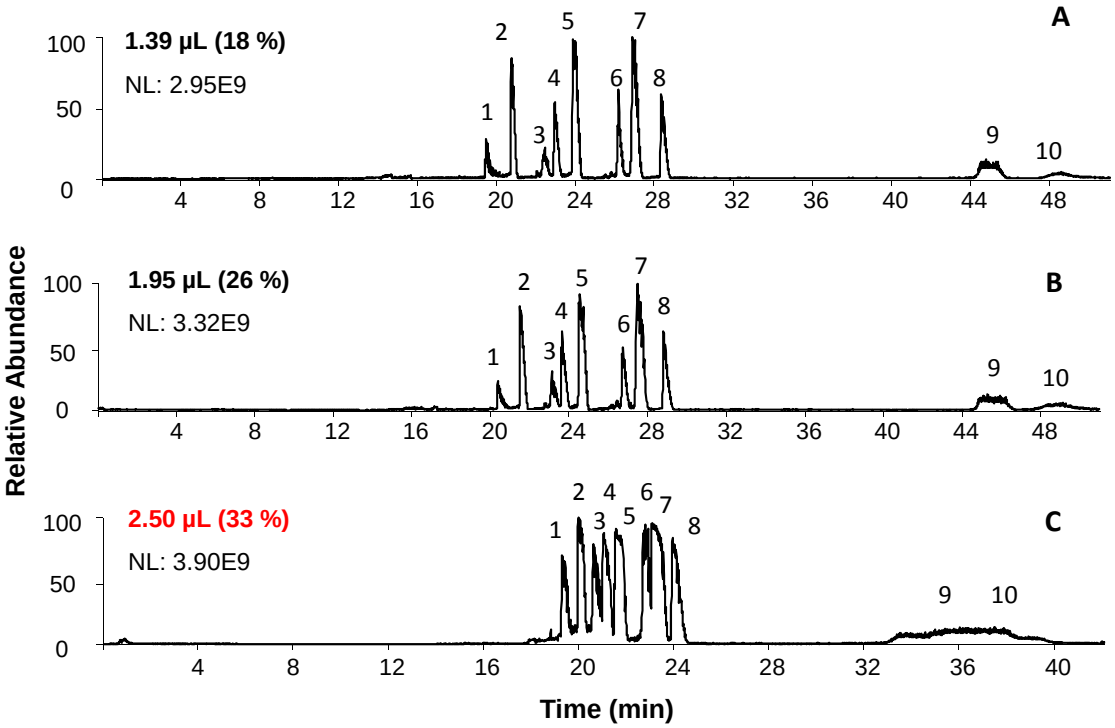

Figure 4.3 Extracted ion chromatograms (EICs) of CITP/CZE separations using a 10 peptide mixture solution at different sample loading volumes.

The labeled peaks from 1 to 10 are melittin, kemptide, substance p, bradykinin, angiotensin I, renin, neurotensin, angiotensin II, leu-enkephalin, and fibrinopeptide A, respectively.

Table 4-1 SRM transitions and parameters used in this study.

Compound Name	Sequence	Precursor Ion (m/z)	Product Ion (m/z)	Dwell Time (msec)	Collision Energy (V)
Leu-enkephalin	**[YGGFL+H]$^{+}$**	**556.3**	**397.2 (a_4^+)**	**25**	**19**
		556.3	425.2 (b_4^+)	25	16
		556.3	278.1 (b_3^+)	25	25
Angiotensin II	**[DRVYIHPF+2H]$^{2+}$**	**523.8**	**263.1 (y_2^+)**	**25**	**20**
		523.8	784.4 (b_6^+)	25	18
		523.8	647.4 (b_5^+)	25	22
Kemptide	**[LRRASLG+2H]$^{2+}$**	**386.7**	**567.3 (b_5^+-NH_3)**	**25**	**18**
		386.7	409.3 (b_3^+-NH_3)	25	25
		386.7	539.4 (a_5^+-NH_3)	25	22
BSA peptide I	[LVNELTEFAK+2H]$^{2+}$	582.3	951.5 (y_8^+)	25	18
		582.3	595.3 (y_5^+)	25	20
		582.3	837.4 (y_7^+)	25	16
BSA peptide II	*[HLVDEPQNLIK+2H]$^{2+}$*	*653.4*	*712.4 (y_6^+)*	*25*	*26*
		653.4	251.2 (b_2^+)	25	26
		653.4	1056.7 (y_9^+)	25	23
BSA peptide III	[CCTESLVNR+2H]$^{2+}$	512.7	637.2 (b_6^+)	25	17
		512.7	581.7 (a_6^+ - 28)	25	16

The bolded transitions indicate the transition used for quantification of each peptide. The non bolded/italicized transitions were used to confirm the peptide's identity. The italicized transition of BSA peptide was used to monitor the platform's reproducibility and calibration.

4.3.2 Performance Characterization of the Sheathless CITP/CZE-MS Interface

Following the initial sample loading volume optimization, the CITP/CZE- QQQ MS instrumental platform with the new sheathless interface was characterized systematically using the ten peptides spiked in 50 nM BSA digest in 25 mM LE at different concentrations. The mass spectrometry was operated in a highly sensitive SRM mode in which specific precursor-to-fragment ion transitions were monitored for each analyte in the sample solution. Three peptides (leu-enkephalin, kemptide and angiotensin II) in the sample mixture were chosen as the representative peptide targets in this study due to their good electrospray ionization efficiencies from our previous study[190] and three peptides from BSA digest were also chosen to evaluate the stability of the instrument platform. Three most abundant transitions for each selected peptide, as listed in Table 4-1, were monitored in all the CITP/CZE-SRM MS analyses.

The advantage of analyte focusing was evaluated by comparing CITP/CZE with CZE at the same sample loading volume. With 2.5 μL sample loading and identical experimental setup as well as operating parameters, a broad kemptide peak with a flat top peak intensity caused by the long sample plug was resulted from CZE operation. In contrast, a sharp narrow peak was obtained in CITP/CZE separation mode which displays a 77 times higher peak intensity implying an approximately two orders of magnitude gain in signal intensity in CITP/CZE mode as compared to CZE only mode (Figure 4.4).

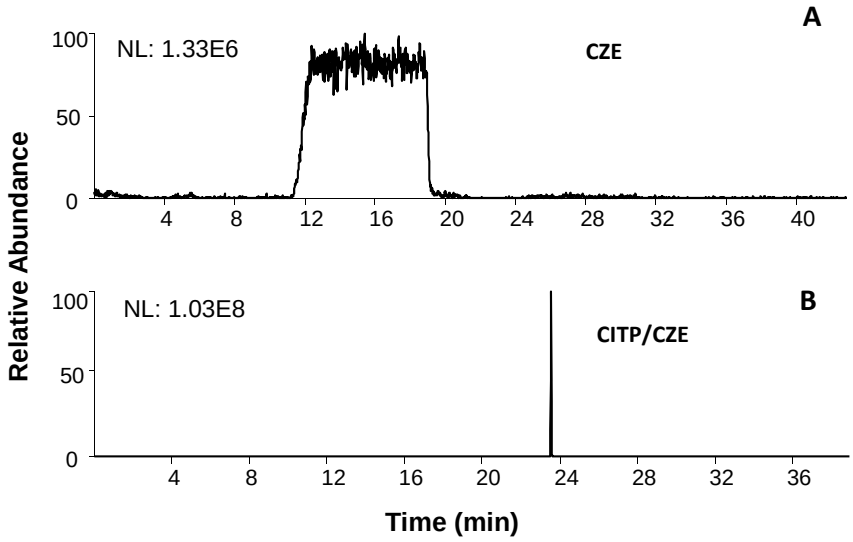

Figure 4.4 EICs for kemptide from A) CZE-MS and B) CITP/CZE-MS analyses.

Sample condition: 2.5 μL of 50 nM peptide in 50 nM BSA digest using solvent 0.1 M acetic acid in deionized water for CZE and 2.5 μL of 50 nM peptide in 50 nM BSA digest using 25 mM ammonium acetate in deionized water for CITP/CZE.

One of the unique features of the new sheathless CITP/CZE-MS interface developed in this study is its capability to use large i.d. separation capillary for increased sample loading volume and small i.d. emitter capillary for stable nanoESI operation simultaneously, both which are critical to the sensitivity achieved. This is evident by comparing the performance of the new interface with a conventional sheathless CITP/CZE-MS interface in which a single capillary (30 μm i.d., 360 μm o.d., and 95 cm long) was used for both CTIP/CZE separation and nanoESI operation[113,195].The same sample as in the focusing experiment (Figure 4.4) was used for the evaluation. With the same 33% of the sample loading volume with respect to the total capillary volume, 220 nL sample was loaded using the conventional sheathless CITP/CZE-MS interface while 2.5 μL sample was loaded using the new sheathless CITP/CZE interface. Separations in both interface configurations were performed under equal linear velocity of 0.75 cm/min to achieve similar separation quality, corresponding to 60 nL/min in the new interface and 5 nL/min in the conventional single capillary interface. Figure 4.5 shows the sensitivity comparison between these two interfaces using kemptide EIC. While similar peak widths were observed for both interface configurations, the kemptide peak intensity using the new CITP/CZE-MS interface (Figure 4.5A) shows a 11 fold improvement as compared to using the conventional sheathless CITP/CZE-MS interface (Figure 4.5B), which is consistent with the increase of the sample loading volume using the new interface.

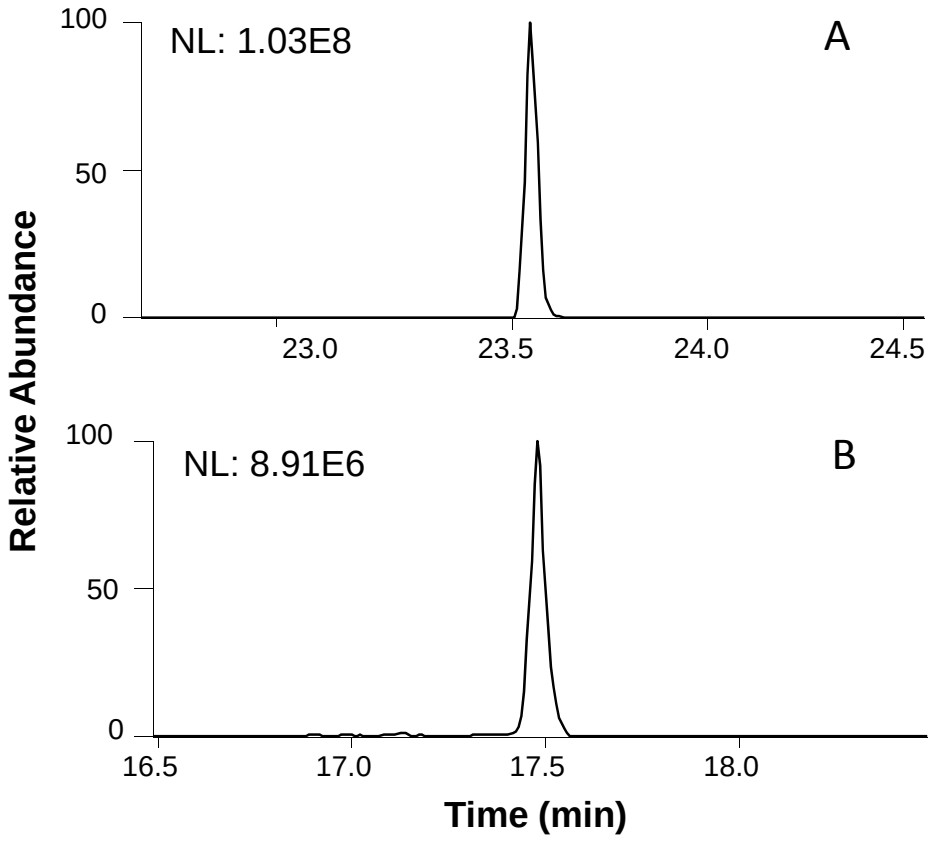

Figure 4.5 Sensitivity comparison of kemptide EIC using interfaces with different sizes

A) the new sheathless CTIP/CZE-MS interface with a 100 μm i.d. separation capillary and a 20 μm i.d. ESI emitter, and B) a conventional sheathless CITP/CZE-MS interface with a single 30 μm i.d. capillary for both CITP/CZE separation and ESI emitter. Sample condition: 50 nM target peptides spiked in 50 nM BSA digest in 25 mM LE.

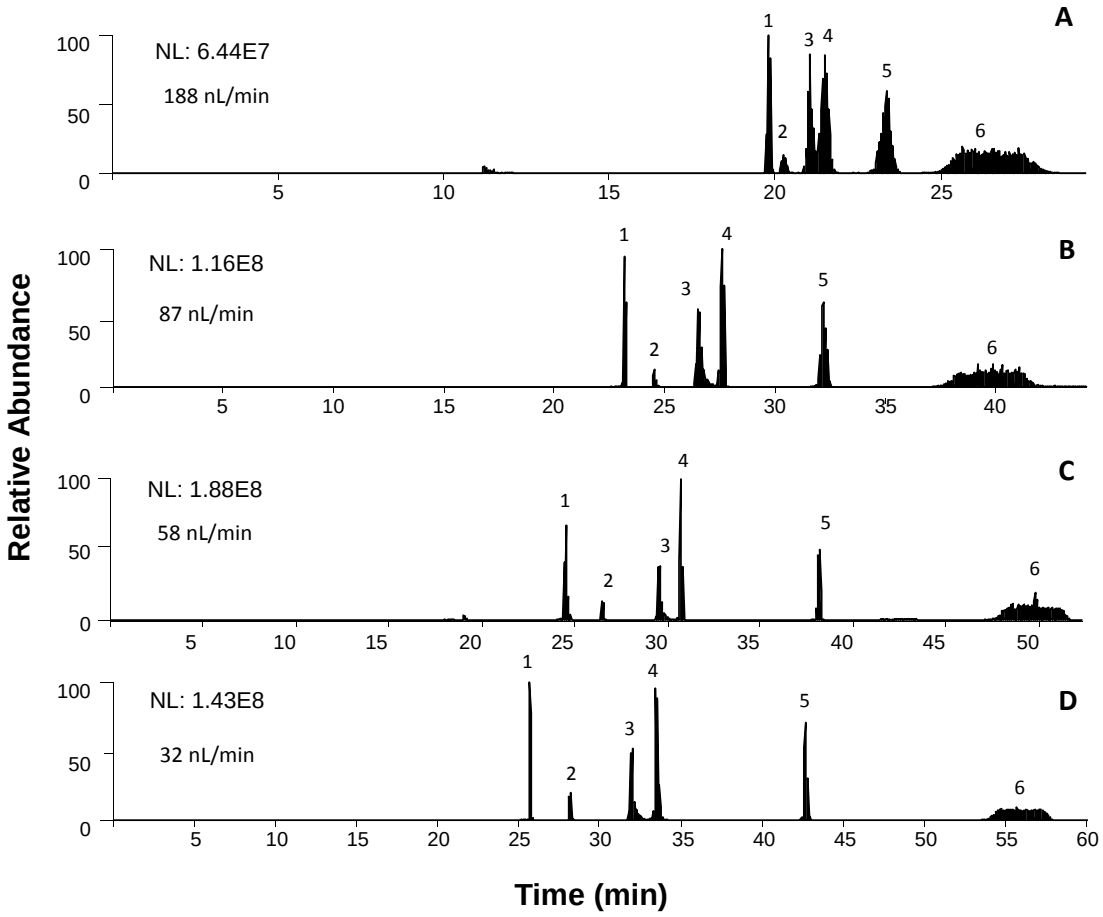

Figure 4.6 SRM TIC of CITP/CZE separations at different flow rates.

The labeled peaks from 1 to 6 are kemptide, BSA peptide III, BSA peptide II, angiotensin II, BSA peptide I, and leu-enkephalin, respectively. Sample condition: 50 nM target peptides in 50 nM BSA digest and 25 mM LE.

The benefit of operating electrospray at reduced flow rate was further demonstrated by operating the sheathless CTIP/CZE-ESI-SRM MS at different flow rates ranging from 30 nL/min to 377 nL/min. Figure 4.6 shows the total ion chromatogram (TIC) for kemptide, angiotensin II, leu-enkephalin and three selected BSA peptides from the CTIP/CZE-ESI-SRM MS analyses using the new sheathless interface at four representative ESI flow rates of 188 nL/min, 87 nL/min, 58 nL/min and 32 nL/min, respectively. As the flow rate decreased from 188 nL/min (Figure 4.6A) to 32 nL/min (Figure 4.6D), the effective separation window for all six monitored peptides increased from 10 min to 33 min and all the peptide peaks became increasingly separated from each other indicating a higher separation resolution at a lower ESI flow rate. The best CITP/CZE separation was achieved at 32 nL/min while a complete loss of separation was observed at the flow rate exceeding 261 nL/min.

Figure 4.7 further shows the change of peak elution time, peak width and peak intensity as a function of ESI flow rate. While the retention time for all the peptide peaks consistently increases with the decrease of the ESI flow rate (Figure 4.7A), the peak widths remain essentially unchanged (Figure 4.7B). More importantly, the intensity for all the peptide peaks increases as the flow rate decreases (Figure 4.7C) down to 58 nL/min because of higher ESI efficiency at lower flow rate. The observed decrease of the peak intensity at 32 nL/min flow rate for angiotensin II and leu-enkephalin relative to the peak intensity at 58 nL/min might be related to the stability of the electrospray implying an even smaller i.d. ESI emitter is needed. The peak capacity of the CITP/CZE separation can be also estimated based on the experimental measurements shown in Figure 4.6 and Figure 4.7. In Table 4-2, the peak capacity at different flow rates was calculated using the

average peak width at half peak height for five peptide peaks with Leu-enkephalin peak (peak 6) excluded from the peak width calculation due to its incomplete focusing. A peak capacity as high as over 200 was estimated for the sheathless CITP/CZE separation at 32 nL/min and good separation efficiency can be maintained at ESI flow rate lower than 100 nL/min.

4.3.3 Targeted Peptide Quantification

The analytical utility of the sheathless CITP/CZE-SRM MS was further evaluated for its linear dynamic range, limit of quantification (LOQ), and reproducibility. Triplicate analyses were performed using peptides (Table 4-1) spiked in 50 nM BSA digest at different concentrations from 10 pM to 500 nM. Flow rate of 60 nL/min was used in the CITP/CZE-SRM MS quantification due to the overall good ESI stability, peak capacity and sensitivity as discussed above. Quantification of each peptide was carried out using the most abundant transition (bolded in Table 4-1). One additional BSA peptide (italicized in Table 4-1) was also monitored as "internal standard" during each CITP/CZE-ESI-MS analysis to ensure the measurement stability and correct the small variations of run to run sample loading volume and analyte peak intensity.

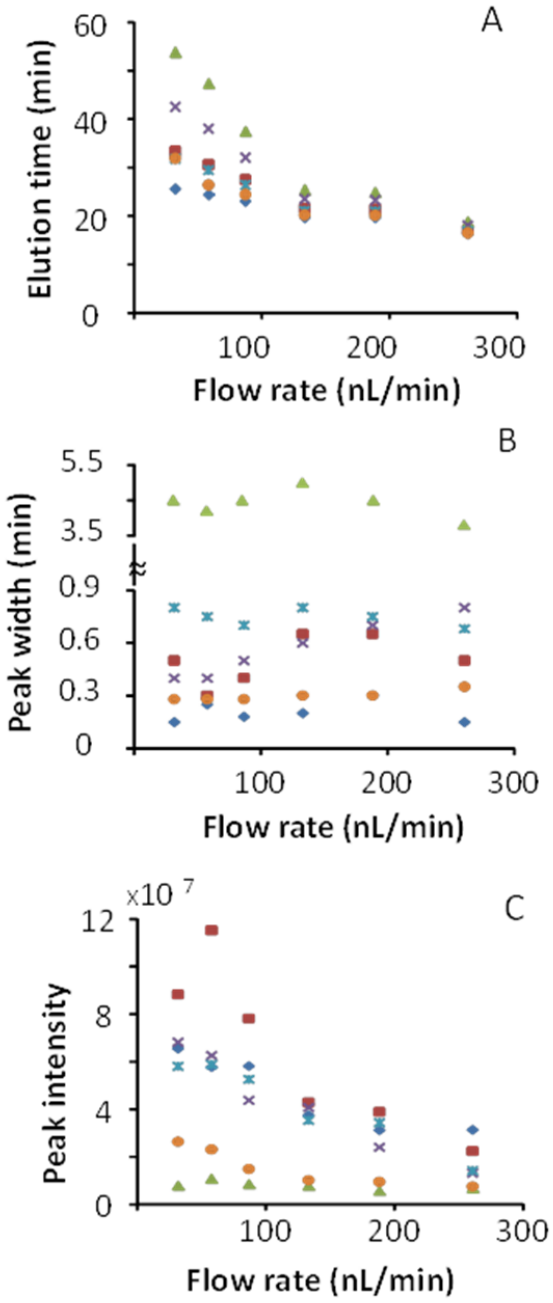

Figure 4.7 CITP/CZE peak elution time (A), peak width (B) and peak intensity (C) at different flow rates.

kemptide (◆), angiotensin II (■), leu-enkephalin (▲), BSA peptide I (×), BSA peptide II (✱), and BSA peptide III (●).

Table 4-2 Peak capacity under different flow rates.

Peak width at half height (min)					Average	Separation window (min)	peak capacity
kemptide	BSA peptide III	Angiotensin II	BSA peptide I	BSA peptide II			
0.055	0.090	0.137	0.130	0.100	0.102	18 - 28	176 - 275
0.085	0.099	0.074	0.131	0.130	0.104	15 - 23	144 - 221
0.068	0.105	0.154	0.180	0.138	0.129	10 - 14	76 - 109
0.055	0.117	0.186	0.340	0.095	0.159	6	38
0.070	0.130	0.206	0.210	0.092	0.142	5	35
0.031	0.095	0.247	0.330	0.175	0.176	3	17

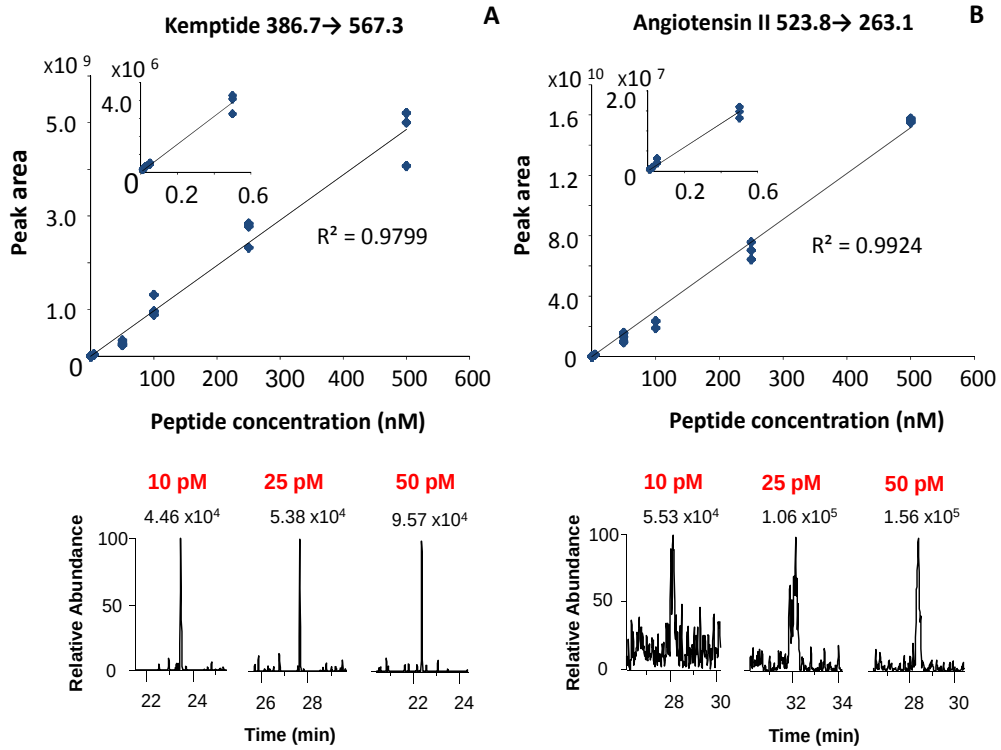

Concentration (nM)		0.010	0.025	0.05	0.5	5	50	100	250	500
CV (%)	Kemptide	12	8	6	11	22	15	18	9	10
	Angiotensin II	1	8	22	8	6	21	10	7	1

Figure 4.8 CITP/CZE-SRM MS quantification of kemptide (A) and angiotensin II (B) in BSA digest matrix.

Top: Calibration curve between peak area and sample concentration; Middle: EICs from SRM measurements at 10 pM, 25 pM, 50 pM sample concentrations; Bottom: peak area CV at different concentrations.

Figure 4.8 shows the CITP/CZE-nanoESI-SRM MS quantification results for kemptide (Figure 4.8A) and angiotensin II (Figure 4.8B). Good linearity ($R^2 > 0.97$) for both targeted peptides between the concentration and peak area was observed in the concentration range from 10 pM to 500 nM, indicating 4.5 orders of magnitude linear dynamic range. Based on the signal-to-noise ratio (S/N) and the measurement CV shown in Figure 4.8, The LOQs for both kemptide and angiotensin II is estimated to be at 10 pM which corresponds to 25 attomoles total sample loading. The LOQ for kemptide is significantly better than the LOQ for angiotensin II mainly due to the better CITP focusing and lower chemical background for kemptide. The LOQ for leu-enkephalin was estimated to be about 500 pM (data not shown) due to insufficient CITP focusing. Good measurement reproducibility was also observed as the CVs for all the peak area and peak elution time measurements were less than 22 % and less than 10% respectively (Table 4-3).

Table 4-3 Retention time deviation of triplicate CITP/CZE-SRM MS analyses at different sample concentrations.

Concentration (Mol/L)	Kemptide	Angiotensin II	Leu-enkephalin	BSA peptide III	BSA peptide II	BSA peptide I	Average
1.0E-11	7%	2%		2%	3%	0%	3%
2.5E-11	5%	8%		6%	7%	9%	7%
5.0E-11	5%	5%		5%	5%	6%	5%
5.0E-10	9%	9%	10%	9%	9%	9%	9%
5.0E-09	5%	6%	0%	6%	6%	8%	5%
5.0E-08	5%	7%	7%	6%	6%	7%	6%
1.0E-07	4%	5%	0%	5%	5%	0%	3%
2.5E-07	1%	2%	4%	1%	2%	3%	2%
5.0E-07	9%	2%	1%	9%	2%	2%	4%
Average	6%	5%	4%	5%	5%	5%	

4.4 Conclusion

A detailed experimental evaluation of the new sheathless CITP/CZE-MS interface in this study showed its capabilities of both high sample loading capacity and stable nanoESI operation and demonstrated its utility in achieving high sensitivity CITP/CZE-nanoESI SRM MS sample quantification. Sample loading volume in μL range for CITP/CZE separation is provided by using a large bore separation capillary in the new interface without the degradation of separation quality, enabling a sample loading capacity comparable to that in typical nanoLC separations. The new interface also allows stable, dilution free ESI operation at low nanoliters per minute flow rate which was shown to simultaneously improve the CITP/CZE separation quality and MS detection sensitivity. The high accuracy for sample quantification (CV < 22%) and the low picomolar LOQ using the new sheathless CITP/CZE-ESI-SRM MS instrument platform make it suited for high sensitivity quantitative sample analysis. This sheathless CITP/CZE-MS interface design can be easily coupled to multiple mass spectrometers or used in different CE operation modes for ultrasensitive analysis. It may also provide a basis for coupling with other separation methods to perform multidimensional separations. Our future work will focus on exploring the potential of the new sheathless CITP/CZE-MS for high sensitivity proteomics measurements.

4.5 Acknowledgements

This work was partially supported by grants from the National Institutes of Health: National Cancer Institute (1R33CA155252), National Institute of General Medical Sciences (8 P41 GM103493-10), National Cancer Institute (R21 CA143177), and

National Institute of General Medical Science (R21 GM103536). All the experiments were performed in the Environmental Molecular Sciences Laboratory, a U.S. DOE national scientific user facility located at the Pacific Northwest National Laboratory (PNNL) in Richland, Washington. PNNL is a multi-program national laboratory operated by Battelle for the DOE under Contract DE-AC05-76RL01830.

Chapter 5 : Conclusion

Understanding disease-related changes including protein expression level, post-translational modifications and functional pathway has profound impact in our understanding of how disease occurs and develops, which is essential to develop effective stradegies for disease prevention and treatment. While the conventional discovery based approaches have encountered challenges in obtaining biological and clinical relevant information, a shift in proteomic field began to take place from discovery proteomics to targeted proteomics. Sensitive, reproducible and quantitative analysis focused on a subset of the proteome not only helps to reduce the sample complexity, more importantly it allows researchers to address specific biological questions to their line of inquiry. In addition, targeted proteomics enables matching of the proteomic data to the data mountain generated from high-throughput biology experiments like DNA sequencing and genome analysis for researchers to utilize and build on this knowledge.

Our goal was to demonstrate the application of a CITP/CZE based multidimensional separation platform in targeted tissue proteomic analysis, which provides selective analyte enrichment and high resolving power with minimal interference from the cell heterogeneity in samples. We also wanted to provide a CITP/CZE based hyphenation strategy as an alternative to the nanoLC-MS systems, which would allow ultrasensitive quantitation with optimal enrichment and resolving power while improving the throughput and versatility compared with nanoLC-MS.

5.1 Realization of Research Objectives

5.1.1 Targeted Tissue Proteomic through CITP/CZE Based Multidimensional Platform

Considering sample complexity and cell heterogeneity of human tissues, disease related information can only be obtained from homogeneous cell population that is free from interference and misleading information from unwanted cells. Targeted analysis was performed on homogeneous tumor cells microdissected from astrocytoma tumor tissues using LCM to identify confident biomarker candidate. The selective enriching capability of CITP/CZE towards low abundance analytes in complex protein/peptide mixtures and the intrinsic high resolving power together with LCM displayed a synergetic effort in reducing the complexity as well as the dynamic range of proteins which always pose great challenges in analysis of biological samples.

Comparing other multidimensional separation platform such as MuDPIT which consists of SCX and RPLC as first and second separation, or 2D RPLC which utilizes high pH and low pH RPLC, the CITP/CZE-nanoRPLC-ESI-MS platform demonstrated significant advantages in several aspects. First of all, CITP/CZE provides pre-concentration of analytes which can improve signal intensity with several orders of magnitudes while none of the fore-mentioned separation platform performs sample enriching, let alone selective enrichment which brings the trace analytes to more detectable region of MS. Secondly, CITP/CZE displayed outstanding resolving power with more than 80% of peptides detected only in one fraction, comparing with only 40% in SCX separation as a result of low resolving power. Peptide overlapping in multiple fractions is likely to cause loss of sensitivity because of analyte dilution as well as increasing the chance of peak overlapping in detection. Thirdly, CE and RPLC separate analytes based on different

physiochemical properties generating “orthogonal separation” when coupled together, where co-eluting peptides in one dimension are likely to get well separated in the other dimension. Low pH-high pH-RPLC multidimensional separation, on the other hand, only demonstrates small orthogonality between the two dimensions which in turns would be expected to display inferior separation power comparing with CE-RPLC separation.

The utilization of the CITP/CZE based multidimensional separation platform achieved successive handling of 1 μg of each sample loading and displayed comprehensive identification of more than 3000 unique proteins with 19% attributed to membrane proteins. Comparative proteomics and pathway function mapping allowed identification of confident biomarkers which were further validated using immuno quantification assay.

5.1.2 Online CITP/CZE-ESI-SRM MS for Targeted Quantification

The second goal, of providing ultrasensitive targeted quantification techniques through CITP/CZE was achieved in online coupling with SRM MS via both sheathliquid and sheathless interfaces which demonstrate both robustness and sensitivity. Again, the selective enrichment and high resolving power of CITP/CZE plays a key role in achieving ultrasensitive quantification of target peptides in biological background at LOQ of 10 pM while good CV and S/N was achieved even at the limit point of sample concentration. The online interfacing of CITP/CZE with MS through in house developed interfaces were designed to optimally reserve the enriching factor and resolving power by minimizing sheathliquid dilution and dead volume for peak broadening.

In interface design and development, factors like sample loading capacity, electrolysis interference, firm electric contact and nano flow rate operation in addition to dilution and dead volume were our top concerns. In sheathliquid interface design, we avoided the use

of metal in the main separation path and adopted an off-path waste line to ESI voltage application to eliminate the electrolysis interruption of the separation procedure. And electrokinetic pumped sheathflow was employed instead of pressure pumped flow to operate ESI at nano range. In order to further improve the sensitivity of the platform, a sheathless interface was then developed to substitute the sheathliquid design. We preserved the usage of large bore capillary to ensure the sample loading capacity which is essential to sensitive detection of trace analytes and managed to couple with improved ionization efficiency with nanoESI operation via small size porous emitter. Overall, the work in the chapter 3 and 4 demonstrates the excellent capability of online CITP/CZE-ESI-MS through both sheathliquid and sheathless interface for targeted quantitative analysis, proving the platform to be a potential powerful tool in biomarker validation research field for improved sensitivity and throughput.

5.2 Future Research Directions

5.2.1 Application in Real Samples with High Complexity

Work introduced in Chapter 3 and 4 utilized sample of medium complexity as proof of concept demonstration and was more focused on fundamental aspects of technology development of the online CITP/CZE-ESI-SRM MS platform. Further application of the platform to complex samples like human saliva, plasma or to particular research subjects such as PTM analysis will help validate the capability of the analysis platform within a more specific research context and determine the strength and weakness towards different research objectives where more improvements and adjustment can be inspired and implemented.

Our work on online CITP/CZE-MS for quantitation in SRM mode was the first work published to the best of our knowledge, so it has been hard to test the performance improvement over other existing interfaces or platform. It would be valuable to test same samples on other literature published interfaces or on commercial products with same experiment conditions to get a side-by-side comparison for better understanding of the performance of this platform. Moreover, in order to achieve our goal as to provide a platform as an alternative for current LC-MS system it would be beneficial to conduct a direct comparison between these two platforms to understand the differences and advantages.

5.2.2 Incorporation of LC based separation for multidimensional separation platform

Although we have adopted a multidimensional separation platform as described in Chapter 2, the LC separation performed as the second dimension has always been a bottleneck for higher throughput analysis. Therefore, the length and size of LC column is also limited to obtain reasonable analysis time in trade for separation performance. In addition, the analyte enrichment is compromised during fraction collection where in theory the greatest signal increase is expected.

Concerning the effectiveness of the interface development to couple CITP/CZE with MS and the proven performance, switching the order of CITP/CZE and LC separation should have significant improvement in terms of sensitivity, throughput and provides much room to further improve the performance of the multidimensional separation platform without sacrificing throughput. Firstly, the concentrated analyte bands can be detected in their optimal concentration which will be big advantage toward the low abundance compounds in the sample. Secondly, the dimension of LC separation can be extended and separation

be performed at longer duration to achieve better separation without slowing down the entire throughput. Thirdly, large sample loading is enabled which will in turn benefit the detection sensitivity of trace analytes.

In my future studies, I plan to employ an LC system that is adopted from PRISM system as describe in one of co-workers previous publications which has proven to display outstanding separation and sensitivity. The LC separation would consist of a 200 μm i.d. 50 cm long capillary column packed with 3 μm C18 particles and 100 min or even longer LC run would be employed. Fraction collected from LC separation would be sequentially injected into the online sheathless CITP/CZE-ESI-SRM MS platform described in Chapter 4 for further separation, selective concentration and targeted quantitation. Analysis results would be compared with single dimension CITP/CZE-ESI-SRM MS as well as conventional PRISM system to provide useful insight of the capabilities of the new two-dimensional separation platform.

5.2.3 Application in fields other than proteomics

Capillary electrophoresis is known for its versatility in different operation mode and its wide compatibility with different samples from small molecules like amino acids, metabolites to large molecules like peptides or even intact proteins. In addition, the high resolving power of CE separation is often useful to separation isomers which are inseparable in LC. Having demonstrated the feasibility and capability of the online CE-MS platform in peptides, we would like to examine the use of the platform in other fields of study such as metabolomics or intact proteins which does not usually behave well in LC separation due to the similarity in structures and extreme small/large molecular

weight. The long term goal is to develop applicable analyzing platforms based on this online CITP/CZE-ESI-MS platform for wide applications in a broad scope of fields.

References

(1) Xue, A.; Gandy, R. C.; Chung, L.; Baxter, R. C.; Smith, R. C.: Discovery of diagnostic biomarkers for pancreatic cancer in immunodepleted serum by SELDI-TOF MS. *Pancreatology* **2012**, *12*, 124-129.

(2) Kosanam, H.; Prassas, I.; Chrystoja, C. C.; Soleas, I.; Chan, A.; Dimitromanolakis, A.; Blasutig, I. M.; Ruckert, F.; Gruetzmann, R.; Pilarsky, C.; Maekawa, M.; Brand, R.; Diamandis, E. P.: LAMC2: A promising new pancreatic cancer biomarker identified by proteomic analysis of pancreatic adenocarcinoma tissues. *Mol Cell Proteomics* **2013**.

(3) McKinney, K. Q.; Lee, J.-G.; Sindram, D.; Russo, M. W.; Han, D. K.; Bonkovsky, H. L.; Hwang, S.-I.: Identification of differentially expressed proteins from primary versus metastatic pancreatic cancer cells using subcellular proteomics. *Cancer Genomics Proteomics* **2012**, *9*, 257-263.

(4) Wang, Y.; Kuramitsu, Y.; Ueno, T.; Suzuki, N.; Yoshino, S.; Iizuka, N.; Zhang, X.; Akada, J.; Oka, M.; Nakamura, K.: Proteomic differential display identifies upregulated vinculin as a possible biomarker of pancreatic cancer. *Oncol Rep* **2012**, *28*, 1845-1850.

(5) Takadate, T.; Onogawa, T.; Fukuda, T.; Motoi, F.; Suzuki, T.; Fujii, K.; Kihara, M.; Mikami, S.; Bando, Y.; Maeda, S.; Ishida, K.; Minowa, T.; Hanagata, N.; Ohtsuka, H.; Katayose, Y.; Egawa, S.; Nishimura, T.; Unno, M.: Novel prognostic protein markers of resectable pancreatic cancer identified by coupled shotgun and targeted proteomics using formalin-fixed paraffin-embedded tissues. *Int J Cancer* **2013**, *132*, 1368-1382.

(6) Tan, F.; Jiang, Y.; Sun, N.; Chen, Z.; Lv, Y.; Shao, K.; Li, N.; Qiu, B.; Gao, Y.; Li, B.; Tan, X.; Zhou, F.; Wang, Z.; Ding, D.; Wang, J.; Sun, J.; Hang, J.; Shi, S.; Feng, X.; He, F.; He, J.: Identification of isocitrate dehydrogenase 1 as a potential diagnostic and prognostic biomarker for non-small cell lung cancer by proteomic analysis. *Mol Cell Proteomics* **2012**, *11*.

(7) Gamez-Pozo, A.; Sanchez-Navarro, I.; Calvo, E.; Agullo-Ortuno, M. T.; Lopez-Vacas, R.; Diaz, E.; Camafeita, E.; Nistal, M.; Madero, R.; Espinosa, E.; Lopez, J. A.; Fresno Vara, J. Á.: PTRF/cavin-1 and MIF proteins are identified as non-small cell lung cancer biomarkers by label-free proteomics. *PLoS One* **2012**, *7*.

(8) Yang, J.; Song, Y.-C.; Song, T.-S.; Hu, X.-Y.; Guo, Y.-M.; Li, Z.-F.; Dang, C.-X.; Huang, C.: Identification of novel low molecular weight serum peptidome biomarkers for non-small cell lung cancer (NSCLC). *J Clin Lab Anal* **2012**, *26*, 148-154.

(9) Chen, W.-L.; Kuo, K.-T.; Chou, T.-Y.; Chen, C.-L.; Wang, C.-H.; Wei, Y.-H.; Wang, L.-S.: The role of cytochrome c oxidase subunit Va in non-small cell lung carcinoma cells: association with migration, invasion and prediction of distant metastasis. *BMC Cancer* **2012**, *12*, 273-273.

(10) Kang, J.-H.; Mori, T.; Kitazaki, H.; Niidome, T.; Takayama, K.; Nakanishi, Y.; Katayama, Y.: Kinase activity of protein kinase cα in serum as a diagnostic biomarker of human lung cancer. *Anticancer Res* **2013**, *33*, 485-488.

(11) Liu, Y.; Luo, X.; Hu, H.; Wang, R.; Sun, Y.; Zeng, R.; Chen, H.: Integrative proteomics and tissue microarray profiling indicate the association between overexpressed serum proteins and non-small cell lung cancer. *PLoS One* **2012**, *7*.

(12) Kikuchi, T.; Hassanein, M.; Amann, J. M.; Liu, Q.; Slebos, R. J. C.; Rahman, S. M. J.; Kaufman, J. M.; Zhang, X.; Hoeksema, M. D.; Harris, B. K.; Li, M.; Shyr, Y.; Gonzalez, A. L.; Zimmerman, L. J.; Liebler, D. C.; Massion, P. P.; Carbone, D. P.: In-depth proteomic analysis of nonsmall cell lung cancer to discover molecular targets and candidate biomarkers. *Mol Cell Proteomics* **2012**, *11*, 916-932.

(13) Ueda, K.; Tatsuguchi, A.; Saichi, N.; Toyama, A.; Tamura, K.; Furihata, M.; Takata, R.; Akamatsu, S.; Igarashi, M.; Nakayama, M.; Sato, T.-A.; Ogawa, O.; Fujioka, T.; Shuin, T.; Nakamura, Y.; Nakagawa, H.: Plasma Low-molecular-weight Proteome Profiling Identified Neuropeptide-Y as a Prostate Cancer Biomarker Polypeptide. *J Proteome Res* **2013**.

(14) Takakura, M.; Yokomizo, A.; Tanaka, Y.; Kobayashi, M.; Jung, G.; Banno, M.; Sakuma, T.; Imada, K.; Oda, Y.; Kamita, M.; Honda, K.; Yamada, T.; Naito, S.; Ono, M.: Carbonic anhydrase I as a new plasma biomarker for prostate cancer. *ISRN Oncol* **2012**, *2012*, 768190-768190.

(15) Qian, X.; Li, C.; Pang, B.; Xue, M.; Wang, J.; Zhou, J.: Spondin-2 (SPON2), a more prostate-cancer-specific diagnostic biomarker. *PLoS One* **2012**, *7*.

(16) Profumo, A.; Mangerini, R.; Rubagotti, A.; Romano, P.; Damonte, G.; Guglielmini, P.; Facchiano, A.; Ferri, F.; Ricci, F.; Rocco, M.; Boccardo, F.: Complement C3f serum levels may predict breast cancer risk in women with gross cystic disease of the breast. *J Proteomics* **2013**, *85*, 44-52.

(17) Washam, C. L.; Byrum, S. D.; Leitzel, K.; Ali, S. M.; Tackett, A. J.; Gaddy, D.; Sundermann, S. E.; Lipton, A.; Suva, L. J.: Identification of PTHrP(12-48) as a plasma

biomarker associated with breast cancer bone metastasis. *Cancer Epidemiol Biomarkers Prev* **2013**, *22*, 972-983.

(18) Xiang, M.; Zhou, W.; Gao, D.; Fang, X.; Liu, Q.: Inhibitor of apoptosis protein-like protein-2 as a novel serological biomarker for breast cancer. *Int J Mol Sci* **2012**, *13*, 16737-16750.

(19) Semaan, S. M.; Wang, X.; Marshall, A. G.; Sang, Q.-X. A.: Identification of Potential Glycoprotein Biomarkers in Estrogen Receptor Positive (ER+) and Negative (ER-) Human Breast Cancer Tissues by LC-LTQ/FT-ICR Mass Spectrometry. *J Cancer* **2012**, *3*, 269-284.

(20) Hodgkinson, V. C.; Agarwal, V.; Elfadl, D.; Fox, J. N.; McManus, P. L.; Mahapatra, T. K.; Kneeshaw, P. J.; Drew, P. J.; Lind, M. J.; Cawkwell, L.: Pilot and feasibility study: comparative proteomic analysis by 2-DE MALDI TOF/TOF MS reveals 14-3-3 proteins as putative biomarkers of response to neoadjuvant chemotherapy in ER-positive breast cancer. *J Proteomics* **2012**, *75*, 2745-2752.

(21) Greenwood, C.; Metodieva, G.; Al-Janabi, K.; Lausen, B.; Alldridge, L.; Leng, L.; Bucala, R.; Fernandez, N.; Metodiev, M. V.: Stat1 and CD74 overexpression is co-dependent and linked to increased invasion and lymph node metastasis in triple-negative breast cancer. *J Proteomics* **2012**, *75*, 3031-3040.

(22) Yang, W. S.; Moon, H.-G.; Kim, H. S.; Choi, E.-J.; Yu, M.-H.; Noh, D.-Y.; Lee, C.: Proteomic approach reveals FKBP4 and S100A9 as potential prediction markers of therapeutic response to neoadjuvant chemotherapy in patients with breast cancer. *J Proteome Res* **2012**, *11*, 1078-1088.

(23) Yan, H.; Yang, K.; Xiao, H.; Zou, Y.-J.; Zhang, W.-B.; Liu, H.-Y.: Over-expression of cofilin-1 and phosphoglycerate kinase 1 in astrocytomas involved in pathogenesis of radioresistance. *CNS Neurosci Ther* **2012**, *18*, 729-736.

(24) Banerjee, H. N.; Mahaffey, K.; Riddick, E.; Banerjee, A.; Bhowmik, N.; Patra, M.: Search for a diagnostic/prognostic biomarker for the brain cancer glioblastoma multiforme by 2D-DIGE-MS technique. *Mol Cell Biochem* **2012**, *367*, 59-63.

(25) Hu, Y.; Ylivinkka, I.; Chen, P.; Li, L.; Hautaniemi, S.; Nyman, T. A.; Keski-Oja, J.; Hyytiainen, M.: Netrin-4 promotes glioblastoma cell proliferation through integrin β4 signaling. *Neoplasia* **2012**, *14*, 219-227.

(26) Song, J. Y.; Bae, H. S.; Koo, D. H.; Lee, J. K.; Jung, H. H.; Lee, K. W.; Lee, N. W.: Candidates for tumor markers of cervical cancer discovered by proteomic analysis. *J Korean Med Sci* **2012**, *27*, 1479-1485.

(27) Drake, R. R.; White, K. Y.; Fuller, T. W.; Igwe, E.; Clements, M. A.; Nyalwidhe, J. O.; Given, R. W.; Lance, R. S.; Semmes, O. J.: Clinical collection and protein properties of expressed prostatic secretions as a source for biomarkers of prostatic disease. *J Proteomics* **2009**, *72*, 907-917.

(28) Schaaij-Visser, T. B. M.; de Wit, M.; Lam, S. W.; Jimenez, C. R.: The cancer secretome, current status and opportunities in the lung, breast and colorectal cancer context. *Biochim Biophys Acta* **2013**.

(29) Whelan, S. A.; He, J.; Lu, M.; Souda, P.; Saxton, R. E.; Faull, K. F.; Whitelegge, J. P.; Chang, H. R.: Mass spectrometry (LC-MS/MS) identified proteomic biosignatures of breast cancer in proximal fluid. *J Proteome Res* **2012**, *11*, 5034-5045.

(30) Fijneman, R. J. A.; de Wit, M.; Pourghiasian, M.; Piersma, S. R.; Pham, T. V.; Warmoes, M. O.; Lavaei, M.; Piso, C.; Smit, F.; Delis-van Diemen, P. M.; van Turenhout, S. T.; Terhaar sive Droste, J. S.; Mulder, C. J. J.; Blankenstein, M. A.; Robanus-Maandag, E. C.; Smits, R.; Fodde, R.; van Hinsbergh, V. W. M.; Meijer, G. A.; Jimenez, C. R.: Proximal fluid proteome profiling of mouse colon tumors reveals biomarkers for early diagnosis of human colorectal cancer. *Clin Cancer Res* **2012**, *18*, 2613-2624.

(31) Principe, S.; Kim, Y.; Fontana, S.; Ignatchenko, V.; Nyalwidhe, J. O.; Lance, R. S.; Troyer, D. A.; Alessandro, R.; Semmes, O. J.; Kislinger, T.; Drake, R. R.; Medin, J. A.: Identification of prostate-enriched proteins by in-depth proteomic analyses of expressed prostatic secretions in urine. *J Proteome Res* **2012**, *11*, 2386-2396.

(32) Hoskins, E. R.; Hood, B. L.; Sun, M.; Krivak, T. C.; Edwards, R. P.; Conrads, T. P.: Proteomic analysis of ovarian cancer proximal fluids: validation of elevated peroxiredoxin 1 in patient peripheral circulation. *PLoS One* **2011**, *6*.

(33) White, K. Y.; Rodemich, L.; Nyalwidhe, J. O.; Comunale, M. A.; Clements, M. A.; Lance, R. S.; Schellhammer, P. F.; Mehta, A. S.; Semmes, O. J.; Drake, R. R.: Glycomic characterization of prostate-specific antigen and prostatic acid phosphatase in prostate cancer and benign disease seminal plasma fluids. *J Proteome Res* **2009**, *8*, 620-630.

(34) Wang, P.; Whiteaker, J. R.; Paulovich, A. G.: The evolving role of mass spectrometry in cancer biomarker discovery. *Cancer Biol Ther* **2009**, *8*, 1083-1094.

(35) Espina, V.; Heiby, M.; Pierobon, M.; Liotta, L. A.: Laser capture microdissection technology. *Expert Rev Mol Diagn* **2007**, *7*, 647-657.

(36) Shekouh, A. R.; Thompson, C. C.; Prime, W.; Campbell, F.; Hamlett, J.; Herrington, C. S.; Lemoine, N. R.; Crnogorac-Jurcevic, T.; Buechler, M. W.; Friess, H.; Neoptolemos, J. P.; Pennington, S. R.; Costello, E.: Application of laser capture microdissection combined with two-dimensional electrophoresis for the discovery of differentially regulated proteins in pancreatic ductal adenocarcinoma. *Proteomics* **2003**, *3*, 1988-2001.

(37) Liu, Y.; Wu, J.; Yan, G.; Hou, R.; Zhuang, D.; Chen, L.; Pang, Q.; Zhu, J.: Proteomic analysis of prolactinoma cells by immuno-laser capture microdissection combined with online two-dimensional nano-scale liquid chromatography/mass spectrometry. *Proteome Sci* **2010**, *8*, 2-2.

(38) Zhu, J.; Nie, S.; Wu, J.; Lubman, D. M.: Target proteomic profiling of frozen pancreatic CD24+ adenocarcinoma tissues by immuno-laser capture microdissection and nano-LC-MS/MS. *J Proteome Res* **2013**, *12*, 2791-2804.

(39) Karring, H.; Poulsen, E. T.; Runager, K.; Thogersen, I. B.; Klintworth, G. K.; Hojrup, P.; Enghild, J. J.: Serine protease HtrA1 accumulates in corneal transforming growth factor beta induced protein (TGFBIp) amyloid deposits. *Mol Vis* **2013**, *19*, 861-876.

(40) Kirkpatrick, D. S.; Gerber, S. A.; Gygi, S. P.: The absolute quantification strategy: a general procedure for the quantification of proteins and post-translational modifications. *Methods* **2005**, *35*, 265-273.

(41) Addona, T. A.; Abbatiello, S. E.; Schilling, B.; Skates, S. J.; Mani, D. R.; Bunk, D. M.; Spiegelman, C. H.; Zimmerman, L. J.; Ham, A.-J. L.; Keshishian, H.; Hall, S. C.; Allen, S.; Blackman, R. K.; Borchers, C. H.; Buck, C.; Cardasis, H. L.; Cusack, M. P.;

Dodder, N. G.; Gibson, B. W.; Held, J. M.; Hiltke, T.; Jackson, A.; Johansen, E. B.; Kinsinger, C. R.; Li, J.; Mesri, M.; Neubert, T. A.; Niles, R. K.; Pulsipher, T. C.; Ransohoff, D.; Rodriguez, H.; Rudnick, P. A.; Smith, D.; Tabb, D. L.; Tegeler, T. J.; Variyath, A. M.; Vega-Montoto, L. J.; Wahlander, A.; Waldemarson, S.; Wang, M.; Whiteaker, J. R.; Zhao, L.; Anderson, N. L.; Fisher, S. J.; Liebler, D. C.; Paulovich, A. G.; Regnier, F. E.; Tempst, P.; Carr, S. A.: Multi-site assessment of the precision and reproducibility of multiple reaction monitoring-based measurements of proteins in plasma. *Nat Biotechnol* **2009**, *27*, 633-641.

(42) Prakash, A.; Rezai, T.; Krastins, B.; Sarracino, D.; Athanas, M.; Russo, P.; Zhang, H.; Tian, Y.; Li, Y.; Kulasingam, V.; Drabovich, A.; Smith, C. R.; Batruch, I.; Oran, P. E.; Fredolini, C.; Luchini, A.; Liotta, L.; Petricoin, E.; Diamandis, E. P.; Chan, D. W.; Nelson, R.; Lopez, M. F.: Interlaboratory reproducibility of selective reaction monitoring assays using multiple upfront analyte enrichment strategies. *J Proteome Res* **2012**, *11*, 3986-3995.

(43) Mustafa, G. M.; Petersen, J. R.; Ju, H.; Cicalese, L.; Snyder, N.; Haidacher, S. J.; Denner, L.; Elferink, C.: Biomarker Discovery for Early Detection of Hepatocellular Carcinoma (HCC)in Hepatitis C (HCV) Infected Patients. *Mol Cell Proteomics* **2013**.

(44) Everley, R. A.; Kunz, R. C.; McAllister, F. E.; Gygi, S. P.: Increasing Throughput in Targeted Proteomics Assays: 54-Plex Quantitation in a Single Mass Spectrometry Run. *Analytical Chemistry* **2013**, *85*, 5340-5346.

(45) Hood, L.: Systems biology: integrating technology, biology, and computation. *Mech Ageing Dev* **2003**, *124*, 9-16.

(46) Aebersold, R.; Cravatt, B. F.: Proteomics--advances, applications and the challenges that remain. *Trends Biotechnol* **2002**, *20*, 1-2.

(47) Drube, J.; Zurbig, P.; Schiffer, E.; Lau, E.; Ure, B.; Gluer, S.; Kirschstein, M.; Pape, L.; Decramer, S.; Bascands, J.-L.; Schanstra, J. P.; Mischak, H.; Ehrich, J. H. H.: Urinary proteome analysis identifies infants but not older children requiring pyeloplasty. *Pediatr Nephrol* **2010**, *25*, 1673-1678.

(48) Theodorescu, D.; Schiffer, E.; Bauer, H. W.; Douwes, F.; Eichhorn, F.; Polley, R.; Schmidt, T.; Schofer, W.; Zurbig, P.; Good, D. M.; Coon, J. J.; Mischak, H.: Discovery and validation of urinary biomarkers for prostate cancer. *Proteomics Clin Appl* **2008**, *2*, 556-570.

(49) Schiffer, E.; Vlahou, A.; Petrolekas, A.; Stravodimos, K.; Tauber, R.; Geschwend, J. E.; Neuhaus, J.; Stolzenburg, J.-U.; Conaway, M. R.; Mischak, H.; Theodorescu, D.: Prediction of muscle-invasive bladder cancer using urinary proteomics. *Clin Cancer Res* **2009**, *15*, 4935-4943.

(50) Schiffer, E.; Bick, C.; Grizelj, B.; Pietzker, S.; Schofer, W.: Urinary proteome analysis for prostate cancer diagnosis: cost-effective application in routine clinical practice in Germany. *Int J Urol* **2012**, *19*, 118-125.

(51) Haubitz, M.; Good, D. M.; Woywodt, A.; Haller, H.; Rupprecht, H.; Theodorescu, D.; Dakna, M.; Coon, J. J.; Mischak, H.: Identification and validation of urinary biomarkers for differential diagnosis and evaluation of therapeutic intervention in anti-neutrophil cytoplasmic antibody-associated vasculitis. *Mol Cell Proteomics* **2009**, *8*, 2296-2307.

(52) Zimmerli, L. U.; Schiffer, E.; Zurbig, P.; Good, D. M.; Kellmann, M.; Mouls, L.; Pitt, A. R.; Coon, J. J.; Schmieder, R. E.; Peter, K. H.; Mischak, H.; Kolch, W.; Delles, C.; Dominiczak, A. F.: Urinary proteomic biomarkers in coronary artery disease. *Mol Cell Proteomics* **2008**, *7*, 290-298.

(53) von Zur Muhlen, C.; Schiffer, E.; Zuerbig, P.; Kellmann, M.; Brasse, M.; Meert, N.; Vanholder, R. C.; Dominiczak, A. F.; Chen, Y. C.; Mischak, H.; Bode, C.; Peter, K.: Evaluation of urine proteome pattern analysis for its potential to reflect coronary artery atherosclerosis in symptomatic patients. *J Proteome Res* **2009**, *8*, 335-345.

(54) Snell-Bergeon, J. K.; Maahs, D. M.; Ogden, L. G.; Kinney, G. L.; Hokanson, J. E.; Schiffer, E.; Rewers, M.; Mischak, H.: Evaluation of urinary biomarkers for coronary artery disease, diabetes, and diabetic kidney disease. *Diabetes Technol Ther* **2009**, *11*, 1-9.

(55) Jantos-Siwy, J.; Schiffer, E.; Brand, K.; Schumann, G.; Rossing, K.; Delles, C.; Mischak, H.; Metzger, J.: Quantitative urinary proteome analysis for biomarker evaluation in chronic kidney disease. *J Proteome Res* **2009**, *8*, 268-281.

(56) Kistler, A. D.; Mischak, H.; Poster, D.; Dakna, M.; Wuthrich, R. P.; Serra, A. L.: Identification of a unique urinary biomarker profile in patients with autosomal dominant polycystic kidney disease. *Kidney Int* **2009**, *76*, 89-96.

(57) Good, D. M.; Zurbig, P.; Argiles, A.; Bauer, H. W.; Behrens, G.; Coon, J. J.; Dakna, M.; Decramer, S.; Delles, C.; Dominiczak, A. F.; Ehrich, J. H. H.; Eitner, F.; Fliser, D.; Frommberger, M.; Ganser, A.; Girolami, M. A.; Golovko, I.; Gwinner, W.; Haubitz, M.; Herget-Rosenthal, S.; Jankowski, J.; Jahn, H.; Jerums, G.; Julian, B. A.; Kellmann, M.; Kliem, V.; Kolch, W.; Krolewski, A. S.; Luppi, M.; Massy, Z.; Melter,

M.; Neususs, C.; Novak, J.; Peter, K.; Rossing, K.; Rupprecht, H.; Schanstra, J. P.; Schiffer, E.; Stolzenburg, J.-U.; Tarnow, L.; Theodorescu, D.; Thongboonkerd, V.; Vanholder, R.; Weissinger, E. M.; Mischak, H.; Schmitt-Kopplin, P.: Naturally occurring human urinary peptides for use in diagnosis of chronic kidney disease. *Mol Cell Proteomics* **2010**, *9*, 2424-2437.

(58) Raedler, T. J.; Wittke, S.; Jahn, H.; Koessler, A.; Mischak, H.; Wiedemann, K.: Capillary electrophoresis mass spectrometry as a potential tool to detect lithium-induced nephropathy: Preliminary results. *Prog Neuropsychopharmacol Biol Psychiatry* **2008**, *32*, 673-678.

(59) Weissinger, E. M.; Schiffer, E.; Hertenstein, B.; Ferrara, J. L.; Holler, E.; Stadler, M.; Kolb, H.-J.; Zander, A.; Zurbig, P.; Kellmann, M.; Ganser, A.: Proteomic patterns predict acute graft-versus-host disease after allogeneic hematopoietic stem cell transplantation. *Blood* **2007**, *109*, 5511-5519.

(60) Haselberg, R.; de Jong, G. J.; Somsen, G. W.: Capillary electrophoresis-mass spectrometry for the analysis of intact proteins 2007-2010. *Electrophoresis* **2011**, *32*, 66-82.

(61) Albalat, A.; Mischak, H.; Mullen, W.: Clinical application of urinary proteomics/peptidomics. *Expert Rev Proteomics* **2011**, *8*, 615-629.

(62) Mischak, H.; Schanstra, J. P.: CE-MS in biomarker discovery, validation, and clinical application. *Proteomics Clin Appl* **2011**, *5*, 9-23.

(63) Metzger, J.; Chatzikyrkou, C.; Broecker, V.; Schiffer, E.; Jaensch, L.; Iphoefer, A.; Mengel, M.; Mullen, W.; Mischak, H.; Haller, H.; Gwinner, W.: Diagnosis of

subclinical and clinical acute T-cell-mediated rejection in renal transplant patients by urinary proteome analysis. *Proteomics Clin Appl* **2011**, *5*, 322-333.

(64) Zuberovic, A.; Wetterhall, M.; Hanrieder, J.; Bergquist, J.: CE MALDI-TOF/TOF MS for multiplexed quantification of proteins in human ventricular cerebrospinal fluid. *Electrophoresis* **2009**, *30*, 1836-1843.

(65) Wiese, S.; Reidegeld, K. A.; Meyer, H. E.; Warscheid, B.: Protein labeling by iTRAQ: a new tool for quantitative mass spectrometry in proteome research. *Proteomics* **2007**, *7*, 340-350.

(66) Wang, W.; Guo, T.; Rudnick, P. A.; Song, T.; Li, J.; Zhuang, Z.; Zheng, W.; Devoe, D. L.; Lee, C. S.; Balgley, B. M.: Membrane proteome analysis of microdissected ovarian tumor tissues using capillary isoelectric focusing/reversed-phase liquid chromatography-tandem MS. *Anal Chem* **2007**, *79*, 1002-1009.

(67) Guo, T.; Wang, W.; Rudnick, P. A.; Song, T.; Li, J.; Zhuang, Z.; Weil, R. J.; DeVoe, D. L.; Lee, C. S.; Balgley, B. M.: Proteome analysis of microdissected formalin-fixed and Paraffin-embedded tissue specimens. *J Histochem Cytochem* **2007**, *55*, 763-772.

(68) Liu, H.; Sadygov, R. G.; Yates, J. R.: A model for random sampling and estimation of relative protein abundance in shotgun proteomics. *Anal Chem* **2004**, *76*, 4193-4201.

(69) Ishihama, Y.; Oda, Y.; Tabata, T.; Sato, T.; Nagasu, T.; Rappsilber, J.; Mann, M.: Exponentially modified protein abundance index (emPAI) for estimation of absolute protein amount in proteomics by the number of sequenced peptides per protein. *Mol Cell Proteomics* **2005**, *4*, 1265-1272.

(70) Balgley, B. M.; Wang, W.; Song, T.; Fang, X.; Yang, L.; Lee, C. S.: Evaluation of confidence and reproducibility in quantitative proteomics performed by a capillary isoelectric focusing-based proteomic platform coupled with a spectral counting approach. *Electrophoresis* **2008**, *29*, 3047-3054.

(71) Dai, L.; Li, C.; Shedden, K. A.; Misek, D. E.; Lubman, D. M.: Comparative proteomic study of two closely related ovarian endometrioid adenocarcinoma cell lines using cIEF fractionation and pathway analysis. *Electrophoresis* **2009**, *30*, 1119-1131.

(72) Hanrieder, J.; Zuberovic, A.; Bergquist, J.: Surface modified capillary electrophoresis combined with in solution isoelectric focusing and MALDI-TOF/TOF MS: a gel-free multidimensional electrophoresis approach for proteomic profiling--exemplified on human follicular fluid. *J Chromatogr A* **2009**, *1216*, 3621-3628.

(73) An, Y.; Cooper, J. W.; Balgley, B. M.; Lee, C. S.: Selective enrichment and ultrasensitive identification of trace peptides in proteome analysis using transient capillary isotachophoresis/zone electrophoresis coupled with nano-ESI-MS. *Electrophoresis* **2006**, *27*, 3599-3608.

(74) Fang, X.; Yang, L.; Wang, W.; Song, T.; Lee, C.; Devoe, D.; Balgley, B.: Comparison of Electrokinetics-Based Multidimensional Separations Coupled with Electrospray Ionization-Tandem Mass Spectrometry for Characterization of Human Salivary Proteins. *Anal Chem* **2007**, *79*, 5785-5792.

(75) Fang, X.; Wang, W.; Yang, L.; Chandrasekaran, K.; Kristian, T.; Balgley, B. M.; Lee, C. S.: Application of capillary isotachophoresis-based multidimensional separations coupled with electrospray ionization-tandem mass spectrometry for characterization of mouse brain mitochondrial proteome. *Electrophoresis* **2008**, *29*, 2215-2223.

(76) Fang, X.; Balgley, B. M.; Wang, W.; Park, D. M.; Lee, C. S.: Comparison of multidimensional shotgun technologies targeting tissue proteomics. *Electrophoresis* **2009**, *30*, 4063-4070.

(77) Wolters, D. A.; Washburn, M. P.; Yates, J. R.: An automated multidimensional protein identification technology for shotgun proteomics. *Anal Chem* **2001**, *73*, 5683-5690.

(78) Jinawath, N.; Vasoontara, C.; Jinawath, A.; Fang, X.; Zhao, K.; Yap, K.-L.; Guo, T.; Lee, C. S.; Wang, W.; Balgley, B. M.; Davidson, B.; Wang, T.-L.; Shih, I.-M.: Oncoproteomic analysis reveals co-upregulation of RELA and STAT5 in carboplatin resistant ovarian carcinoma. *PLoS One* **2010**, *5*.

(79) Chen, Z.; Fadiel, A.; Xia, Y.: Functional duality of merlin: A conundrum of proteome complexity. *Med Hypotheses* **2006**, *67*, 1095-1098.

(80) Huang, K.-C.; Park, D. C.; Ng, S.-K.; Lee, J. Y.; Ni, X.; Ng, W.-C.; Bandera, C. A.; Welch, W. R.; Berkowitz, R. S.; Mok, S. C.; Ng, S.-W.: Selenium binding protein 1 in ovarian cancer. *Int J Cancer* **2006**, *118*, 2433-2440.

(81) Chekhun, V. F.; Lukyanova, N. Y.; Urchenko, O. V.; Kulik, G. I.: The role of expression of the components of proteome in the formation of molecular profile of human ovarian carcinoma A2780 cells sensitive and resistant to cisplatin. *Exp Oncol* **2005**, *27*, 191-195.

(82) Smith-Beckerman, D. M.; Fung, K. W.; Williams, K. E.; Auersperg, N.; Godwin, A. K.; Burlingame, A. L.: Proteome changes in ovarian epithelial cells derived from women with BRCA1 mutations and family histories of cancer. *Mol Cell Proteomics* **2005**, *4*, 156-168.

(83) Duan, Z.; Foster, R.; Bell, D. A.; Mahoney, J.; Wolak, K.; Vaidya, A.; Hampel, C.; Lee, H.; Seiden, M. V.: Signal transducers and activators of transcription 3 pathway activation in drug-resistant ovarian cancer. *Clin Cancer Res* **2006**, *12*, 5055-5063.

(84) Haura, E. B.; Zheng, Z.; Song, L.; Cantor, A.; Bepler, G.: Activated epidermal growth factor receptor-Stat-3 signaling promotes tumor survival in vivo in non-small cell lung cancer. *Clin Cancer Res* **2005**, *11*, 8288-8294.

(85) Chen, L.-F.; Greene, W. C.: Shaping the nuclear action of NF-kappaB. *Nat Rev Mol Cell Biol* **2004**, *5*, 392-401.

(86) Olivares, J. A.; Nguyen, N. T.; Yonker, C. R.; Smith, R. D.: On-line mass spectrometric detection for capillary zone electrophoresis. *Analytical Chemistry* **1987**, *59*, 1230-1232.

(87) Smith, R. D.; Udseth, H. R.: Capillary zone electrophoresis-MS. *Nature* **1988**, *331*, 639-640.

(88) Mokaddem, M.; Gareil, P.; Belgaied, J.-E.; Varenne, A.: A new insight into suction and dilution effects in capillary electrophoresis coupled to mass spectrometry via an electrospray ionization interface. Part I-Suction effect. *Electrophoresis* **2008**, *29*, 1957-1964.

(89) Mokaddem, M.; Gareil, P.; Belgaied, J.-E.; Varenne, A.: New insight into suction and dilution effects in CE coupled to MS via an ESI interface. II--dilution effect. *Electrophoresis* **2009**, *30*, 1692-1697.

(90) Yan, X.; Essaka, D. C.; Sun, L.; Zhu, G.; Dovichi, N. J.: Bottom-up proteome analysis of E. coli using capillary zone electrophoresis-tandem mass spectrometry with an electrokinetic sheath-flow electrospray interface. *Proteomics* **2013**, *13*, 2546-2551.

(91) Wojcik, R.; Dada, O. O.; Sadilek, M.; Dovichi, N. J.: Simplified capillary electrophoresis nanospray sheath-flow interface for high efficiency and sensitive peptide analysis. *Rapid Communications in Mass Spectrometry* **2010**, *24*, 2554-2560.

(92) Cargile, B. J.; Bundy, J. L.; Freeman, T. W.; Stephenson, J. L.: Gel based isoelectric focusing of peptides and the utility of isoelectric point in protein identification. *J Proteome Res* **2004**, *3*, 112-119.

(93) Iwasaki, M.; Miwa, S.; Ikegami, T.; Tomita, M.; Tanaka, N.; Ishihama, Y.: One-dimensional capillary liquid chromatographic separation coupled with tandem mass spectrometry unveils the Escherichia coli proteome on a microarray scale. *Anal Chem* **2010**, *82*, 2616-2620.

(94) Xia, S.; Tao, D.; Yuan, H.; Zhou, Y.; Liang, Z.; Zhang, L.; Zhang, Y.: Nano-flow multidimensional liquid chromatography platform integrated with combination of protein and peptide separation for proteome analysis. *J Sep Sci* **2012**, *35*, 1764-1770.

(95) Wachs, T.; Sheppard, R. L.; Henion, J.: Design and applications of a self-aligning liquid junction-electrospray interface for capillary electrophoresis-mass spectrometry. *J Chromatogr B Biomed Appl* **1996**, *685*, 335-342.

(96) Wilm, M.; Mann, M.: Analytical Properties of the Nanoelectrospray Ion Source. *Analytical Chemistry* **1996**, *68*, 1-8.

(97) Wilm, M. S.; Mann, M.: Electrospray and Taylor-Cone theory, Dole's beam of macromolecules at last? *International Journal of Mass Spectrometry and Ion Processes* **1994**, *136*, 167-180.

(98) Bahr, U.; Pfenninger, A.; Karas, M.; Stahl, B.: High-Sensitivity Analysis of Neutral Underivatized Oligosaccharides by Nanoelectrospray Mass Spectrometry. *Analytical Chemistry* **1997**, *69*, 4530-4535.

(99) Zamfir, A. D.: Recent advances in sheathless interfacing of capillary electrophoresis and electrospray ionization mass spectrometry. *Journal of Chromatography A* **2007**, *1159*, 2-13.

(100) Wahl, J. H.; Gale, D. C.; Smith, R. D.: Sheathless capillary electrophoresis-electrospray ionization mass spectrometry using 10 μm I.D. capillaries: Analyses of tryptic digests of cytochrome c. *Journal of Chromatography A* **1994**, *659*, 217-222.

(101) Maziarz, E. P.; Lorenz, S.; White, T.; Wood, T.: Polyaniline: A conductive polymer coating for durable nanospray emitters. *Journal of the American Society for Mass Spectrometry* **2000**, *11*, 659-663.

(102) Chang, Y. Z.; Her, G. R.: Sheathless Capillary Electrophoresis/Electrospray Mass Spectrometry Using a Carbon-Coated Fused-Silica Capillary. *Analytical Chemistry* **1999**, *72*, 626-630.

(103) Cao, P.; Moini, M.: A novel sheathless interface for capillary electrophoresis/electrospray ionization mass spectrometry using an in-capillary electrode. *Journal of the American Society for Mass Spectrometry* **1997**, *8*, 561-564.

(104) Figeys, D.; Ducret, A.; Yates, J. R.; Aebersold, R.: Protein identification by solid phase microextraction[mdash]capillary zone electrophoresis[mdash]microelectrospray[mdash]tandem mass spectrometry. *Nat Biotech* **1996**, *14*, 1579-1583.

(105) Moini, M.: Simplifying CE-MS operation. 2. Interfacing low-flow separation techniques to mass spectrometry using a porous tip. *Anal Chem* **2007**, *79*, 4241-4246.

(106) Faserl, K.; Sarg, B.; Kremser, L.; Lindner, H.: Optimization and Evaluation of a Sheathless Capillary Electrophoresis–Electrospray Ionization Mass Spectrometry Platform for Peptide Analysis: Comparison to Liquid Chromatography–Electrospray Ionization Mass Spectrometry. *Analytical Chemistry* **2011**, *83*, 7297-7305.

(107) Haselberg, R.; Ratnayake, C. K.; de Jong, G. J.; Somsen, G. W.: Performance of a sheathless porous tip sprayer for capillary electrophoresis–electrospray ionization-mass spectrometry of intact proteins. *Journal of Chromatography A* **2010**, *1217*, 7605-7611.

(108) Ramautar, R.; Shyti, R.; Schoenmaker, B.; Groote, L.; Derks, R. E.; Ferrari, M.; Maagdenberg, A. J. M.; Deelder, A.; Mayboroda, O.: Metabolic profiling of mouse cerebrospinal fluid by sheathless CE-MS. *Anal Bioanal Chem* **2012**, *404*, 2895-2900.

(109) Busnel, J.-M.; Schoenmaker, B.; Ramautar, R.; Carrasco-Pancorbo, A.; Ratnayake, C.; Feitelson, J. S.; Chapman, J. D.; Deelder, A. M.; Mayboroda, O. A.: High capacity capillary electrophoresis-electrospray ionization mass spectrometry: coupling a porous sheathless interface with transient-isotachophoresis. *Anal Chem* **2010**, *82*, 9476-9483.

(110) Ramautar, R.; Busnel, J.-M.; Deelder, A. M.; Mayboroda, O. A.: Enhancing the coverage of the urinary metabolome by sheathless capillary electrophoresis-mass spectrometry. *Anal Chem* **2012**, *84*, 885-892.

(111) Heemskerk, A. A. M.; Busnel, J.-M.; Schoenmaker, B.; Derks, R. J. E.; Klychnikov, O.; Hensbergen, P. J.; Deelder, A. M.; Mayboroda, O. A.: Ultra-low flow

electrospray ionization-mass spectrometry for improved ionization efficiency in phosphoproteomics. *Anal Chem* **2012**, *84*, 4552-4559.

(112) Heemskerk, A. A.; Wuhrer, M.; Busnel, J. M.; Koeleman, C. A.; Selman, M. H.; Vidarsson, G.; Kapur, R.; Schoenmaker, B.; Derks, R. J.; Deelder, A. M.: Coupling porous sheathless interface MS with transient-ITP in neutral capillaries for improved sensitivity in glycopeptide analysis. *Electrophoresis* **2013**, *34*, 383-387.

(113) Faserl, K.; Sarg, B.; Kremser, L.; Lindner, H.: Optimization and evaluation of a sheathless capillary electrophoresis-electrospray ionization mass spectrometry platform for peptide analysis: comparison to liquid chromatography-electrospray ionization mass spectrometry. *Anal Chem* **2011**, *83*, 7297-7305.

(114) Lacroix, M.; Abi-Said, D.; Fourney, D. R.; Gokaslan, Z. L.; Shi, W.; DeMonte, F.; Lang, F. F.; McCutcheon, I. E.; Hassenbusch, S. J.; Holland, E.; Hess, K.; Michael, C.; Miller, D.; Sawaya, R.: A multivariate analysis of 416 patients with glioblastoma multiforme: prognosis, extent of resection, and survival. *J Neurosurg* **2001**, *95*, 190-198.

(115) Ichimura, K.; Ohgaki, H.; Kleihues, P.; Collins, V. P.: Molecular pathogenesis of astrocytic tumours. *J Neurooncol* **2004**, *70*, 137-160.

(116) Holland, E. C.: Gliomagenesis: genetic alterations and mouse models. *Nat Rev Genet* **2001**, *2*, 120-129.

(117) Maher, E. A.; Furnari, F. B.; Bachoo, R. M.; Rowitch, D. H.; Louis, D. N.; Cavenee, W. K.; DePinho, R. A.: Malignant glioma: genetics and biology of a grave matter. *Genes Dev* **2001**, *15*, 1311-1333.

(118) Kitange, G. J.; Templeton, K. L.; Jenkins, R. B.: Recent advances in the molecular genetics of primary gliomas. *Curr Opin Oncol* **2003**, *15*, 197-203.

(119) Sallinen, S. L.; Sallinen, P. K.; Haapasalo, H. K.; Helin, H. J.; Helen, P. T.; Schraml, P.; Kallioniemi, O. P.; Kononen, J.: Identification of differentially expressed genes in human gliomas by DNA microarray and tissue chip techniques. *Cancer Res* **2000**, *60*, 6617-6622.

(120) Bachoo, R. M.; Maher, E. A.; Ligon, K. L.; Sharpless, N. E.; Chan, S. S.; You, M. J.; Tang, Y.; DeFrances, J.; Stover, E.; Weissleder, R.; Rowitch, D. H.; Louis, D. N.; DePinho, R. A.: Epidermal growth factor receptor and Ink4a/Arf: convergent mechanisms governing terminal differentiation and transformation along the neural stem cell to astrocyte axis. *Cancer Cell* **2002**, *1*, 269-277.

(121) Maher, E. A.; Brennan, C.; Wen, P. Y.; Durso, L.; Ligon, K. L.; Richardson, A.; Khatry, D.; Feng, B.; Sinha, R.; Louis, D. N.; Quackenbush, J.; Black, P. M.; Chin, L.; DePinho, R. A.: Marked genomic differences characterize primary and secondary glioblastoma subtypes and identify two distinct molecular and clinical secondary glioblastoma entities. *Cancer Res* **2006**, *66*, 11502-11513.

(122) Ohnishi, M.; Matsumoto, T.; Nagashio, R.; Kageyama, T.; Utsuki, S.; Oka, H.; Okayasu, I.; Sato, Y.: Proteomics of tumor-specific proteins in cerebrospinal fluid of patients with astrocytoma: usefulness of gelsolin protein. *Pathol Int* **2009**, *59*, 797-803.

(123) Schuhmann, M. U.; Zucht, H. D.; Nassimi, R.; Heine, G.; Schneekloth, C. G.; Stuerenburg, H. J.; Selle, H.: Peptide screening of cerebrospinal fluid in patients with glioblastoma multiforme. *Eur J Surg Oncol* **2010**, *36*, 201-207.

(124) Kumar, D. M.; Thota, B.; Shinde, S. V.; Prasanna, K. V.; Hegde, A. S.; Arivazhagan, A.; Chandramouli, B. A.; Santosh, V.; Somasundaram, K.: Proteomic

identification of haptoglobin α2 as a glioblastoma serum biomarker: implications in cancer cell migration and tumor growth. *J Proteome Res* **2010**, *9*, 5557-5567.

(125) Nirmalan, N. J.; Harnden, P.; Selby, P. J.; Banks, R. E.: Mining the archival formalin-fixed paraffin-embedded tissue proteome: opportunities and challenges. *Mol Biosyst* **2008**, *4*, 712-720.

(126) Rifai, N.; Gillette, M. A.; Carr, S. A.: Protein biomarker discovery and validation: the long and uncertain path to clinical utility. *Nat Biotechnol* **2006**, *24*, 971-983.

(127) Cottingham, K.: Tissues tell the real tale of breast cancer. *J Proteome Res* **2007**, *6*, 2052-2052.

(128) Melchior, K.; Tholey, A.; Heisel, S.; Keller, A.; Lenhof, H.-P.; Meese, E.; Huber, C. G.: Proteomic study of human glioblastoma multiforme tissue employing complementary two-dimensional liquid chromatography- and mass spectrometry-based approaches. *J Proteome Res* **2009**, *8*, 4604-4614.

(129) Li, N.; Zhang, J.; Liang, Y.; Shao, J.; Peng, F.; Sun, M.; Xu, N.; Li, X.; Wang, R.; Liu, S.; Lu, Y.: A controversial tumor marker: is SM22 a proper biomarker for gastric cancer cells? *J Proteome Res* **2007**, *6*, 3304-3312.

(130) Iwadate, Y.; Sakaida, T.; Hiwasa, T.; Nagai, Y.; Ishikura, H.; Takiguchi, M.; Yamaura, A.: Molecular classification and survival prediction in human gliomas based on proteome analysis. *Cancer Res* **2004**, *64*, 2496-2501.

(131) Odreman, F.; Vindigni, M.; Gonzales, M. L.; Niccolini, B.; Candiano, G.; Zanotti, B.; Skrap, M.; Pizzolitto, S.; Stanta, G.; Vindigni, A.: Proteomic studies on low- and high-grade human brain astrocytomas. *J Proteome Res* **2005**, *4*, 698-708.

(132) Li, J.; Zhuang, Z.; Okamoto, H.; Vortmeyer, A. O.; Park, D. M.; Furuta, M.; Lee, Y. S.; Oldfield, E. H.; Zeng, W.; Weil, R. J.: Proteomic profiling distinguishes astrocytomas and identifies differential tumor markers. *Neurology* **2006**, *66*, 733-736.

(133) Gimenez, M.; Souza, V. C. d. O.; Izumi, C.; Barbieri, M. R.; Chammas, R.; Oba-Shinjo, S. M.; Uno, M.; Marie, S. K. N.; Rosa, J. C.: Proteomic analysis of low- to high-grade astrocytomas reveals an alteration of the expression level of raf kinase inhibitor protein and nucleophosmin. *Proteomics* **2010**, *10*, 2812-2821.

(134) Bonner, R. F.; Emmert-Buck, M.; Cole, K.; Pohida, T.; Chuaqui, R.; Goldstein, S.; Liotta, L. A.: Laser capture microdissection: molecular analysis of tissue. *Science* **1997**, *278*, 1481-1481.

(135) Gebauer, P.; Bocek, P.: Recent progress in capillary isotachophoresis. *Electrophoresis* **2000**, *21*, 3898-3904.

(136) Foret, F.; Szoko, E.; Karger, B. L.: Trace analysis of proteins by capillary zone electrophoresis with on-column transient isotachophoretic preconcentration. *Electrophoresis* **1993**, *14*, 417-428.

(137) Stegehuis, D. S.; Irth, H.; Tjaden, U. R.; Van der Greef, J.: Isotachophoresis as an on-line concentration pretreatment technique in capillary electrophoresis. *J Chromatogr* **1991**, *538*, 393-402.

(138) Rappsilber, J.; Ryder, U.; Lamond, A. I.; Mann, M.: Large-scale proteomic analysis of the human spliceosome. *Genome Res* **2002**, *12*, 1231-1245.

(139) Furuta, M.; Weil, R. J.; Vortmeyer, A. O.; Huang, S.; Lei, J.; Huang, T.-N.; Lee, Y.-S.; Bhowmick, D. A.; Lubensky, I. A.; Oldfield, E. H.; Zhuang, Z.: Protein patterns

and proteins that identify subtypes of glioblastoma multiforme. *Oncogene* **2004**, *23*, 6806-6814.

(140) Zhuang, Z.; Lee, Y. S.; Zeng, W.; Furuta, M.; Valyi-Nagy, T.; Johnson, M. D.; Vnencak-Jones, C. L.; Woltjer, R. L.; Weil, R. J.: Molecular genetic and proteomic analysis of synchronous malignant gliomas. *Neurology* **2004**, *62*, 2316-2319.

(141) Yang, L.; Lee, C. S.; Hofstadler, S. A.; Smith, R. D.: Characterization of microdialysis acidification for capillary isoelectric focusing-microelectrospray ionization mass spectrometry. *Anal Chem* **1998**, *70*, 4945-4950.

(142) Geer, L. Y.; Markey, S. P.; Kowalak, J. A.; Wagner, L.; Xu, M.; Maynard, D. M.; Yang, X.; Shi, W.; Bryant, S. H.: Open mass spectrometry search algorithm. *J Proteome Res* **2004**, *3*, 958-964.

(143) Elias, J. E.; Haas, W.; Faherty, B. K.; Gygi, S. P.: Comparative evaluation of mass spectrometry platforms used in large-scale proteomics investigations. *Nat Methods* **2005**, *2*, 667-675.

(144) Balgley, B. M.; Laudeman, T.; Yang, L.; Song, T.; Lee, C. S.: Comparative evaluation of tandem MS search algorithms using a target-decoy search strategy. *Mol Cell Proteomics* **2007**, *6*, 1599-1608.

(145) Krogh, A.; Larsson, B.; von Heijne, G.; Sonnhammer, E. L.: Predicting transmembrane protein topology with a hidden Markov model: application to complete genomes. *J Mol Biol* **2001**, *305*, 567-580.

(146) Eisen, M. B.; Spellman, P. T.; Brown, P. O.; Botstein, D.: Cluster analysis and display of genome-wide expression patterns. *Proc Natl Acad Sci U S A* **1998**, *95*, 14863-14868.

(147) Lin, B.; White, J. T.; Lu, W.; Xie, T.; Utleg, A. G.; Yan, X.; Yi, E. C.; Shannon, P.; Khrebtukova, I.; Lange, P. H.; Goodlett, D. R.; Zhou, D.; Vasicek, T. J.; Hood, L.: Evidence for the presence of disease-perturbed networks in prostate cancer cells by genomic and proteomic analyses: a systems approach to disease. *Cancer Res* **2005**, *65*, 3081-3091.

(148) He, F.; Sun, Y. E.: Glial cells more than support cells? *Int J Biochem Cell Biol* **2007**, *39*, 661-665.

(149) Hart, M. J.; Callow, M. G.; Souza, B.; Polakis, P.: IQGAP1, a calmodulin-binding protein with a rasGAP-related domain, is a potential effector for cdc42Hs. *EMBO J* **1996**, *15*, 2997-3005.

(150) Grohmanova, K.; Schlaepfer, D.; Hess, D.; Gutierrez, P.; Beck, M.; Kroschewski, R.: Phosphorylation of IQGAP1 modulates its binding to Cdc42, revealing a new type of rho-GTPase regulator. *J Biol Chem* **2004**, *279*, 48495-48504.

(151) Li, Z.; McNulty, D. E.; Marler, K. J. M.; Lim, L.; Hall, C.; Annan, R. S.; Sacks, D. B.: IQGAP1 promotes neurite outgrowth in a phosphorylation-dependent manner. *J Biol Chem* **2005**, *280*, 13871-13878.

(152) Mischak, H.; Delles, C.; Klein, J.; Schanstra, J. P.: Urinary proteomics based on capillary electrophoresis-coupled mass spectrometry in kidney disease: discovery and validation of biomarkers, and clinical application. *Adv Chronic Kidney Dis* **2010**, *17*, 493-506.

(153) Gamagedara, S.; Ma, Y.: Biomarker analysis for prostate cancer diagnosis using LC-MS and CE-MS. *Bioanalysis* **2011**, *3*, 2129-2142.

(154) Simionato, A. V. C.; Carrilho, E.; Maggi Tavares, M. F.: CE-MS and related techniques as a valuable tool in tumor biomarkers research. *Electrophoresis* **2010**, *31*, 1214-1226.

(155) Barbas, C.; Moraes, E. P.; Villasenor, A.: Capillary electrophoresis as a metabolomics tool for non-targeted fingerprinting of biological samples. *J Pharm Biomed Anal* **2011**, *55*, 823-831.

(156) Monton, M. R. N.; Soga, T.: Metabolome analysis by capillary electrophoresis-mass spectrometry. *J Chromatogr A* **2007**, *1168*, 237-246.

(157) Rodriguez Robledo, V.; Smyth, W. F.: The application of CE-MS in the trace analysis of environmental pollutants and food contaminants. *Electrophoresis* **2009**, *30*, 1647-1660.

(158) Ravelo-Perez, L. M.; Asensio-Ramos, M.; Hernandez-Borges, J.; Rodriguez-Delgado, M. A.: Recent food safety and food quality applications of CE-MS. *Electrophoresis* **2009**, *30*, 1624-1646.

(159) Ban, E.; Park, S. H.; Kang, M.-J.; Lee, H.-J.; Song, E. J.; Yoo, Y. S.: Growing trend of CE at the omics level: the frontier of systems biology--an update. *Electrophoresis* **2012**, *33*, 2-13.

(160) Desiderio, C.; Rossetti, D. V.; Iavarone, F.; Messana, I.; Castagnola, M.: Capillary electrophoresis--mass spectrometry: recent trends in clinical proteomics. *J Pharm Biomed Anal* **2010**, *53*, 1161-1169.

(161) Suntornsuk, L.: Recent advances of capillary electrophoresis in pharmaceutical analysis. *Anal Bioanal Chem* **2010**, *398*, 29-52.

(162) Smith, R. D.; Barinaga, C. J.; Udseth, H. R.: Improved electrospray ionization interface for capillary zone electrophoresis-mass spectrometry. *analytical chemistry* **1988**, *60*, 1948-1952.

(163) Smith, R. D.; Olivares, J. A.; Nguyen, N. T.; Udseth, H. R.: Capillary zone electrophoresis-mass spectrometry using an electrospray ionization interface. *analytical chemistry* **1988**, *60*, 436-441.

(164) Lee, E. D.; Muck, W.; Henion, J. D.; Covey, T. R.: On-line capillary zone electrophoresis-ion spray tandem mass spectrometry for the determination of dynorphins. *J Chromatogr* **1988**, *458*, 313-321.

(165) Haselberg, R.; de Jong, G. J.; Somsen, G. W.: Capillary electrophoresis-mass spectrometry of intact basic proteins using Polybrene-dextran sulfate-Polybrene-coated capillaries: system optimization and performance. *Anal Chim Acta* **2010**, *678*, 128-134.

(166) Huhn, C.; Ramautar, R.; Wuhrer, M.; Somsen, G. W.: Relevance and use of capillary coatings in capillary electrophoresis-mass spectrometry. *Anal Bioanal Chem* **2010**, *396*, 297-314.

(167) Liu, Y.; Fu, X.; Bai, Y.; Zhai, M.; Liao, Y.; Liao, J.; Liu, H.: Improvement of reproducibility and sensitivity of CE analysis by using the capillary coated dynamically with carboxymethyl chitosan. *Anal Bioanal Chem* **2011**, *399*, 2821-2829.

(168) Kelly, R. T.; Page, J. S.; Luo, Q.; Moore, R. J.; Orton, D. J.; Tang, K.; Smith, R. D.: Chemically etched open tubular and monolithic emitters for nanoelectrospray ionization mass spectrometry. *Anal Chem* **2006**, *78*, 7796-7801.

(169) Ramautar, R.; Heemskerk, A. A. M.; Hensbergen, P. J.; Deelder, A. M.; Busnel, J.-M.; Mayboroda, O. A.: CE-MS for proteomics: Advances in interface development and application. *J Proteomics* **2012**, *75*, 3814-3828.

(170) Maxwell, E. J.; Zhong, X.; Zhang, H.; van Zeijl, N.; Chen, D. D. Y.: Decoupling CE and ESI for a more robust interface with MS. *Electrophoresis* **2010**, *31*, 1130-1137.

(171) Meng, Z.; Veenstra, T. D.: Targeted mass spectrometry approaches for protein biomarker verification. *J Proteomics* **2011**, *74*, 2650-2659.

(172) Rangiah, K.; Hwang, W.-T.; Mesaros, C.; Vachani, A.; Blair, I. A.: Nicotine exposure and metabolizer phenotypes from analysis of urinary nicotine and its 15 metabolites by LC-MS. *Bioanalysis* **2011**, *3*, 745-761.

(173) Blair, I. A.: Analysis of endogenous glutathione-adducts and their metabolites. *Biomed Chromatogr* **2010**, *24*, 29-38.

(174) Kim, K.; Kim, S. J.; Yu, H. G.; Yu, J.; Park, K. S.; Jang, I.-J.; Kim, Y.: Verification of biomarkers for diabetic retinopathy by multiple reaction monitoring. *J Proteome Res* **2010**, *9*, 689-699.

(175) Kuzyk, M. A.; Smith, D.; Yang, J.; Cross, T. J.; Jackson, A. M.; Hardie, D. B.; Anderson, N. L.; Borchers, C. H.: Multiple reaction monitoring-based, multiplexed, absolute quantitation of 45 proteins in human plasma. *Mol Cell Proteomics* **2009**, *8*, 1860-1877.

(176) Jeong, J.-S.; Kim, S.-K.; Park, S.-R.: Capillary electrophoresis mass spectrometry with sheathless electrospray ionization for high sensitivity analysis of underivatized amino acids. *Electrophoresis* **2012**, *33*, 2112-2121.

(177) Li, Y.; Wojcik, R.; Dovichi, N. J.; Champion, M. M.: Quantitative Multiple Reaction Monitoring of Peptide Abundance Introduced via a Capillary Zone Electrophoresis-Electrospray Interface. *Anal Chem* **2012**, *84*, 6116-6121.

(178) Kuhr, W. G.: Capillary electrophoresis. *analytical chemistry* **1990**, *62*, 403R-414R.

(179) Ibrahim, Y.; Tang, K.; Tolmachev, A. V.; Shvartsburg, A. A.; Smith, R. D.: Improving mass spectrometer sensitivity using a high-pressure electrodynamic ion funnel interface. *J Am Soc Mass Spectrom* **2006**, *17*, 1299-1305.

(180) Krenkova, J.; Foret, F.: On-line CE/ESI/MS interfacing: Recent developments and applications in proteomics. *PROTEOMICS* **2012**, *12*, 2978-2990.

(181) Ramautar, R.; Mayboroda, O. A.; Somsen, G. W.; de Jong, G. J.: CE-MS for metabolomics: Developments and applications in the period 2008–2010. *ELECTROPHORESIS* **2011**, *32*, 52-65.

(182) Herrero, M.; Ibañez, E.; Cifuentes, A.: Capillary electrophoresis-electrospray-mass spectrometry in peptide analysis and peptidomics. *ELECTROPHORESIS* **2008**, *29*, 2148-2160.

(183) Haselberg, R.; de Jong, G. J.; Somsen, G. W.: Low-Flow Sheathless Capillary Electrophoresis–Mass Spectrometry for Sensitive Glycoform Profiling of Intact Pharmaceutical Proteins. *Analytical Chemistry* **2013**, *85*, 2289-2296.

(184) Thakur, D.; Rejtar, T.; Karger, B. L.; Washburn, N. J.; Bosques, C. J.; Gunay, N. S.; Shriver, Z.; Venkataraman, G.: Profiling the Glycoforms of the Intact α Subunit of Recombinant Human Chorionic Gonadotropin by High-Resolution Capillary Electrophoresis−Mass Spectrometry. *Analytical Chemistry* **2009**, *81*, 8900-8907.

(185) Ramautar, R.; Busnel, J.-M.; Deelder, A. M.; Mayboroda, O. A.: Enhancing the Coverage of the Urinary Metabolome by Sheathless Capillary Electrophoresis-Mass Spectrometry. *Analytical Chemistry* **2011**, *84*, 885-892.

(186) Lee, R.; West, D.; Phillips, S. M.; Britz-McKibbin, P.: Differential Metabolomics for Quantitative Assessment of Oxidative Stress with Strenuous Exercise and Nutritional Intervention: Thiol-Specific Regulation of Cellular Metabolism with N-Acetyl-l-Cysteine Pretreatment. *Analytical Chemistry* **2010**, *82*, 2959-2968.

(187) Ibáñez, C.; Simó, C.; Martín-Álvarez, P. J.; Kivipelto, M.; Winblad, B.; Cedazo-Mínguez, A.; Cifuentes, A.: Toward a Predictive Model of Alzheimer's Disease Progression Using Capillary Electrophoresis–Mass Spectrometry Metabolomics. *Analytical Chemistry* **2012**, *84*, 8532-8540.

(188) Bachmann, S.; Bakry, R.; Huck, C. W.; Polato, F.; Corradini, D.; Bonn, G. K.: Peptide mapping using capillary electrophoresis offline coupled to matrix-assisted laser desorption ionization time of flight mass spectrometry. *ELECTROPHORESIS* **2011**, *32*, 2830-2839.

(189) Dong, Y.-M.; Chien, K.-Y.; Chen, J.-T.; Lin, S.-J.; Wang, T.-C. V.; Yu, J.-S.: Site-specific separation and detection of phosphopeptide isomers with pH-mediated stacking capillary electrophoresis-electrospray ionization-tandem mass spectrometry. *Journal of Separation Science* **2013**, n/a-n/a.

(190) Wang, C.; Lee, C. S.; Smith, R. D.; Tang, K.: Ultrasensitive Sample Quantitation via Selected Reaction Monitoring Using CITP/CZE-ESI-Triple Quadrupole MS. *Anal Chem* **2012**, *84*, 10395-10403.

(191) Wen, Y.; Li, J.; Ma, J.; Chen, L.: Recent advances in enrichment techniques for trace analysis in capillary electrophoresis. *ELECTROPHORESIS* **2012**, *33*, 2933-2952.

(192) Kašička, V.: Recent developments in CE and CEC of peptides (2009–2011). *ELECTROPHORESIS* **2012**, *33*, 48-73.

(193) Tong, W.; Link, A.; Eng, J. K.; Yates, J. R.: Identification of Proteins in Complexes by Solid-Phase Microextraction/Multistep Elution/Capillary Electrophoresis/Tandem Mass Spectrometry. *Analytical Chemistry* **1999**, *71*, 2270-2278.

(194) Busnel, J.-M.; Schoenmaker, B.; Ramautar, R.; Carrasco-Pancorbo, A.; Ratnayake, C.; Feitelson, J. S.; Chapman, J. D.; Deelder, A. M.; Mayboroda, O. A.: High capacity capillary electrophoresis-electrospray ionization mass spectrometry: coupling a porous sheathless interface with transient-isotachophoresis. *Analytical chemistry* **2010**, *82*, 9476-9483.

(195) Heemskerk, A. A.; Busnel, J.-M.; Schoenmaker, B.; Derks, R. J.; Klychnikov, O.; Hensbergen, P. J.; Deelder, A. M.; Mayboroda, O. A.: Ultra-Low Flow Electrospray Ionization-Mass Spectrometry for Improved Ionization Efficiency in Phosphoproteomics. *Analytical chemistry* **2012**, *84*, 4552-4559.